Multi-functional nanocomposites for the mechanical actuation and magnetoelectric conversion

Jiawei Zhang

N° d'ordre 2011-ISAL-0132 **Année 2011**

THESE

Multi-functional Nanocomposites for the Mechanical Actuation and Magnetoelectric Conversion

By

Jiawei Zhang

A thesis submitted in fulfilment of the requirements for the degree of

Doctor of Philosophy

School of doctorate: Electronic, Electrotechnic and Automatic (EEA)

INSA-LYON

Lyon, France

13 December 2011

Advisory Committee:

Advisor	Prof. Laurent LEBRUN
Co-Advisor	Prof. Benoit GUIFFARD
Reviewer	Prof. Colette LACABANNE
Reviewer	Dr. Yves BERNARD (HDR)
Committee Member	Dr. François BAUER
Committee Member	Prof. Daniel GUYOMAR

LGEF Laboratory, Department of Electrical Engineering, INSA-Lyon

SIGLE	ECOLE DOCTORALE	NOM ET COORDONNEES DU RESPONSABLE
CHIMIE	**CHIMIE DE LYON** **http://www.edchimie-lyon.fr** Insa : R. GOURDON	M. Jean Marc LANCELIN Université de Lyon – Collège Doctoral Bât ESCPE 43 bd du 11 novembre 1918 69622 VILLEURBANNE Cedex Tél : 04.72.43 13 95 directeur@edchimie-lyon.fr
E.E.A.	**ELECTRONIQUE, ELECTROTECHNIQUE, AUTOMATIQUE** **http://edeea.ec-lyon.fr** Secrétariat : M.C. HAVGOUDOUKIAN eea@ec-lyon.fr	M. Gérard SCORLETTI Ecole Centrale de Lyon 36 avenue Guy de Collongue 69134 ECULLY Tél : 04.72.18 60 97 Fax : 04 78 43 37 17 Gerard.scorletti@ec-lyon.fr
E2M2	**EVOLUTION, ECOSYSTEME, MICROBIOLOGIE, MODELISATION** **http://e2m2.universite-lyon.fr** Insa : H. CHARLES	Mme Gudrun BORNETTE CNRS UMR 5023 LEHNA Université Claude Bernard Lyon 1 Bât Forel 43 bd du 11 novembre 1918 69622 VILLEURBANNE Cédex Tél : 04.72.43.12.94 e2m2@biomserv.univ-lyon1.fr
EDISS	**INTERDISCIPLINAIRE SCIENCES-SANTE** **http://ww2.ibcp.fr/ediss** Sec : Safia AIT CHALAL Insa : M. LAGARDE	M. Didier REVEL Hôpital Louis Pradel Bâtiment Central 28 Avenue Doyen Lépine 69677 BRON Tél : 04.72.68 49 09 Fax :04 72 35 49 16 Didier.revel@creatis.uni-lyon1.fr
INFOMATHS	**INFORMATIQUE ET MATHEMATIQUES** http://infomaths.univ-lyon1.fr	M. Johannes KELLENDONK Université Claude Bernard Lyon 1 INFOMATHS Bâtiment Braconnier 43 bd du 11 novembre 1918 69622 VILLEURBANNE Cedex Tél : 04.72. 44.82.94 Fax 04 72 43 16 87 infomaths@univ-lyon1.fr
Matériaux	**MATERIAUX DE LYON** Secrétariat : M. LABOUNE PM : 71.70 –Fax : 87.12 Bat. Saint Exupéry Ed.materiaux@insa-lyon.fr	M. Jean-Yves BUFFIERE INSA de Lyon MATEIS Bâtiment Saint Exupéry 7 avenue Jean Capelle 69621 VILLEURBANNE Cédex Tél : 04.72.43 83 18 Fax 04 72 43 85 28 Jean-yves.buffiere@insa-lyon.fr
MEGA	**MECANIQUE, ENERGETIQUE, GENIE CIVIL, ACOUSTIQUE** Secrétariat : M. LABOUNE PM : 71.70 –Fax : 87.12 Bat. Saint Exupéry mega@insa-lyon.fr	M. Philippe BOISSE INSA de Lyon Laboratoire LAMCOS Bâtiment Jacquard 25 bis avenue Jean Capelle 69621 VILLEURBANNE Cedex Tél :04.72.43.71.70 Fax : 04 72 43 72 37 Philippe.boisse@insa-lyon.fr
ScSo	**ScSo*** M. OBADIA Lionel Sec : Viviane POLSINELLI Insa : J.Y. TOUSSAINT	M. OBADIA Lionel Université Lyon 2 86 rue Pasteur 69365 LYON Cedex 07 Tél : 04.78.69.72.76 Fax : 04.37.28.04.48 Lionel.Obadia@univ-lyon2.fr

*ScSo : Histoire, Geographie, Aménagement, Urbanisme, Archéologie, Science politique, Sociologie, Anthropologie

RESUME

L'effet magnétoélectrique (ME) se traduit par la possibilité d'induire une magnétisation à l'aide d'un champ électrique (effet direct) ou celle d'induire une polarisation électrique à l'aide d'un champ magnétique (effet inverse). Les composites laminés qui possèdent de grands coefficients ME ont généré beaucoup d'intérêt dans le domaine des capteurs, des modulateurs, des interrupteurs et des inverseurs de phase.

Dans cette thèse, nous présentons les performances de composites dits laminés à deux ou trois couches. Il a été montré que l'on pouvait obtenir des performances en conversion magnéto-électrique directe en associant des phases magnétostrictives et piézoélectriques. Une modélisation de leur comportement basée sur un oscillateur mécanique a été proposée. Elle a été en particulier utilisée pour simuler le couplage mécanique entre deux couches.

Une autre approche pour développer des dispositifs originaux a consisté à utiliser un champ magnétique alternatif pour induire des courants de Foucault dans des électrodes métalliques et une Force de Lorentz en présence d'un deuxième champ magnétique continu. Si ces électrodes recouvrent un matériau piézoélectrique, la force de Lorentz sera alors convertie en signal électrique suivant l'effet direct. Cette approche permet donc de développer des dispositifs de conversion électromagnétique sans phase magnétique. Différents prototypes utilisant un bimorphe piézoélectrique, un film de PVDF et une céramique piézoélectrique ont été réalisés et caractérisés. Un signal électrique proportionnel à la composante continue du champ magnétique a été mis en évidence, ce qui ouvre des applications pour la détection magnétique.

Cette thèse s'est également intéressée à l'augmentation du coefficient d'électrostriction par injection de charges électriques en utilisant la technique de décharge Corona. Cette étude a été réalisée sur du polypropylène, connu pour sa capacité à stocker des charges électriques. Le mécanisme de stockage de charge et l'effet sur l'électrostriction ont été étudiées par la mesure du potentiel de surface, la mesure des courants thermo-stimulés, la calorimétrie différentielle et l'interférométrie Laser. L'injection de charges a contribué à une augmentation de la permittivité et par la même à celle du coefficient d'électrostriction, en accord avec un modèle simple de distribution de charges dans l'échantillon.

ABSTRACT

Magnetoelectric (ME) interactions in matter correspond to the appearance of magnetization by means of an electric field (direct effect) or the appearance of electric polarization by means of a magnetic field (converse effect). The composite laminates which possess large ME coefficient, have attracted much attention in the field of sensors, modulators, switches and phase inverters. In this thesis, we report on the ME performances of the bi- and tri- layered composites. It is shown that their ME couplings can be achieved by combining magnetostrictive and piezoelectric layers. A model based on a driven damped oscillation is established for the piezoelectric/magnetostrictive laminated composite. It is used to simulate the mechanical coupling between the two layers. In addition, we report that the ME coupling can be achieved without magnetic phase but only with eddy current induced Lorentz forces in the metal electrodes of a piezoelectric material induced by ac magnetic field. The models based on the Lorentz effect inducing ME coupling in PZT unimorph bender, polyvinylidene fluoride (PVDF) film and PZT ceramic disc are thus established. The results show the good sensitivity and linear ME response versus dc magnetic field change. Thus, the room temperature magnetic field detection is achievable using the product property between magnetic forces and piezoelectricity.

Besides, we report on the electrostrictive performance of cellular polypropylene electret after high-voltage corona poling. We use the Surface Potential test, Thermal Stimulated Depolarization Current experiment and Differential Scanning Calorimetry experiment to analyse its charge storage mechanism. The result show that the electrostrictive coefficient and relative permittivity of the charged samples increase. Last but not least, in order to explain this phenomenon, a mathematic model based on the charged sample has been established.

I am a slow walker, but I never walk backwards.

Abraham Lincoln

Acknowledgments

I would like to express my sincere gratitude to my advisors, Prof. Laurent Lebrun and Prof. Benoit Guiffard, for giving me the opportunity to work on exciting projects. I would especially like to thank both of them for their warm guidance, encouragement and support throughout my Ph.D research at the INSA-Lyon. I deeply appreciate all the time and effort they spent discussing my projects and advising me. I also appreciate all their precious corrections to my papers and thesis, attentive consideration and encouragement they gave me. It would not have been possible to accomplish my scientific goals without their guidance. Also, without their selfless help, I can not get my research work done within few years.

I also would like to express my gratitude to the committee members:
Prof. Colette Lacabanne, Dr. Yves Bernard, Prof. François Bauer, Prof. Daniel Guyomar for their insightful, invaluable comments and suggestions that improved the quality of this work.

In addition, the same gratitude goes to Dr. Rabah Belouadah, Dr. Pierre-Jean Cottinet, Dr. Lauric Garbuio, Dr. Gael Sebald, Dr. Mickaë Lallart, Dr. Abdelowahed Hajjaji, Dr. Benjamin Ducharne and Dr. Jean-Fabien Capsal. It was a great opportunity and honor to join the Laboratory of Electrical Engineering and Ferroelectricity (LGEF), learn magnetical, mechanical and electrical characterizations of the composites films and discuss on theoretical and technical issues of my research work with them. Thanks also go to Dr. Laurence Seveyrat, Mr. Frederic Defromerie and Mrs. Véronique Perin for machining the art-like device for my research and experiments.

I am also grateful for all the supports from Evelyne Dorieux, secretary of our laboratory. Thanks to all of her hard work, I can devote all my time to my studies and researches.

I would like to thank all members and colleagues in LGEF, as well as Bo Li, Ting Li and other friends in France who constantly help me not only in research but also in many aspects of my life during my Ph.D. study, though I can't list all of their names.

I also appreciate China Scholarship Council (CSC) for financial support.

Last but not least, I want to thank my families who constantly support my every pursuit.

Table of Contents

Nomenclature

A	Area
B	Magnetic induction vector
C	Capacitance
D	Electric displacement
d_{33}	Piezoelectric coefficients
E	Electric field
e	Electromotive forces
e_{31}	Piezoelectric strain coefficient
F	Force
f	Frequency
H_{dc}	dc Magnetic field
h_{ac}	ac Magnetic field
I	Current
J	Current density
$k(r)$	Eddy current surface density
M	Moment
M_{33}	Electrical field related electrostrcitive coefficient
P	Polarization
Q	Electrical charges
Q_m	Mechanical quality factor of piezoelectric ceramic
Q_{corona}	Charge quantity ater corona poling
R	Resistance
r	Radius
S	Strain
s	Elastic compliance
T	Stress
th	Thickness
V	Voltage

v	Velocity
Y	Young's modulus
y	Film deflection
α	The first order magnetoelectric coefficient
β	The second order magnetoelectric coefficient
ε	Permittivity
ε_0	Permittivity of free space (8.85×10^{-12} F m^{-1})
ε_r	Relative permittivity
λ	Magnetostriction coefficient
ρ	Charge density
δ_1	Stress magnetostrictive coefficient
$tan\delta$	Loss tangent
ϕ	Magnetic flux
φ	Phase shift
Φ_{loop}	Magnitude of magnetic flux
ω	Angular velocity
μ_0	Permeability of free space (1.2566×10^{-6} $WbA^{-1}m^{-1}$)

Introduction

Magnetoelectric (ME) effect, triggered much interests because of its potential of the crosscorrelation between the electric and magnetic properties of matter for technical applications such as magnetic field sensors, transducers, actuators and so on. Normally, the ME effect in composite materials with two or more phases is generated through the product property between magnetostriction and piezoelectricity. The strain induced by applied magnetic field, passes on to the piezoelectric phase, where an electric polarization appears. While, the converse effect is also possible to be put into application, in which applied electric field on the piezoelectric material produce sample's strain, which can be transferred as stress to the magnetostrictive material inducing magnetization [1]. During the last decade, many works have been realized on two types of ME composites: the particulate and the laminate composites. Particulate composites where magnetic particles are embedded in piezoelectric ceramic exhibit poor ME activity because of the high temperature process (sintering) which induces cracks, porosity in the compound. The ME effect has been found larger in laminate (multi-layered) composites owing to the macroscopic separation of magnetostrictive and piezoelectric phases, yielding a better interface coupling.

To our knowledge, very few studies have been devoted to the ME effect in laminate composites including magnetostrictive polymeric layer. For this reason, in the present thesis work, we have studied the ME effect based on magneto-elastic-electric effect in bi- and trilayered composites consisting of thermoplastic polyurethane (PU) filled with magnetically hard magnetite

Fe_3O_4 or Terfenol-D (TeD) magnetostrictive alloy. The layer of magnetostrictive polymer composite was bonded with piezoelectric polyvinylidene fluoride (PVDF) or piezoelectric lead zirconate titanate (PZT) ceramic layer. Besides, another ME effect in two-phase composites consisting of piezoelectric and metal (i.e. Fe, Al) may be envisaged. This ME coupling in composites without magnetic phase is expected to be based on the product property between Lorentz forces and piezoelectricity. The modelings with the aim to establish the coupling mechanisms between different phases of the laminates composites need to be developed.

On the other hand, electroactive polymers present many advantages as compared to classical ferroelectric materials. They can be prepared at low cost, molded into various shapes and deposited on large surfaces. They are also lightweight and can generate high levels of strain [2-4]. Recently, new types of polymer composites, obtained by filling a polymeric matrix with conductive nanofillers (i.e., carbon nanopowder, carbon nanotubes, etc.), have been synthesized. These composites exhibit large strains at medium electric fields and consequently appear to be promising electroactive materials for actuation with high electrostrictive coefficients [2, 3]. As these outstanding properties seem to be linked to the space charge distribution, it seems to be interesting to evaluate the actuation performance of a dielectric material in which only electrical charges have been injected instead of filling it with nano-objects.

The most well-known technique for injecting charges is the high-voltage corona treatment. The sample is placed under a metallic grid onto which a negative potential is applied. A high voltage generator is connected to metallic needles in order to inject charges within the polymer. Various parameters (temperature, grid voltage, position of the needles) control the quantity of the injected charges and their profile within the materials. Several papers have described this process and the equipment in detail [5-7].

Beyond the various available materials, cellular polypropylene (PP) is a well known polymer for its ability to store electrical charge when subjected to the corona poling and for having ferroelectric-like properties (like remnant electrical field-induced polarization and converse piezoelectric effect, i.e. strain directly proportional to the electric field) caused by charged lens-like voids which are responsible for a strong anisotropy within the polymer. It has therefore been given the name ferroelectret [8-13]. However, few studies have been done on that how injected charge affects electrostriction property of charged cellular PP, which corresponds to a strain proportional to the square of the electric field.

Negative corona-charged PP has been widely studied [14-17]. By using the Thermal Stimulated Depolarization Current (TSDC) method, detrapped charges and a relaxation of the polarization have been observed by Ono et al.4 Furthermore, the Laser Induced Pressure Pulse (LIPP) technique has also been used in former investigations for displaying the charge distribution [5]. By integration of the TSC current, the quantity of charges can be calculated.

Objectives of this work

The first objective of this study is to investigate the magnetoelectric effect of multi-layered polymers including PU layer filled with magnetically hard magnetite Fe_3O_4 or TeD and PVDF film. In particular, we design an analytical modeling to evaluate the influence of the first and second-order ME coefficients on the dc magnetic field-induced phase switching phenomenon between dynamic ME current and the applied ac magnetic field.

The second objective of this work is to explore the ME effect in a metal-piezoelectric laminates without magnetic ordering. Three distinct configurations are envisaged: piezoelectric unimorph bender with PZT ceramic,

PVDF single layer and piezoelectric ceramic disc. We work out the modeling of their output ME current.

Thirdly, the goal has been to evaluate the effect of charge injection on the apparent electrostrictive coefficient of cellular Polypropylene (PP) by combining surface voltage measurements, and the TSDC and DSC methods which can give the information on stability and quantity of injected charge, as well as crystallinity, and evaluate enhanced electrostrictive response by these methods. In order to explore the application potential of such a readily manufacturable polymer, the effect of its surface roughness on the charge injection has been also explored, which can influence the charge injection of cellular polymer and its electrostrictive response. The charges retain ability and charge storage mechanisms have been analyzed.

Thesis Outline

The thesis consists of six chapters. The literatures review concerning to the development history and application of magnetoelectric and electrostrictive effect have been reported in Chapter 1.

Chapter 2 presents the fabrication procedures of multi-layered composites. The set-ups and configuration of their magnetoelectric experiments have been presented in detail.

Chapter 3 gives the corona poling set-up and a series of experimental techniques used to perform Surface Potential Decay test, Thermal Stimulated Depolarization Current experiment, Differential Scanning Calorimetry experiement and electrostrictive experiment of cellular polypropylene after corona treatment.

Chapter 4 describes the results and includes the discussions of the magnetoelectric experiments of laminate composites. The calculation modelings have also been described.

In Chapter 5, the results, discussions and modeling of corona-charged cellular polypropylene have been given.

In Chapter 6, the conclusions and future promising works are presented.

Chapter 1. Literatures review and general concepts of Magnetoelectric and Electrostrictive effects

1.1 Introduction

In the first part of this chapter, the magnetoelectric (ME) effect (including both direct and converse magnetoelectric effects) is defined. Representative composite materials which have the significant magnetoelectric effect are introduced. Finally, after introduction of the magnetoelectric effects and the Multiferroic composite materials, some novel applications (i.e. data storage, magnetic field sensors, and actuators) are presented.

In the second part of this chapter, the electrostrictive effect is explained. Development history and modern applications of electrets and electroactive polymers which always attracted the interest of scientists in many fields are introduced. In particular, a lot of works have been devoted to the enhancement of the electrostatic and electrostrictive properties. As an example, the Corona poling of the electrets have been widely studied as well as the filling of eletroactive polymer with nano-sized conductive particles.

1.2 Magnetoelectric effect

1.2.1 Review of magnetoelectric effect

In single-phase compounds and at microscopic level, magnetoelectric effect originates from the interactions of the ions in lattice sites: single-ion anisotropy, symmetric superexchange, antisymmetric superexchange, dipolar interactions and Zeeman energy [1]. In composites, macroscopic magnetoelectric effect is the combination of two types of materials property such as magnetostriction and piezoelectricity [18-20]. It is can be classified as the so-called direct ME effect and the converse ME effect. The former one can be described as the induced electrical polarization (P) under magnetic field (H) and can be expressed as:

$$\Delta P = \alpha \Delta H \quad \text{or} \quad \Delta E = \alpha_E \Delta H \tag{1.1}$$

where α and α_E are the ME and ME voltage coefficient respectively. Under applied alternating magnetic field, the magnetostrictive phase produces strain which is transferred to the piezoelectric phase that converts strain into electric charge. It is denoted that, based on ME coupling, the modulation of electric polarization can be due to applying a magnetic field or a ME voltage output can be caused by an applied magnetic field on the samples.

On the other hand, under applied electric field piezoelectric phase produces strain which is transferred on to the magnetostrictive phase that converts it into magnetic field. So the converse ME response is the appearance of a magnetization (M) upon an applied electric field (E):

$$\Delta M = \alpha \Delta E \tag{1.2}$$

Here, α is the ME magnetization coefficient. Thus, magnetoelectric (ME) effect measurement are usually performed under two distinctly different conditions which refer to the electric polarization induced by an applied magnetic field or the magnetization induced by an external electric field [18-20]. For the former situation, the induced polarization is $\delta P=\alpha\delta H$, where α, the second rank of magnetoelectric susceptibility tensor and is expressed in the SI units of s/m ($\alpha=4\pi P/H=4\pi M/E$ is dimensionless in Gaussian units). α usually determined by measuring δP for an applied ac field δH. On the other hand, α_E, ME voltage coefficient, can be determined by δE and δH with the expression: $\alpha_E= \delta E/\delta H$, where H is the applied ac field. Then $\alpha=\varepsilon_0.\varepsilon_r.\alpha_E$, where ε_r is the relative permittivity of the tested material.

The polarization and magnetization of ME effect can be derived from the expression of free energy:

$$\begin{aligned} F\left(\vec{E},\vec{H}\right) = F_0 - P_i^s E_i - M_i^s H_i \\ -\frac{1}{2}\varepsilon_0\varepsilon_{ij}E_iE_j - \frac{1}{2}\mu_0\mu_{ij}H_iH_j - \alpha_{ij}E_iH_j \\ -\frac{1}{2}\beta_{ijk}E_iE_jH_k - \frac{1}{2}\gamma_{ijk}H_iE_jH_k - \ldots \end{aligned} \tag{1.3}$$

where P_i^s, M denote the spontaneous polarization and the magnetization respectively, while ε and μ are the electric susceptibility and magnetic susceptibility respectively. Furthermore α corresponds to polarization induced by a magnetic field or magnetization induced by an electric field which denotes the linear ME effect. The coefficients, β and γ are high order tensors of ME effect. Then, the polarization and magnetization can be expressed as Eqs.(1.4) and (1.5) respectively. A lot of researches on the ME effect are focused on the linear ME effect whose prefix “linear” is generally acceptable to be omitted [1, 21].

$$P_i\left(\vec{E},\vec{H}\right) = -\frac{\partial F}{\partial E_i} = P_i^s + \varepsilon_0 \varepsilon_{ij} E_j + \alpha_{ij} H_j + \frac{1}{2}\beta_{ijk} H_j H_k + \gamma_{ijk} H_i E_j + \ldots \quad (1.4)$$

$$M_i\left(\vec{E},\vec{H}\right) = -\frac{\partial F}{\partial H_i} = M_i^s + \mu_0 \mu_{ij} H_j + \alpha_{ij} E_i + \frac{1}{2}\gamma_{ijk} E_j H_k + \beta_{ijk} E_i H_j + \ldots \quad (1.5)$$

1.2.2 History of ME effect

The history of ME effect can be dated back to as early as 1894, when Curie demonstrated that it would be possible for an asymmetric molecular body to polarize directionally under a applied magnetic field [22]. Then, based on symmetry considerations, a linear ME effect occurring in magnetically order crystals was demonstrated in Ref. [23] by Landau and Lifshitz. Subsequently, the first observation of the ME effect can be dated back to 1959 by Dzyaloshinskii [24], who predicted the existence of the ME effect in Cr_2O_3 on the basis of theoretical analysis. This was soon followed by experimental confirmation of an electric-field-induced magnetization in [25] by Astrov and the detection of the magnetic field-induced polarization made by Rado and Folen [26, 27]. In order to observance of the ME effect, the condition that there are the electric and magnetic dipoles coexisting in such material, is the primary requirement [28]. The ME effect offers a number of application opportunities, such as optical wave modulation, M-E data storage and switching, optical diodes, spin-wave generation, amplification, and frequency conversion [29].

In the past 30 years, researchers have developed ME materials with larger coupling coefficient. This developments are explored from following aspects [20]: (1) single phase which includes ceramics and crystals; (2) bulk

composites of piezoelectric ceramics and ferrites such as Cobalt ferrit (CFO)/barium titanium ($BaTiO_3$), nickel ferrite (NFO) / $BaTiO_3$ and $Pb(Zr_{0.52}Ti_{0.48})O_3$ (PZT)–$NiFe_2O_4$ bulk composites [30, 31] etc.; (3) ceramic-metal ME composites such as the two-phase PZT-$Tb_{1-x}Dy_xFe_2$(Terfenol-D) composites [32, 33]; (4) polymer-based ME composites such as the three phase Terfenol-D/PZT/polymer bulk composites [34, 35]; (5) ME composite thin-films [36, 37]. Researchers conducted a series of experiments on ME laminate composites with different details of the composite microstructures, such as component phase properties, volume fraction, grain shape, phase connectivity, field orientations and fabrication methods, etc. [29]. For instance, ME voltage coefficient up to 4.68 V/cm.Oe was achieved at room temperature by Ryu *et al*. using Pb(Zr, Ti)O_3 (PZT) and Terfenol-D laminate composites [38]. Their promising experimental results indicated that the ME voltage coefficient increased with decreasing thickness and increasing piezoelectric voltage constant of the PZT layer.

1.2.3 ME effect in single crystal phase material

The ME effect was first observed about 50 years ago in Cr_2O_3 single crystal, which had a small ME voltage coefficient of $\alpha \approx 20$ mV/cm-Oe and was not sufficient for practical applications [27, 39]. The ME effect in single phase materials requires coexistence of magnetic and electric dipoles in an asymmetric structure. Number of compounds exhibiting ME effect is limited since the coexistence of magnetic and electric order is chemically incompatible [40].

Nowadays, some categories of single-phase magnetoelectric or multiferroic materials are well-known which includes bismuth-based, manganites-based and ferrites-based single-phase materials. $BiFeO_3$ [41], $TbMnO_3$ [42], and $LuFe_2O_4$ [43, 44] are recognized as the representative of these three kinds of sin-

gle-phase material respectively. Some of the research results of their magnetoelectric effect are shown in Fig. 1. 1 and Fig. 1. 2.

Among these single-phase materials, $BiFeO_3$ shows the ME effect observed by T. Zhao, *et. al.* in microscope view, which means that the configuration of micro/nano-scale ferroelectric or ferromagnetic domains changed by an applied magnetic or electric field [45].

The working temperature range makes difficult the practical application of this single phase materials for common applications, because most of them can work only at very low temperature [28] and the magnetoelectric coefficient drops to zero as the temperature reaches the transition temperature [38].

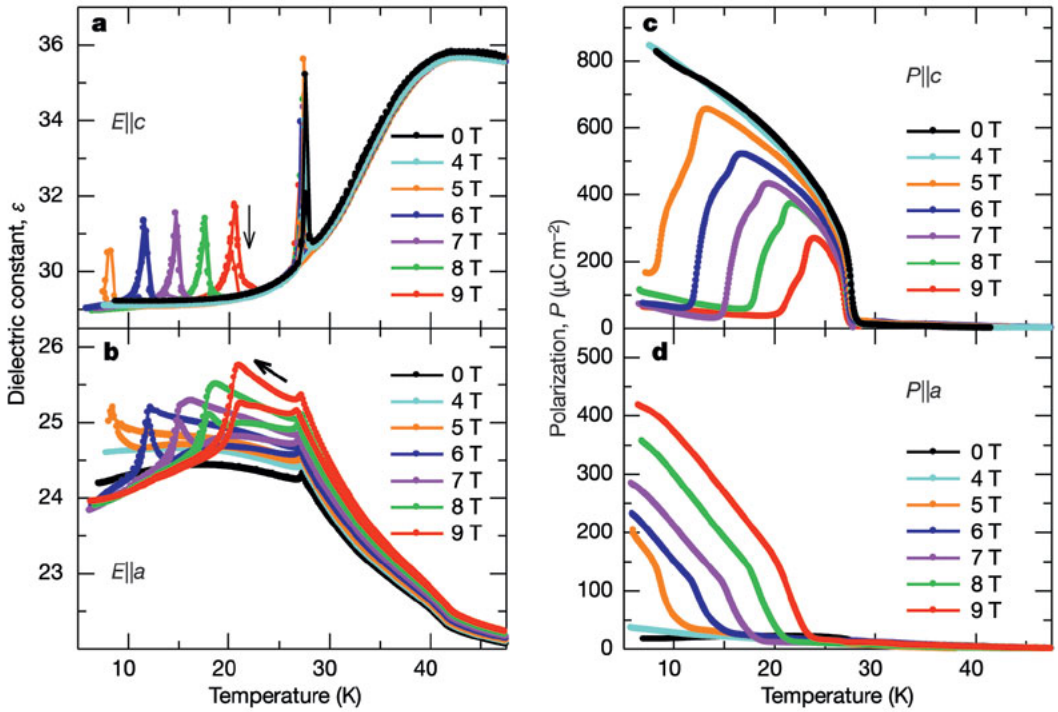

Fig. 1. 1 Direct ME effect of single-phase $TbMnO_3$: Electric polarization induced by an applied magnetic filed [42].

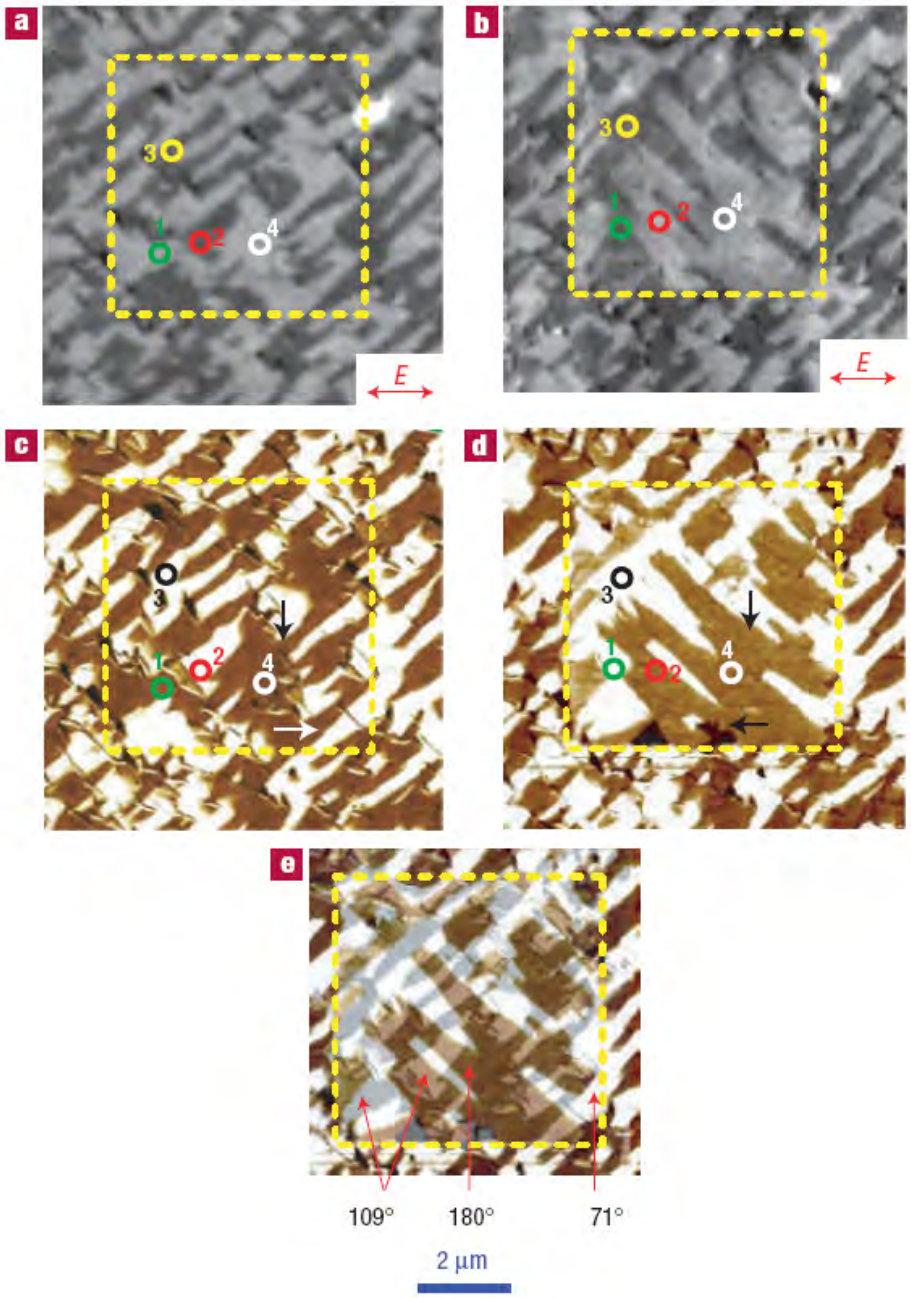

Fig. 1. 2 Converse ME Effect of $BiFeO_3$: magnetization changed by an applied electric field. (Reported by T. Zhao, et al, Nature Materials, 2006) [41]

1.2.4 ME effect in composite materials

The ME effect in composite materials is known as a product tensor property, which is the product of a magnetostrictive and piezoelectric compound [46]. Thanks to the micromechanical coupling, an applied electric field induces a magnetization via the micromechanical coupling between the constituents, or an applied magnetic field induces strain in the magnetostrictive constituent which is passed on to the piezoelectric constituent and induces an electric polarization [1].

For the piezoelectric composites, there are some common connectivity proposals such as 1-3-type fiber composites with fibers of one phase embedded in the matrix of another phase, 0-3-type particulate composites made of piezoelectric and magnetic grains embedded in piezoelectric matrix and 2-2-type laminate composites including piezoelectric and magnetic layers, which are shown in Fig. 1. 3.

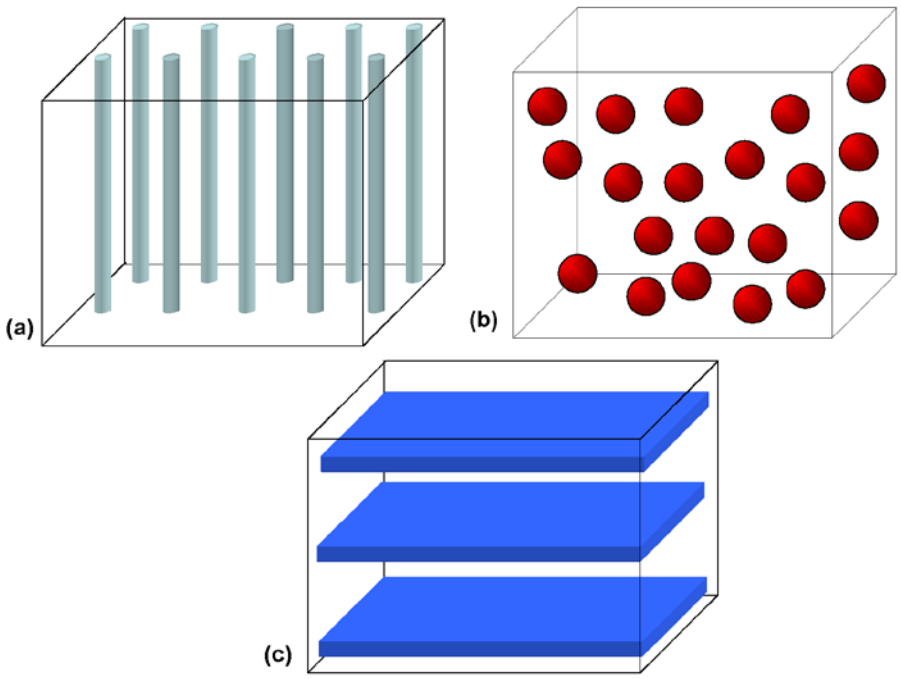

Fig. 1. 3 Schematic illustration of three common types of bulk composites (a) 1-3 fiber/rod composite, (b) 0-3 particulate composite, (c) 2-2 laminate composite [18]

.

After first proposed concept of the ME composite in 1972 by van Suchtelen, the ME effect in bulk composites have drawn ever-increasing interest [18].

Tab. 1. 1ME voltage coefficient for some bulk composites materials [20, 28, 47-58].

	Composite	ME voltage coefficient α_E (mV/cm.Oe)
Ceramic Composite	(0-3) CFO/ BTO	50 @ f_r
	(0-3) NZFO/PZT	155@ 1kHz
	(2-2) NCZF/PZT/ NCZF	782 @1kHz
Ceramic-Alloy Composites	(2-2) Terfenol-D/PMT-PT	10.3×10^3 @1kHz
	(2-2) Terfenol-D/PVDF	1.43×10^3
	(2-1) FeBSiC/PZT-fiber	22×10^3 @ 1Hz and 750×10^3 @ f_r
	(2-2) FeBSiC/PVDF	21.46×10^3 @ 20Hz
	(2-2) FeCoSiB/AIN	3.1×10^3 @ 1Hz and 737×10^3 @ f_r
Polymer-based Composites	(2-2) PZT in PVDF/Terfenol-D in PVDF	80 @ 1kHz and 3×10^3 @ f_r
	(1-3) Terfenol-D in epoxy/PZT	500 @ 100Hz and 18.2×10^3 @ f_r
	(0-3) CFO/P(VDF-TrFE)	40 @ 5kHz

BTO: $BaTiO_3$; CFO: $CoFe_2O_4$; NZFO: $Ni_{0.8}Zn_{0.2}Fe_2O_4$; NCZF: $Ni_{0.6}Cu_{0.2}Zn_{0.2}Fe_2O_4$; AIN: aluminium nitride; PMN-PT: $Pb(Mg,Nb)O_3$-$PbTiO_3$; PVDF: polyvinylidene-fluoride; P(VDF-TrFE): poly(vinylidene fluoride-trifluoroethylene); f_r: electromechanical resonance frequency.

However, most of the theoretical works were undergone which provided quantitative understanding of the ME effect in bulk ceramic composites [20]. ME voltage coefficient of some bulk composites materials at certain frequency have been listed in Tab. 1. 1. The ME effect obtained in compos-

ites is more than a hundred times that of single-phase ME materials and is know as a product tensor property, which is induced by the cross interaction between different ordering of the two phases in the composite.

Coupling between the constituents of laminated double-, triple- or multilayer composites can use glue and epoxy. In layered magnetostrictive/piezoelectric composites, direct ME effect is generated through the magnetic-field induced strain of the magnetostrictive layer which is mechanically coupled to the piezoelectric one subjected to stress variations; this latter transduces the stress to a voltage through its electromechanical conversion ability [1]. The ME coupling in a two-layer structure have been widely studied by several groups who proposed models for ME effect and prediction of ME coefficient [32, 59]. Strictly speaking, the concept of product property between magnetostriction and piezoelectricity clearly corresponds to a ME coupling arising from the combination of two non ME Phases. It has been shown that the efficiency of the micromechanical coupling plays a crucial role. S. Dong investigated a laminate composite made of magnetostrictive Terfenol-D ($Tb_xDy_{1-x}Fe_2$) and piezoelectric ($Pb(Zr_{1-x}Ti_x)O_3$) layer. ME effect of L-L mode (longitudinal magnetized / longitudinal polarized), T-L mode (transverse magnetized / longitudinal polarized) and T-T mode (transverse magnetized / transverse polarized) have been investigated experimentally in [60], in which the maximum ME voltage coefficient 86 mV/Oe under a bias of 500Oe has been got. It was also found that, the ME voltage output can be increased by 10^1-10^3, when the composite sample operating at the electromechanical resonance frequency. It has been shown that laminated composites operated under resonance frequency exhibit ME responses that are orders of magnitude larger than those acquired in single-phase material.

The ME effect in the single piezoelectric phase can not compare with the remarkable ME effect of composites of both magnetic and piezoelectric phases. Thus, ME effect, a coupled magnetic phenomenon via elastic interaction, is a result of the product of the piezoelectric effect (mechani-

cal/electrical effect) and the magnetostrictive effect (magnetic/mechanical effect), which can be denoted by Eqs.(1.6) and (1.7) and shown in Fig. 1. 4. Details of composite microstructure includes: component phase properties, volume fraction, grain shape, phase connectivity, etc.[61].

$$ME_H effect = \frac{Magnetic}{Mechanical} \times \frac{Mechanical}{Electrical} \tag{1.6}$$

$$ME_E effect = \frac{Electrical}{Mechanical} \times \frac{Mechanical}{Magnetic} \tag{1.7}$$

For the direct ME_H effect of a composite, the magnetic phase changes its shape magnetostrictively, when a magnetic field (H) is applied to a composite. Strain induced by this applied magnetic field, passed on to the piezoelectric phase, where an electric polarization appears. While, the converse effect, ME_E, is also possible to be put into application, in which applied electric field (E) on the piezoelectric material produce sample's strain, which can transferred as stress applied to the magnetostrictive material, inducing a magnetization change (ΔM) or domain reorientation through the piezomagnetic effect [1]. Thus, the ME effect in composites depends on the composite microstructure, and coupling interaction across magnetic-piezoelectric interfaces [18]. In addition to their high ME coefficient, the laminated magnetoelectric composites have a relatively simple fabrication method and structure.

Extensive researches have been conducted on the ME effect because of the obvious potential of the coupling between magnetic and electric properties of matter for its technical applications. Then, researchers have made considerable progress towards experimental and theoretical work on ME, and the state of the art in research on the electrodynamics of ME media was summarized in a book written by O'Dell in 1970 [62].

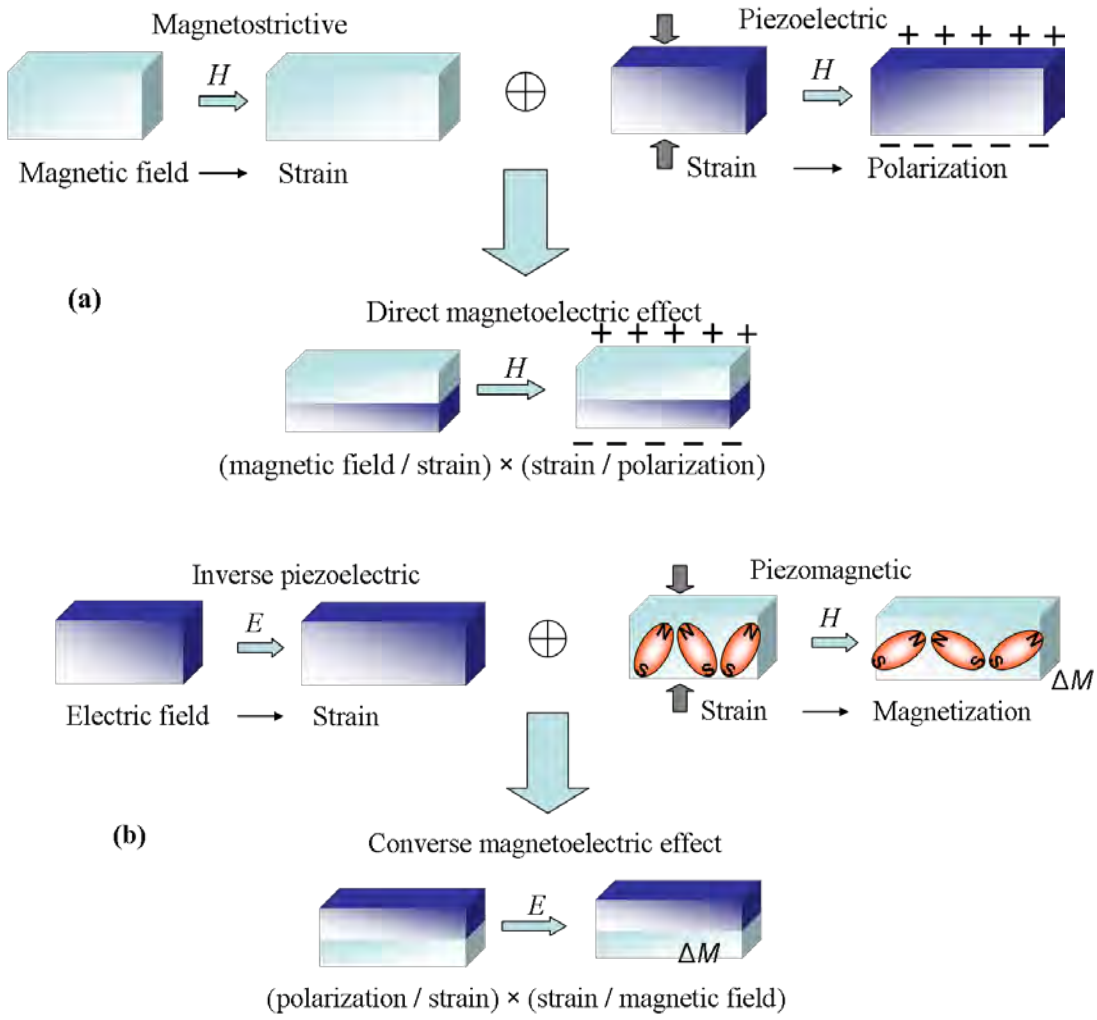

Fig. 1. 4 Schematic illustration of two types of ME effect in laminate composites (a) ME_H effect (b) ME_E effect [63]

However, a general weakness of the ME effect that there was limited number of compounds within it and a limited understanding of microscopic sources of ME behaviour, restricted its useful application and caused a decline of research interest for about two decades. Recently, an impressive revival of the ME effect appeared and some major research topics and trends have been proposed for the future developments. One of these topics concerns structural ME effects in composite materials which contains two or

more constituents. And, the second major topic is associated to multiple (anti-) ferroic ordering [1].

1.2.5 ME coupling as a product property using Lorentz force effect

Very recently, a ME effect based on the product property between Lorentz forces and piezoelectricity has been proposed [64-66]. The ME response triggered by this specific product property may be interesting for applications in ME transducers and sensors. The previous but recent results about this particular ME coupling are presented in the following.

1.2.5.1 Magnetostrictive/piezoelectric laminate composites

The dc magnetic field response of magnetostrictive/piezoelectric magnetoelectric laminates driven by Lorentz force was reported by Jia and co-worker.

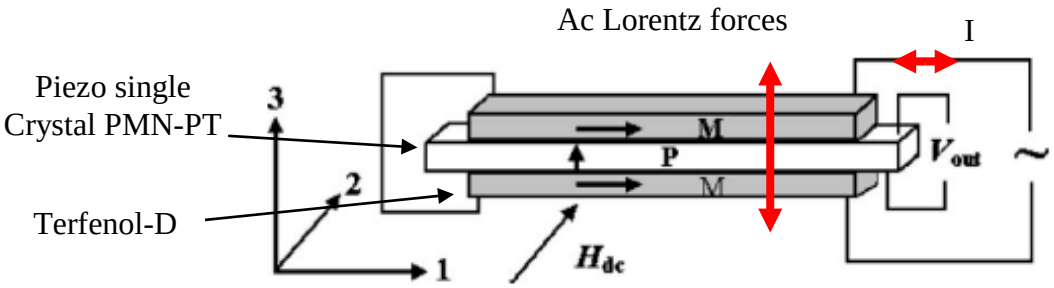

Fig. 1. 5 Magnetostrictive/piezoelectric laminate composite [64]

As shown in Fig. 1. 5, the composite consists of one *L-T* mode ME laminate and one ac current source supplying ac electrical current to Terfenol-D (TeD) alloy strips. Ac current is applied through the two conductive magnetostrictive TeD layers only to induce Lorentz forces within them, in the presence of the dc magnetic field H_{dc}. These Lorentz forces induce stress and strain to the piezoelectric PMN-PT layer sandwiched between the TeD layers. Thus, a second ME coupling is created, in addition to the ME cou-

pling through magnetostriction phenomenon. The Lorentz forces induced ME effect permits dc magnetic field detection along direction 2 and have additional ability to ac field sensing in the direction 1 (L-T mode) using magnetostriction [64]. Researchers got ME coefficient: 6 μV/Oe.A at 1 kHz. However, it requires ac current supply on the electrically conductive Terfenol-D strips.

1.2.5.2 Brass ring around PZT disk

As shown in Fig. 1. 6, a composite consisted of a brass ring and a PZT disk. The ac current was applied circumferentially through the ring. By using the Lorentz force effect from metal strips in the magnetic field when applied with an ac current, the detection of dc magnetic fields can be achieved with a ME coefficient 3.3 μV/Oe.A at 1 kHz [65]. Similarly with previous configuration, the ac current source was also needed.

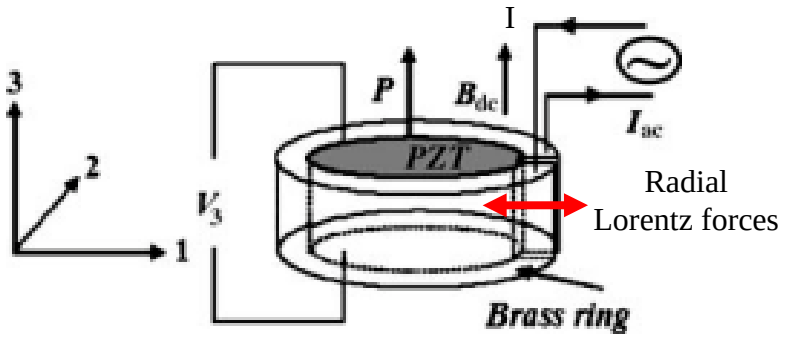

Fig. 1. 6 A ME composite of a brass ring and a PZT disk with Cartesian coordinates [65]

1.2.5.3 Crystal PMN-PT between two aluminium strips

In the work of Leung C.M et.al., an ac current was applied through the strips. Then, the direct coupling of the Lorentz force effect appeared in the aluminium strips in response to a dc magnetic field under an ac electric current with the transverse piezoelectric effect in the PMN-PT plate [66], which was shown in Fig. 1. 7. The measured ME coefficient was 23 μV/Oe.A at 1 kHz.

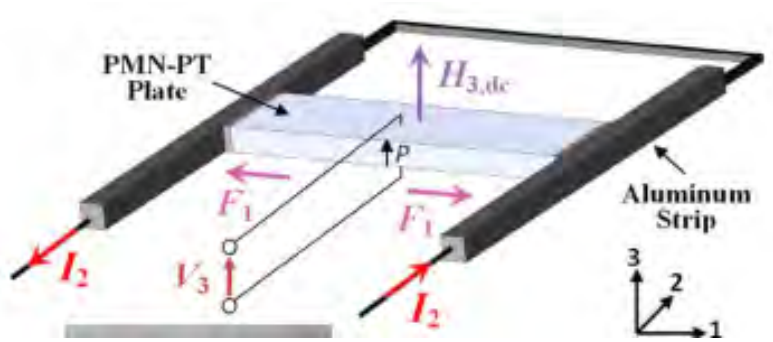

Fig. 1. 7 A dc ME sensor in the Cartesian coordinate system proposed by Leung C.M. et. al. [66] F_1 are Lorentz forces transversely applied to the piezoelectric PMN-PT plate

1.2.6 Applications

Extensive research has been conducted on the magnetoelectric materials, due to their important technological applications as multifunctional devices such as magnetic field sensors for detecting ac or dc fields (thus complementing Hall sensors and current measurement probes), transducers in microwave electronics which converts the microwave magnetic field into a microwave electric field, actuators, data storage applications and so on [1, 34, 55, 67]. Their transductions properties of ME effect could be used in electromagnetic pick-ups and recording heads [28].

For instance, the multiferroic composite thin films could be developed as a magnetoresistive (MR) sensors through their direct ME response [20], in which a constant dc current I is required to detect its resistance ΔR by a read signal of a voltage amplitude change based on the equation $\Delta V = I \times \Delta R$, where ΔR senses the magnetic field change. Thus, the dc test current flow is through the sensor stack in order to measure its change in resistance (i.e. amplitude response signal) as a function of the fringing magnetic flux of the recorded bits, when the reader moves along the recorded track [68]. Vopsaroiu *et al*. proposed a novel magnetic recording head based

on the magneto-electric effect in laminated multiferroic materials, which was much simplified in terms of sensor construction [68]. Their design principle was based on $\Delta V = \alpha \times \delta H$, where δH denoted the stray magnetic field of the record bits. In comparison with former magnetic recording read head (MR) technology, it produced a voltage response without the need for a test current.

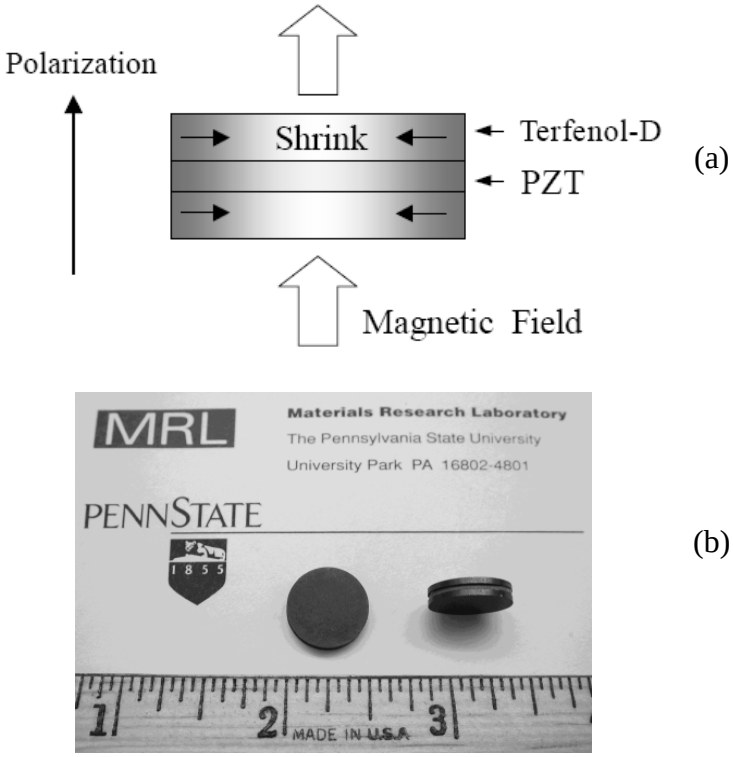

Fig. 1. 8 Magetoelectric laminte composite using TERFENOL-D and PZT discs. (a) Schematic structure; (b) photograph of the sample [38]

Ryu J. and his research group have done extensive research on ME materials for magnetic field sensing and current measurement probes in high-voltage electric transmission systems. As shown in Fig. 1. 8, they investigated a piezoelectric-magnetostrictive composites which were prepared by stacking and bonding Pb(Zr, Ti)O_3 (PZT) and Terfenol-D disks, from which a high ME voltage coefficient of 4.68V/cm.Oe was obtained at room temperature [38].

Furthermore, they may find applications in memory devices, due to their hysteretic nature of the ME effect, and because of the shift in the resonance frequency in a static magnetic or electric bias field the composite materials hold promise in electrically tunable microwave applications such as filters, oscillators, phase shifters [69].

1.3 Electrostrictive effect

1.3.1 Electroactive polymers (EAP)

Electroactive polymers (EAP) are the polymers that change size or shape in response to electrical simulation. EAP materials with electromechanical properties are of great interest in many fields of acoustics where they are used in a large number of applications including loudspeakers, ultrasonic transducers, sonars, actuators and dust-wiper [70]. The impressive advances in improving their actuation strain capability are always attracting the attention of scientists and experts from many fields [71-74]. Other potential applications include interactive tactile Braille readers for the blind and artificial muscles shown in Fig. 1. 9 that can be used to mimic the movements of human, animals and insects for making biologically inspired robots and mechanical devices [71, 75]. As listed in the (Tab. 1. 2), the EAP can be classified into two major groups including: ionic EAP (involving mobility or diffusion of ions and their conjugated substances) and electronic EAP (which are driven by electric field or coulomb forces).

Fig. 1. 9 EAP gripper grabs rocks and works as artificial muscle [76]

Tab. 1. 2 List of the leading EAP materials [77, 78]

Electronic EAP	Ionic EAP
Dielectric EAP	Ionic polymer gels (IPG)
Electrostrictive graft elastomers	Ionic polymer metal composite (IPMC)
Electret polymer	Conductive polymers (CP)
Electrostrictive paper	Carbon nanotubes (CNT)
Electro-viscoelastic elastomers	
Ferroelectric Polymers	
Liquid crystal elastomers (LCE)	

• Ionic EAPs: Their actuation is caused by the displacement of ions inside the polymer. Only a few volts are needed for actuation, but the ionic flow implies a higher electrical power needed for actuation, and energy is needed to keep the actuator at a given position. Examples of ionic EAPS are responsive gels, ionic polymer-metal composites (IPMCs), and conductive polymers. Yet another example is a Bucky gel actuator, which is a polymer-supported layer of polyelectrolyte material made of an ionic liquid sandwiched between two electrode layers consisting of carbon nanotubes [77].

• Electronic EAP: Their actuation is caused by electrostatic forces between two electrodes and/or interaction between dipoles inside the the material, squeezing the polymer. Electronic EAP require no electrical power to keep the actuator at a given position. Electrostrictive polymers and dielectric elastomers are the leading electronic EAP [71].

Thus, there are several kinds of electroactive polymers and the shape change mechanism is somewhat different in case of different types [79]. For many decades, it has been known that some types of polymers can change shape in response to electrical stimulation. As shown in Fig. 1. 10, when subjected to a voltage, dielectrics may become thinner due to their electrostrictive properties [80]. At the very beginning of research on EAP, the studied materials were capable of producing only a relatively small strain. However, since the beginning of the 1990s, some newly developed EAP exhibited large strain [78]. Generally, strain generated by EAP can be as high as two orders of magnitude greater than the rigid and brittle piezoelectric ceramics.

(a) (b)

Fig. 1. 10. Different types of deformation of dielectrics [80]
(a) A nonpolar dielectric without applied voltage; (b) Subjected to a voltage, dielectrics become thinner

1.3.2 Basic properties of electret

An electret, a solid dielectric with a quasi-permanent electric moment, can exhibit an external electric field in the absence of an applied field [81]. As early as 1919 Japanese navy Captain Kawao Wantachi had been able to create an artificial membrane by mixing beeswax with Brazilian palm gum (usually carnauba wax) and resin. The resulting material was then polarised in an electric field, and had maintained its charge for a long time afterward-resulting in the world's very first electret.

The original method, using dipolar polarisation with space charge is applicable to waxes and to polymers like Mylar [82]. Electron beam method (low-energy beams of about 20KeV in vacuum) was used for controlled charging and for research application from the 1960's to today [83]. Corona

method is preferred nowadays for industrial production, often applied at elevated temperatures [84]. Sessler G. M. and Gerhard-Multhaupt R. gave a detailed historical review of the research work performed on electrets [85, 86]. It showed that although heating, ac and dc current could be used as method to prepare the dielectric substance (or move the molecules) at the beginning, pure dc is always required to finally fix the charge.

At the microscopic level, electrets can be classified as real-charge electrets or dipolar-charge electrets [87]. Real-charge electret consists of injected or embedded charges within the dielectric, while dipolar-charge electret is composed of permanent dipoles at the molecular level. Some dielectrics are capable of storing both real and dipolar charges. The macroscopic shape of the electrets can be a film or fiber. Fig. 1. 11 shows the orientation of dipoles within electrets under applied electric field.

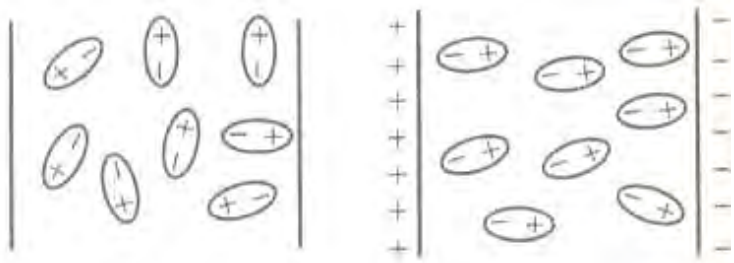

Fig. 1. 11 Orientation of dipoles under electric field [17, 87]

Dipolar-charged electrets can be formed by heating up the material, typically well above the glass transition temperature in the presence of a strong external electric field, and then cooling the material while the field is maintained, thus orienting the dipoles in a semi-permanent configuration. Real-charge electrets can also be formed by exposing the material to a charged plasma or corona.

The distribution of injected sites for real-charge electrets has been an active area of research [88]. The field of electrets has developed rapidly with an increasing number of materials, methods for investigation of charge-

storage phenomena, and the development of creative and exciting applications ranging from air filters to microphones, as well as electrostatic recording, artificial muscle and electret motors and generators [7, 89, 90]. They are also considered for transducer applications, since they mimic piezoelectricity by their unusual electromechanical properties [91].

1.3.3 General concepts of Electrostrictive effect

Generally, electrostriction is defined as quadratic coupling between applied electrical field and strain. The strain S_{ij} and the electric flux density D_m are expressed as:

$$\begin{aligned} S_{ij} &= s^{E}_{ijkl} T_{ij} + M_{mnij} E_n E_m \\ D_m &= \varepsilon_{mn} E_n + 2 M_{mnij} E_n T_{ij} \end{aligned} \tag{1.8}$$

where s_{ijkl}, T_{ij}, M_{mnij} and ε_{mn} are the elastic compliance coefficient, stress, electric field related electrostriction coefficient and linear permittivity respectively [92]. E_m and E_n are the electric field intensity. In our work, we focused on the electrical field induced thickness strain S_3 for a non stressed and low thickness film[93]. In this case, the expression of strain and electric flux density is simplified as:

$$\begin{aligned} S_3 &= s_3 T_3 + M_{33} E_3^{\,2} \\ D_3 &= \varepsilon_{33} E_3 + 2 M_{33} E_3 T_3 \end{aligned} \tag{1.9}$$

Two phenomena named “electrostatic” (Maxwell stress effect) and “electrostriction” are involved in the electrostrictive induced strain [94]. As a consequence, the electrical field related electrostrcitive coefficient M_{33} can be written as [95]:

$$M_{33}^{*} = M_{Maxwell} + M_{electrostrictive} \tag{1.10}$$

where, $M_{Maxwell}$, named as Maxwell stress, is a well-known quantity that results from the electrostatic interaction between two surfaces charged with opposite charges. In the case of a thin film of polymer material, if a voltage is applied in order to create an electric field in the thickness direction of the film, this voltage will generate charges of opposite signs on the two surfaces of the film perpendicular to the thickness direction [96]. This creates an attraction between the two surfaces which results in the deformation of the film. The corresponding stress-Maxwell stress, is related to the square of the electric field, and is therefore a quadratic effect analogous to electrostriction, but one should realize that Maxwell stress is an external effect, independent of intrinsic electromechanical properties of the material such as the ones represented by the electrostrictive coefficients. Nonetheless, this external effect needs to be taken into account in the analysis, because it will contribute to the deformation of the film in exactly the same manner as the electrostrictive effect.

Generally, the relation between the strain and an applied electric field for the electrostrictive materials can be described according to [97, 98]:

$$S_3 = M_{33} E_3^{\,2} \tag{1.11}$$

where E_3 is the applied electrical field, and M_{33} is the the electrostrictive strain coefficients. Consequently, $M_{33}E_3^{\,2}$ represents the strain induced by the electrostriction. For a linear dielectric, M_{33} is equal to $Q_{33}\varepsilon_0^{\,2}(\varepsilon_r-1)^2$ where Q_{33} is the electrostrictive coefficient, and ε_0 and ε_r are the free-space permittivity and the relative permittivity of the tested sample respectively.

In addition to the true electrostrictive contribution ($M_{33}E_3^{\,2}$), one sometimes needs to take into account the Maxwell stress effect contribution

and an apparent electrostrictive coefficient M_{33}^{*} is very often employed [99]. In the case of thickness strain, this additional contribution is assumed to equal to $-(\varepsilon_r.\varepsilon_0 /Y) E_3^2$. Finally M_{33}^{*} can be written as:

$$M_{33}^{*} = Q_{33}\varepsilon_0^2 \left(\varepsilon_r - 1\right)^2 - \frac{\varepsilon_0 \varepsilon_r}{Y} \tag{1.12}$$

Moreover an empirical relationship between the electrostriction coefficient, the permittivity, and the elastic constant has already been established [95], suggesting that the apparent M_{33}^{*} coefficient should be proportional to $\varepsilon_0(\varepsilon_r -1)^2/(Y.\varepsilon_r)$.

1.3.4 Enhanced Electrostrictive performance of cellular polypropylene electret

1.3.4.1 Researches on polypropylene (PP) electret

With the development of science and technology, the application of the foamed polymers has been paid the increasing attention. The functional materials which have high charge-storage ability and high piezoelectric stability are necessary for the air filter, mechanical/acoustic transducers and the piezoelectric sensors [90].

Beyond the various available electrets, cellular polypropylene (PP) is a well known polymer for its ability to store electrical charge when subjected to the corona discharge and for having ferroelectric-like properties (i.e., remnant electrical field-induced polarization) caused by charged lens-like voids which are responsible for a strong anisotropy within the polymer. It has therefore been given the name ferroelectret [8, 9]. However, few studies have been done on that how injected charge affects electromechanical performance of charged cellular PP electrets.

Because of their properties such as lightweight, non-toxic and low price, the commercial used cellular PP film, an ideal electret which can be defined as “Electronic EAP” was researched by a number scholars in recent years. In [9], it was studied by an acoustic method and dielectric resonance spectroscopy. The light emission from barrier discharges in this electret was also quantitatively studied by Qiu X. et. al. [100]. Besides, FTIR analysis was carried out by Sellin N. et. al., in order to analyze the chemical structure changes of PP caused by corona treatment. Furthermore, they analyzed the charged samples by infrared spectroscopy (FTIR/ATR) and atomic force microscopy (AFM) techniques [101].

The pressure expanding treatment and the chemical modification has been applied to cellular polypropylene in order to improve its charge storage stability and the piezoelectricity [102]. As shown in Fig. 1. 12, a scanning electron microscope (SEM) image of PP, the closed-cell voids inside cellular PP have a vertical dimension of several micrometers and a lateral dimension of tens of micrometers [100]. The open-circuit thermally stimulated discharge (TSD) current spectra were studied systematically in [14] as well. At the same time, energy traps inside of polymers have been analysed exactly for the chemically modified cellular PP.

In order to enhance the electret properties, chemical treatment has also been used to cellular PP films in [14]. A mixture solution of H_2SO_4, CrO_3 and H_2O and fluorination in a hydrofluoric acid has been applied during the treatment procedure of cellular polypropylene films. M. Wegener *et al.* pointed that the voids size inside of cellular PP can be increased by the inflation treatment. Thus, the macroscopic dipoles in samples are going to become larger. The inflated samples have shown the excellent d_{33} piezoelectric coefficients [11, 103]. And when temperature of cellular polypropylene is rising up to 60°C, the piezoelectricity activity is decreased [8, 104].

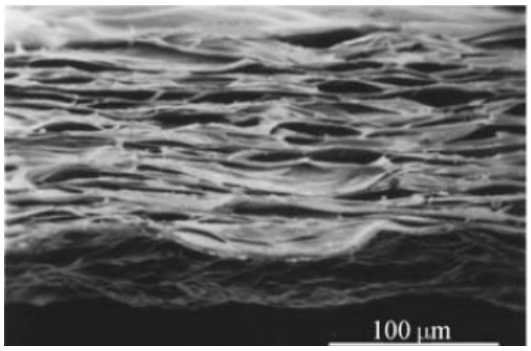

Fig. 1. 12 SEM image of cellular PP after pressure expansion [14]

A simple model for the occurrence of piezoelectricity in polymers has been given in [105, 106]. The elastic behaviours of voids in cellular polymers when they are discharged by DC corona setup have been proposed. They have pointed that cellular polymers exhibit intrinsic (quasi) piezoelectricity. Besides, with the special charging process, the piezoelectric coefficient of the cellular PP is much larger than some of ferroelectric polymers.

In summary, there have been many researches on enhancing piezoelectric properties of polypropylene electrets such as: expansion treatment, chemical modification and charging in gas atmospheres at high pressure [14, 106, 107]. However, little attention was paid to charge cellular PP at high temperature in order to enhance its dipole polarization and electromechanical performance.

1.3.4.2 Basic principles of corona charging technique

Atmosphere corona discharge can enhance the adhesion ability of the polymers and has been extensively applied in photocopiers, electrostatic precipitators, and indoor air cleaners for decades [108-111]. Electron avalanche occuring in the procedure of corona phenomenon is shown in Fig. 1. 13. In application of the electret microphones, preparing the polymer foils by the corona discharge technique has been applied widely [112]. New applications of corona poling have been emerging recently, for example ozone pro-

duction, surface processing, as well as polymer surface treatment [113]. It is a useful technique that can increase adhesive performance, inject real charge into the films and form macro-dipole within them [114]. Their results of corona-discharge show that this surface treatment of polymer film can lead to dramatic increase in the polar and adhesive character of the surface. Other researchers also report that the corona discharge will not only increase the polymers' surface energy, as well as their hydrophilic character, but also generates polar functional groups and the cleavage of chemical bonds [115]. However, the power loss, the generated ozone, the audible noise and electromagnetic interference of corona became main problem in some special occasion, such as over-head high-voltage electric power transmission line [108, 109, 111].

As shown in Fig. 1. 13, during the procedure of corona discharge, the air around vicinity of the cathode is ionized and excited. Meantime, the negative charges and electrons are driven to the anode, obtained by the surface layer of the polymer, and generate new chemical bonds [116].

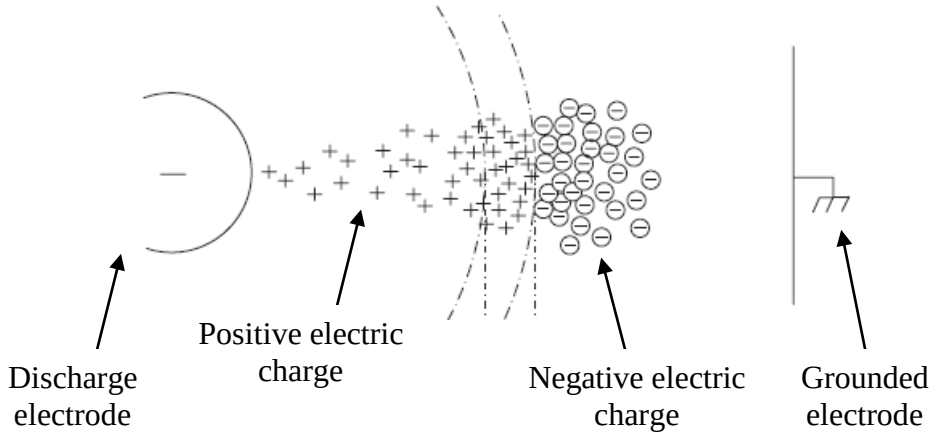

Fig. 1. 13 Development of the negative electric charge avalanche from the cathode [108, 117].

A drawback of the setup shown in Fig. 1. 13 without grid electrode is the relatively large lateral non-uniform charge distribution and thus, the

surface potential could not be controlled as we expected. Thus, in our corona poling experiment, the sample is exposed to a high-voltage in a point-plate arrangement. A grid is inserted between the needle and sample, and the back electrode under the sample is grounded. Such corona poling setup can generate both volume and surface charges. During poling procedure, the surface potential can be regulated by the inserted metallic grid. And the maximum surface potential roughly equals to the applied potential of the grid. This is a simple and speed charging method.

There are two charging techniques, contacting electrodes method and corona discharge method, which are the conventional methods which can be employed to orient dipoles and build up charges inside polymers. The charging method used in our research is corona poling. On the other hand, there are negative and positive corona discharge methods whose working mechanisms can be concluded as followings: There are the sharp distinctions on the secondary electron processes. The number of electrons in negative corona poling is an order of magnitude greater than that in the positive corona poling; the negative corona generate more ozone and less audio noise and electromagnetic interference; negative corona discharge has lower onset fields and higher breakdown voltage than positive corona, thus decrease the need of insulation of the setup [118-120]. In addition, the investigations carried out by Yovcheva T.A *et al*. show that for negative corona charged samples, the oxygen content generated after poling was approximately 2.4 times higher than that in positive corona poled films [121]. Due to the different mechanisms of the positive and negative corona discharge, only the negative corona poling treatment is discussed in our works.

1.3.4.3 Charge storage mechanisms of polymeric electrets

From an applied point of view, it is important to analyze the surface charges storage ability of the polymer after negative corona discharge. Charges stored in polymer electrets could be composed by surface charges

and injected charges which are captured by traps distributed on the surface and in the electret's volume. According to [122], the charge storage capability of an electret polymer film is mainly determined by its chemical nature. For semicrystalline polyolefines, the lamellarcrystals embedded in the amorphous matrix form a heterogeneous morphology, where charge trapping and transport mechanisms depend on the crystallinity. The shallow traps are located in the peripheral and surface layer of the electret film, whereas charges in higher release energy traps are deposited in the central region of the spherulites [123, 124]. There are a number of factors that have effect on the charge storage ability and dipole orientation of polymeric electrets such as chemical impurities, inside voids structure, surface roughness condition, macro-molecular arrangements, particles added in the polymers, chemical composition, discharge conditions (needle and grid voltage, charging time and temperature etc.) and metal electrode spurred on the surface of the electrets etc..

In Ref.[125], the researchers pointed out that the magnitude of the surface voltage on the polymer films due to the corona discharge, associated with charge retain ability, was a function of the strength of the applied voltage to the corona needle, the time relative to the voltage application, and the temperature. According to [126], the results also show that charging polymers at a relative high temperature dramatically increases their charge stability. As the charging temperature is increased, one tends to fill deeper traps because of changes in relative capture and escape probabilities. Besides, the influence of high humidity and porosity on the surface-charge decay and stability was investigated in [127, 128]. The effect of the samples' roughness on the charge stability has been mentioned in [5], but experimental results were not presented their piece of work. In order to explore the application potential of such polymers, this paper gives, for the first time, the numerical results under different charge conditions.

Therefore, the charging behaviour has been found to be associated with some details such as: the sample preparation, surface roughness condition as well as residual stresses [129]. According to [130, 131], the charge forced into the bulk is more permanent than surface charge since it is not removed from the polymer by grounding, and they have also demonstrated that there is a named “memory” effect with the poling current and to the accumulation of trapped charge in the polymer matrix which are released only after the polymer is heated to high above its temperature of glass transition (Tg).

Charge storage mechanism of negative corona-charged PP has been widely studied [14-17]. By using the Thermal Stimulated Depolarization Current (TSDC) method, de-trapped charges and a relaxation of the polarization have been observed by Ono *et al.* [5]. Furthermore, the Laser Induced Pressure Pulse (LIPP) technique has also been used in former investigations for displaying the charge distribution in their research. By integration of the TSDC current, the quantity of charges induced by the high corona voltage treatment can be calculated on such commercial cellular PP.

1.4 Conclusion

The literatures review, development history and application in many fields have been reported on the magnetoelectric and electrostrictive effects.

Firstly, magnetoelectric materials are an important class of multiferroic materials which have received considerable attention in the past decade. The composite laminates which process large ME coefficient, have tremendous application potential on the field of ME sensors, transducers, switches and phase inverters etc..

Secondly, as an electroactive polymer, the cellular polypropylene electret can store a number of charges after corona poling. Efforts on investigating its charge storage mechanism have been made by many scholars.

However, few studies have been done to investigate how the electrostrictive performance of charged cellular PP electret can be influenced by the corona discharge treatment.

Chapter 2. Sample preparation of laminate composites and their magnetoelectric experiments

2.1 Introduction

We report on the magnetoelectric experiment on the bi- and tri-layered composites consisting of polyvinylidene fluoride (PVDF) and polyurethane (PU) filled with magnetically hard magnetite Fe_3O_4 or Terfernol-D (Te-D) magnetostrictive material. PU composite film fabrication procedure has been described in this section, and the magnetoelectric experiments based on PU composite have been presented. Then, a new approach that can achieve the ME coupling using only electroded piezoelectric compounds subjected to ac magnetic flux has been attempted. The magnetoelectric experiment set-up and condition such as magnitude and direction of applied magnetic field on piezoelectric unimorph bender, PVDF film and piezoelectric ceramic disc have been introduced in this chapter. Based on this early prototype, we developed a magnetoelectric sensor which can realize ac/dc magnetic field sensing without applying ac current source on the sample directly.

2.2 Multi-layer polymer composites

The origin of the ME effect is often associated with an interaction mechanism between various compounds of ME matter. In the present case, magnetostrictive and piezoelectric phases were combined to obtain a dramatic enhancement of the ME effects, relative to single phase materials. High magnetoelastic interactions are found for very few magnetostrictive materials. Accordingly, two kinds of magnetostrictive fillers were selected: $Tb_{0.3}Dy_{0.7}Fe_{1.9-1.95}$, commercially known as Terfenol-D (with a highest magnetostriction at room-temperature) at an optimum concentration in PU of 50 wt%, which yields a large ME response, and the 2 wt% Fe_3O_4 powder used as filler in PU for the same reason [132]. In magnetostrictive materials, the strain induced by the applied magnetic field is proportional to the square of the magnetic field. An effective linear operational range can be achieved by applying a (dc) magnetic bias across the structure.

The samples tested in this part were tri- and bi-layered polymer composites consisting of polyvinylidene fluoride (PVDF) and polyurethane (PU) filled with amorphous magnetic Fe_3O_4 micropowder (Aldrich, average particle size: 200 μm) or Terfenol-D (TeD) particles of $<$300 μm in size (Etrema Products, Inc., Ames, IA). For a of magnetic field frequency 1 kHz, the micro-sized magnetic powder used to make the PU composites gives a better response than nano-sized magnetic powder. The compositions of the samples were the following: (PU+2 wt% Fe_3O_4 /PVDF/ PU+2 wt% Fe_3O_4), (PU+2 wt% Fe_3O_4 /PVDF), (PU+50 wt% TeD /PVDF/ PU+50 wt% TeD) and (PU+50 wt% TeD /PVDF).

2.2.1 Film fabrication procedure

Fabrication procedure is as shown in Fig. 2. 1, the selected polyurethane (PU) was the polyether-type thermoplastic TPU5888 from Noveon Company.

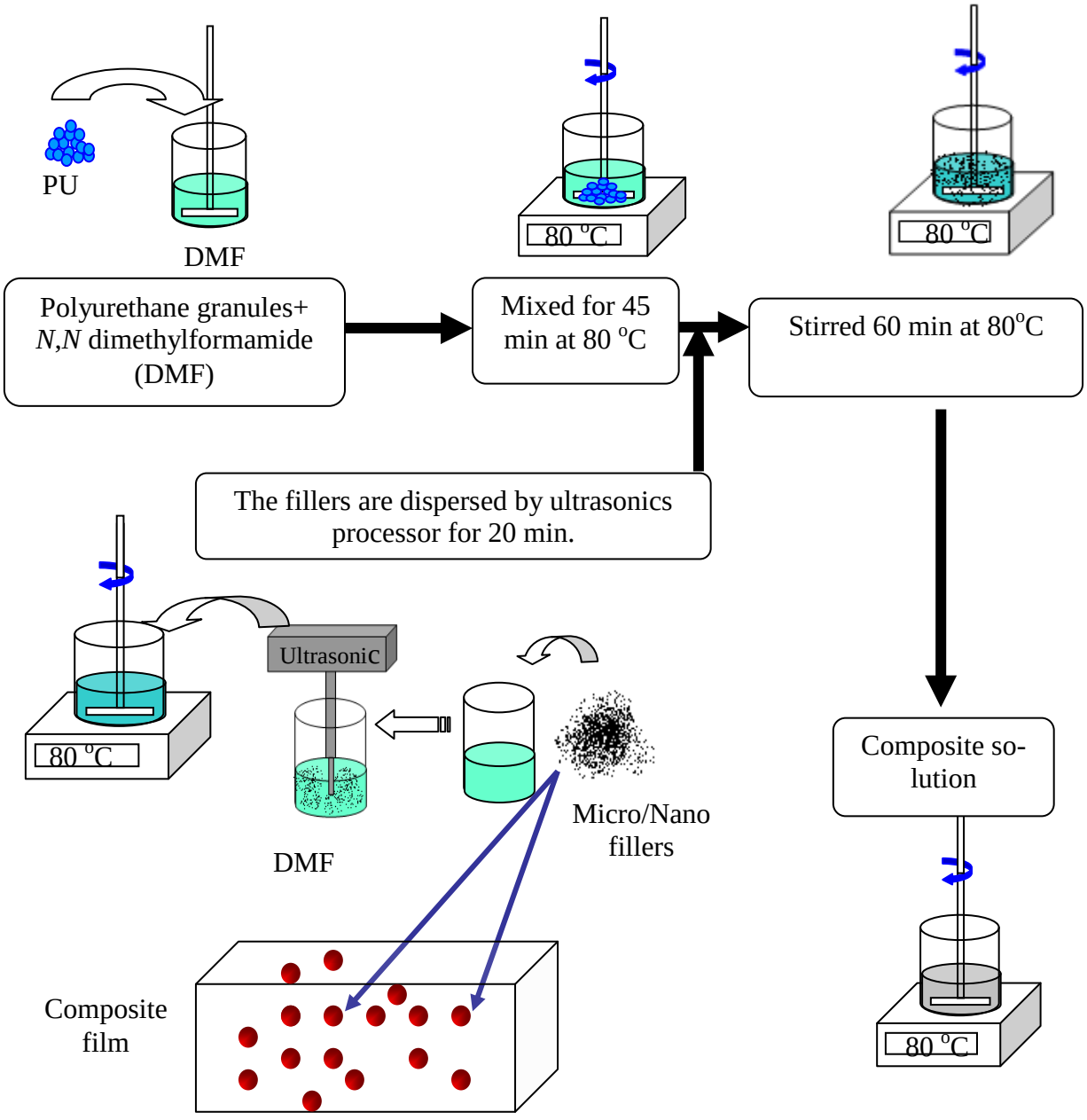

Fig. 2. 1 The fabrication procedure of composite solution

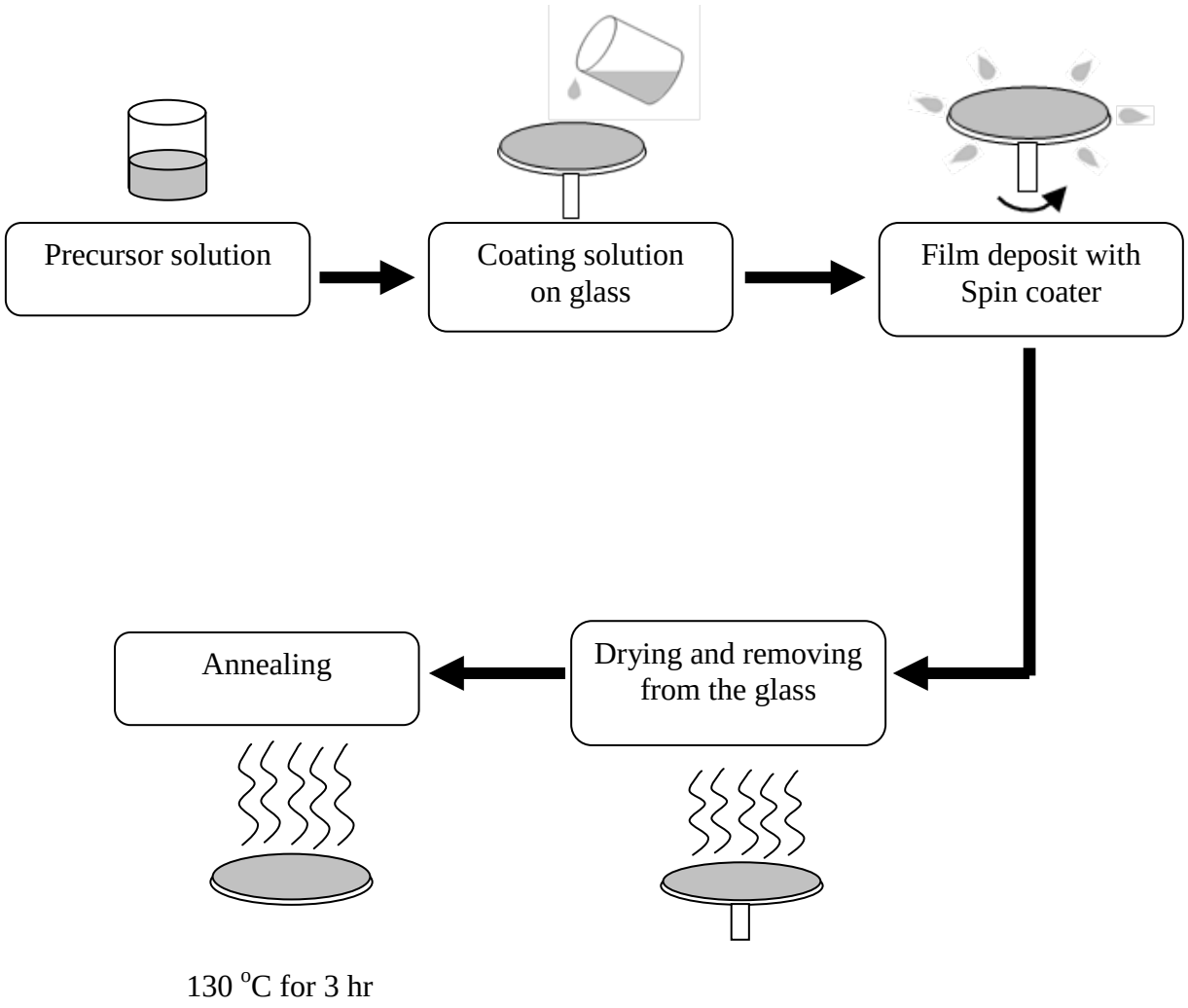

Fig. 2. 2 The fabrication procedure from composite solution to PU composite films

The polymer films were prepared through solution casting. PU granules were first pre-dissolved in N,N-dimethylformamide (DMF) at ~ 80°C for one hour. Then, the fabrication procedure of composite films is shown in Fig. 2. 2. During the fabrication procedure, x wt.% of the magnetic particles (Fe_3O_4 or TeD) were added to the mechanically stirred solution. Stirring was performed at a constant temperature, for between 1.5 hours and 2.5 hours. The mixed solution was subsequently spin coated onto a glass plate, degassed to eliminate voids and dried at 70°C for 6 hours. After this, composite films

were cut into rectangular pieces (~200 microns thick, 40 mm long and 10 mm wide).

2.2.2 Tri- and bi-layered polymer composites fabrication

The PVDF films supplied by PIEZOTECH S.A. Saint-Louis, France, were 25 μm thick, 10 mm wide, 45 mm long and uni-axially stretched along the length direction. Cr/Al Electrodes were sputtered on both surfaces and film polarization direction was perpendicularly to the sample's plane. Finally, the piezoelectric (PVDF sample) and magnetostrictive layers were glued together using an epoxy resin. The multilayer sample was then pressed tightly during several hours, to minimize the effect the glue layer thickness.

2.3 Experiments on piezoelectric unimorph bender and PVDF film

2.3.1 Early ME experiments on piezoelectric unimorph bender and PVDF

The previous studies based on coupling between Lorentz forces and piezoelectricity, are presented in [64-66, 83] and summarized in §1.2.5. The common characteristic of designed ME experiments is the direct ac current appliance on the samples to generate Lorentz Forces. In the present study, an attempt was made to obtain ME coupling in PZT/metal layered composites by designing specific ME set-up which avoids applied ac current directly on the samples. The aluminium plat bonded with silver electroded PZT ceramic, can be made into a unimorph.

The PZT ceramic used in our experiment was a soft-type PZT-P188 (Saint-Gobain Quartz Company) plate of 450 microns thick, 30mm length and 10 mm width. Before poling in the thickness direction, it was electroded on both sides with silver paste (supplied by Degussa) fired at 600°C. Then, after poling, the PZT and an alumina layer of 200 microns thick were epoxied together to create a unimorph bender. The cantilever piezoelectric bender was then clamped at one side and horizontally suspended. In order to predict the ME coefficients in the region around the sample's resonance frequency (4.9 kHz), it was simultaneously subjected to an ac magnetic field h_{ac} (magnitude: H_{ac} = 1 Oe) provided by a Helmholtz coil and a dc bias field (H_{dc} up to 2.2 kOe) generated by permanent magnets [21, 132]. Similarly, the PVDF soft film were 25 μm thick, 10 mm wide, 45 mm long, clamped in the test bench and subjected the same conditions of magnetic field.

In order to observe the influence of magnitude and direction of applied magnetic field, we work out four possible experimental configurations associated with different condition of h_{ac} and H_{dc}. Then, the magnetoelectric response was obtained by measuring the magnetic-field-induced piezoelectric current i_{ME} at room temperature with a current amplifier (Keithley 428, USA) combined with a lock-in amplifier (SR 830 Stanford Research Systems) tuned to the ac field frequency *f*.

2.3.2 Magnetoelectric sensor based on piezoelectric unimorph bender

Based on the former research of magnetoelectric effect of the piezoelectric unimorph bender, we developed a prototype of a ME sensor by using an electric conducting wire with ac current to replace the ac magnetic coils used in the initial setup and the cantilevered piezoelectric unimorph bender. Fig. 2. 3 illustrates the diagram of the designed ac/dc ME sensor in the Cartesian coordinate system. The ac rotating magnetic fields around ac conducting

wire generated magnetic flux in the silver electrodes crossing the thickness direction of unimorph bender, which was the cause of eddy current within the silver electrode. Consequently, there were Lorentz forces in such single phase piezoelectric bender which induced apparent magnetoelectric response without adding any magnetic phase in such new developed sensor.

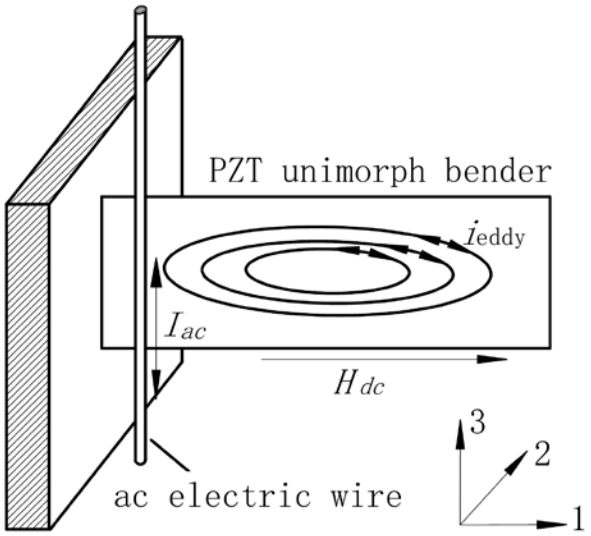

Fig. 2. 3 Schematic diagram of the rectangular shape piezoelectric unimorph bender subjected to ac and dc magnetic fields.

For the magnetoelectric measurement, the photograph of the experimental test bench is shown in Fig. 2. 4. Applied ac current was through a conducting wire which was one part of a closed circuit composed by waveform generator (Agilent 33220A), voltage amplifier (4505 NF Electronics) and a resistance. The wire was put vertically close to PZT unimorph bender with the distance of 4mm, to generate the ac rotating magnetic field h_{ac}, at its bending-mode resonance frequency. Thus, the magnitude of ac magnetic induction B_{ac} is $\mu_0 H_{ac}$ with μ_0 the permeability of free space. The unimorph bender and the conducting wire were inserted between the poles of the electromagnet horizontally and vertically, respectively (Fig. 2. 3 and Fig. 2. 5). This allowed the dc magnetic field H_{dc} appliance along the sample's length (direction "2"). Experimentally, the magnitude of the dc magnetic field on

the proposed ME sensor was measured in the air-gap between the poles of the electromagnet, using a tesla-meter (F.W. Bell 5080) [133-135].

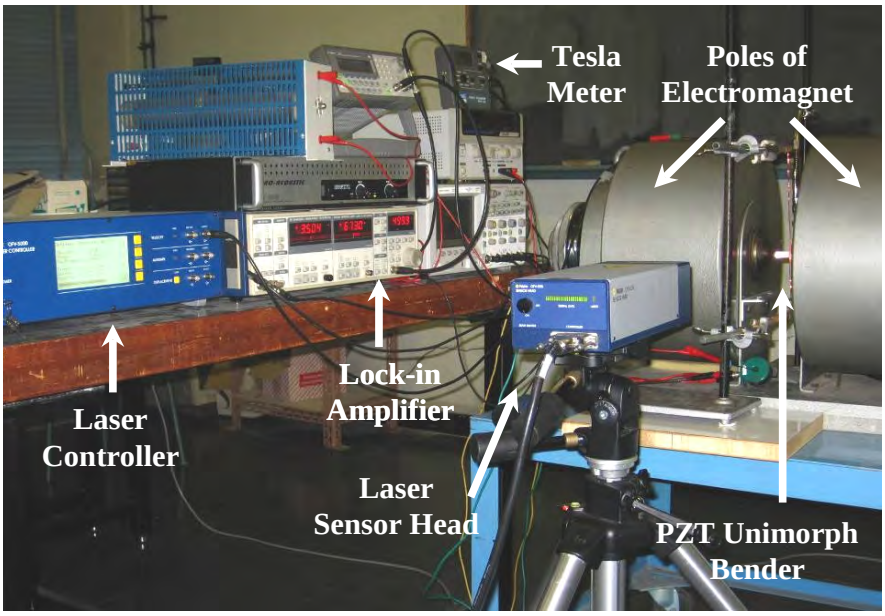

Fig. 2. 4 Photograph of the ME experimental test bench

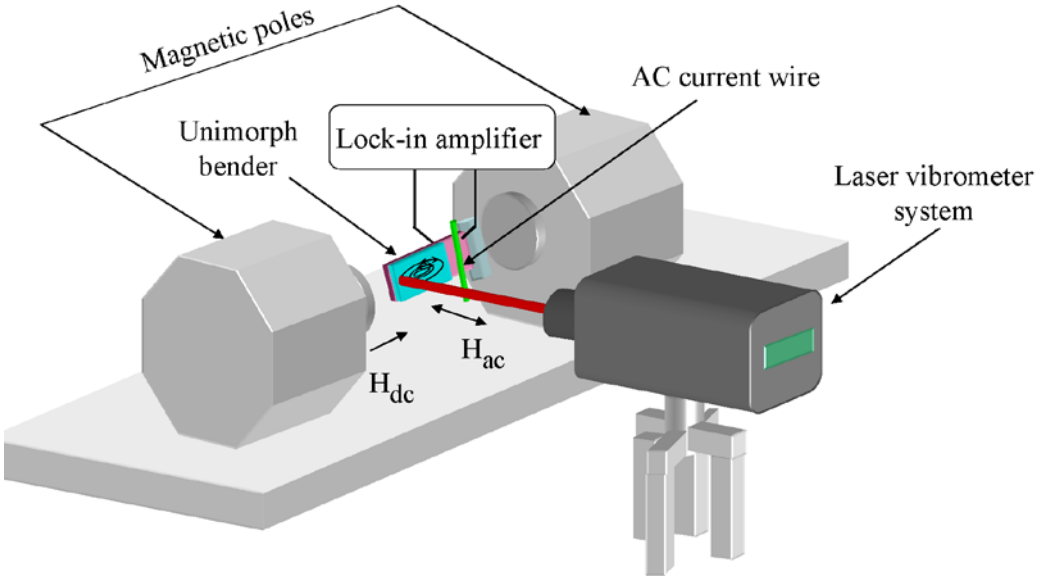

Fig. 2. 5 Schematic drawing of the experimental system of ME sensor and its vibration velocity measurement

As shown in Fig. 2. 5 and Fig. 2. 6, The ac current-induced magnetic field h_{ac} could be estimated close to the sample's plane, which roughly corresponds to an ac field applied in the direction "2". The induced magnetoelectric response was obtained by measuring the magnetic field-induced piezoelectric voltage at room temperature with a lock-in amplifier connected with unimorph bender and tuned to the ac field frequency *f*. The PZT electrodes were connected to the lock-in-amplifier with two thin wires soldered close to its clamped edge. Meanwhile, in order to demonstrate that the studied ME effect was a coupled magnetic and electrical response via mechanical interaction between alumina plate and piezoelectric beam, a velocity measurement was also performed on the edge of the PZT unimorph bender using a laser vibrometer system which was composed by a sensor head (OFV-505 Polytec. France) and a laser controller (OFV-5000 Polytec. France).

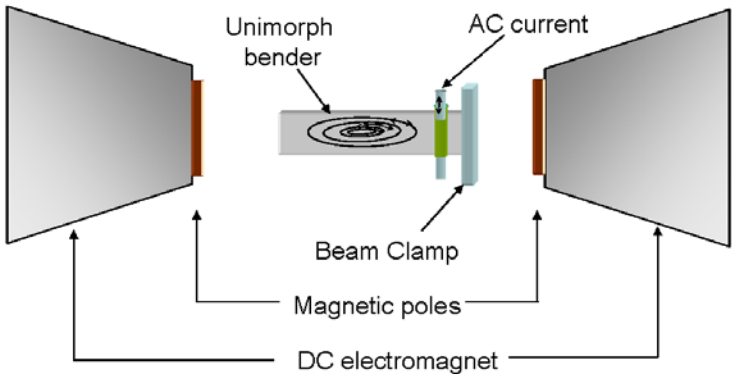

Fig. 2. 6 Detailed schematic drawing PZT unimorph sensor between two magnetic poles

2.3.3 ME experiments on PVDF film

Then, with the aim to observe the same effect as PZT unimorph bender, we have designed a similar ME experiment set-up for the single piezoelectric polymer PVDF supplied by PIEZOTECH S.A. Saint-Louis, France, with the 25μm thick, 10mm wide and 40mm long. As shown in Fig. 2. 7, the

electroded PVDF film was vertically suspended by clamping the upper end. The ME current was obtained by a current amplifier. The magnet field was provided by the same equipments as PZT unimorph bender with the magnitude: H_{dc}: -2k Oe～2k Oe, H_{ac}=1Oe, f_r=60Hz; and their directions shown as in figure. Horizontal deflection (δ) of the free end of the film was measured by the laser vibrometer system.

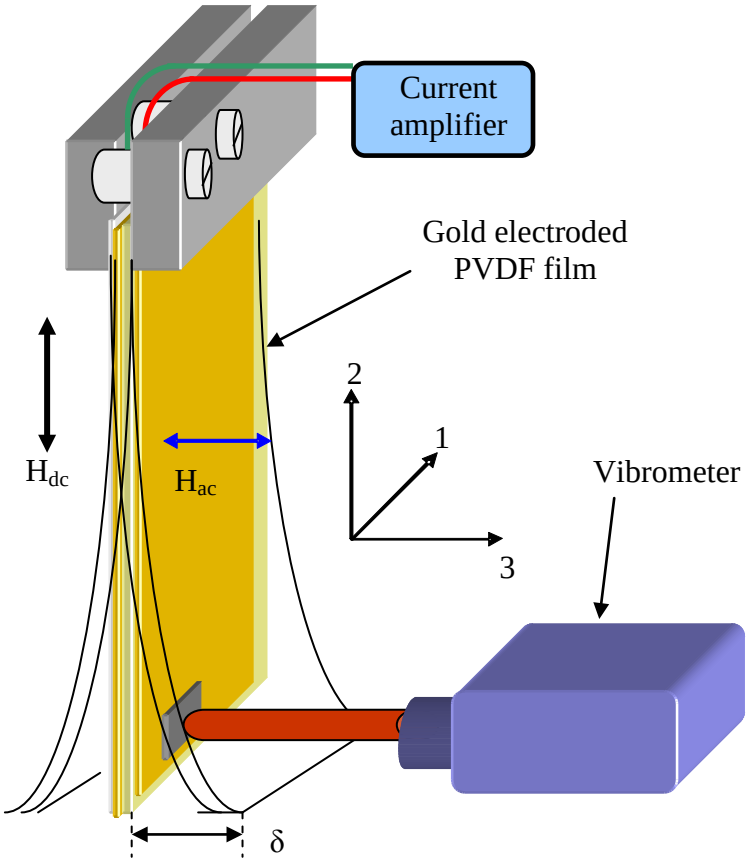

Fig. 2. 7 Schematic diagram of the rectangular shape PVDF film subjected to ac and dc magnetic fields

2.4 Magnetoelectric sensor based on a single piezoelectric ceramic disc

Based on former ME measurement, we can observe the apparent magnetoelectric performance of the unimorph bender and vibration caused by Lorenz force acting on the sample. In order to establish the mathematic modelling and work out the relation between the ME output voltage and Lorenz force induced by eddy current. The studied piezoelectric ceramic sample was changed as a PZT ceramic disc which was elaborated in our Laboratory. The ceramic disc was 500 microns thick with a radius R = 27.5 mm. This high aspect ratio has been deliberately chosen in order to amplify the radial vibration mode since the ceramic has been electrically poled in the thickness direction after silver electrodes deposition on both sides (silver paste supplied by Degussa fired at 600°C).

For magnetoelectric measurement, a dynamic magnetoelectric set up in which both dc and ac magnetic fields can be varied is composed of an electromagnet providing the dc magnetic field appliance (H_{dc}) and two Helmolhtz coils inserted on the poles of the electromagnet to generate the ac magnetic field h_{ac}, (as former $h_{ac}=H_{ac}e^{j\omega t}$ with $j^2=-1$, ω is the angular frequency and the magnitude: H_{ac} = 0.1 Oe i.e. the magnitude of ac magnetic induction is $B_{ac} =\mu_0 H_{ac}=10^{-5}$ T). Thus, in this configuration, both ac and dc fields are parallel each other. The PZT ceramic was inserted vertically between the poles of the electromagnet and its plane was perpendicular to the ac and dc magnetic fields, as shown in Fig. 2. 8. The magnetoelectric response was obtained by measuring the magnetic field-induced piezoelectric current at room temperature with a current amplifier (Stanford) combined with a lock-in amplifier tuned to the ac field frequency $f=\omega/2\pi$. In the following, f_r = 36 kHz which is the electromechanical resonance (EMR) frequency of the tested disc in the radial mode). The two silver electrodes are connected

to the current amplifier with two thin wires soldered close to the edge of the disc, which is suspended in the airgap of the electromagnet. At the same time, in order to demonstrate that the studied ME effect is a coupled magnetic and electrical phenomenon via mechanical interaction, the radial velocity measurements were also performed on the edge of the ceramic using a laser vibrometer (Polytec. France).

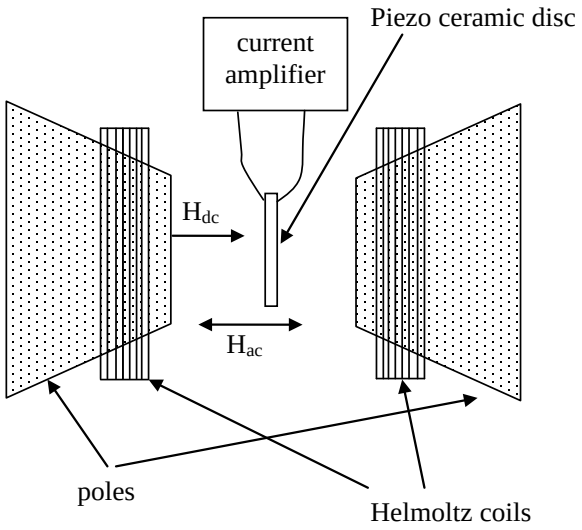

Fig. 2. 8 Schematic diagram of the piezo-ceramic disc in ME measuring system

2.5 Conclusion

In this chapter, we have introduced the magnetoelectric experiments on the composites laminates including PVDF layer and PU laminate filled with magnetically hard magnetite fillers such as Fe_3O_4 or Te-D. Film fabrication procedure including composite solution preparation, film deposition, stir, anneal and conditions of ME experiments including direction and magnitude of applied magnetic field, ac magnetic field frequency have been stated in detail. In addition, we have presented another ME experimental set-up based on Lorentz force induced ME effect made on PZT unimorph bender, piezoelec-

tric PVDF film and PZT ceramic disc. Different conditions of ME experiments such as magnitude and direction of applied magnetic field have been designed out. We try to develop a ME sensor without ac current applied directly on the sample, which is different with previous ME experiments based on Lorentz force and can be used as ac and dc magnetic field sensors and actuators under certain condition.

Chapter 3. Experiments for analysing the charge storage mechanisms and the electrostriction of corona charged cellular PP

3.1 Introduction

In this chapter, we present charged cellular polypropylene with corona poling set-up. A series of experiment including Surface Potential Decay measurement (SPD), Thermal Stimulated Depolarization Current experiment (TSDC), and Differential Scanning Calorimetry experiment (DSC) has been described schematically and literally. Finally, the experiment of electrostrictive performance testing has been introduced, in order to examine electrostriction of the charged films under applied electric filed.

3.2 Experimental setup of corona discharge method

The chosen samples, denoted PQ50 whose thickness and density are 50μm and 600kg/m^3 respectively, were supplied by Sodinor Company

(France). Cellular polypropylene films (4×4cm^2) were charged using a corona triode, which is schematically presented in Fig. 3. 1.

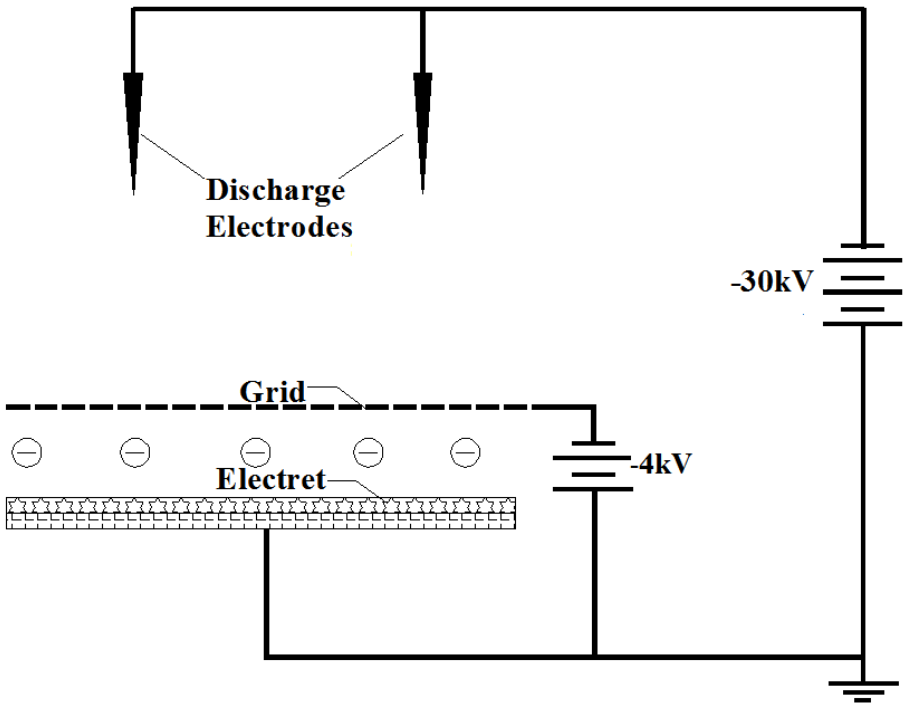

Fig. 3. 1 The corona discharge setup.

The charged films were coated with a gold electrode on one surface (20 nm thick) under high vacuum by a High Resolution Sputter Coater. Then, with a corona triode, the electrical charges were injected for a duration of 10 min through the non-metalized surface of the samples which were placed under a stainless grid (size of mesh screen is 150μm) in order to maintain a uniform surface potential. With the aim of investigating the charge storage performance and its influence on the electrostrictive performance of fully charged cellular PP, the corona voltages were kept at -30 kV and a grid voltage of -4kV was employed.

3.3 Surface potential measurement

Surface potential decay (SPD) measurement have been extensively employed for investigation of electrical characterization of electrets surfaces after corona charging, due to their advantages such as simple and easy to implement, reliability and low cost [136-139]. It is one of the criteria to estimate charge-retaining ability of the polymer.

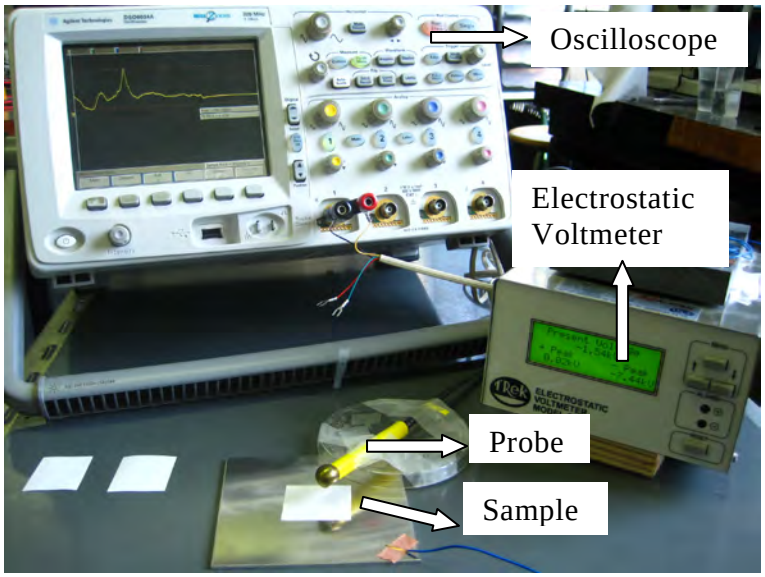

(a)

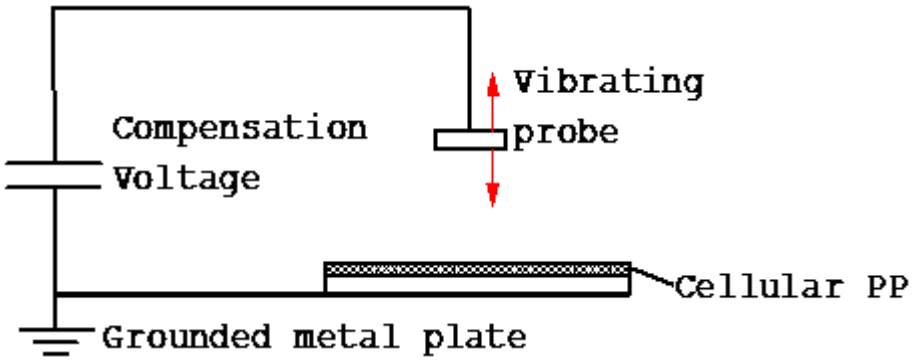

(b)

Fig. 3. 2 (a) photograph of the surface potential test setup (b) Schematic representation of the surface potential measurement setup [140]

Immediately following the corona treatment, in order to observe its charge-decay tendency, the surface potentials of non-charged, and charged cellular PP were measured by an Electrostatic Voltmeter (Model 541 TREK). An electrostatic charge monitoring probe is placed close 1cm to the surface to measure its surface potential through non-contact method. At the same time, the surface potential decay of the charged samples could be recorded with the help of an oscilloscope (DSO6034A Agilent). The surface potential measuring setup used in this work is shown in Fig. 3. 2, in which the probe acts as a vibrating capacitor, formed between the probe and the sample.

3.4 Relative permittivity measurement

The charged films were coated with a gold electrode on two surfaces (20 nm thick) under high vacuum by a High Resolution Sputter Coater (208 HR, Cressington), and their relative permittivity at 0.1Hz was measured by using a permittivity measurement system (1255A Frequency Response Analyzer combined with a 1296 Dielectric Interface, Solartron, United Kingdom).

3.5 Measurement of Young's modulus

Young's modulus, Y, is an indicator of the stiffness of a film. It is determined from the value for the resulting stress applied to the material divided by the value for the applied strain in the same direction. An experiment for measuring the Young's modulus of the film with Ultra-Precision Linear Motor Stage, 50 mm Travel (Newsport XMS 50 France), Motion Controller/Driver (Newsport XPS France), oscilloscope and computer which are shown in Fig. 3. 3. The measured value of Young's modulus of cellular PP is 1GPa.

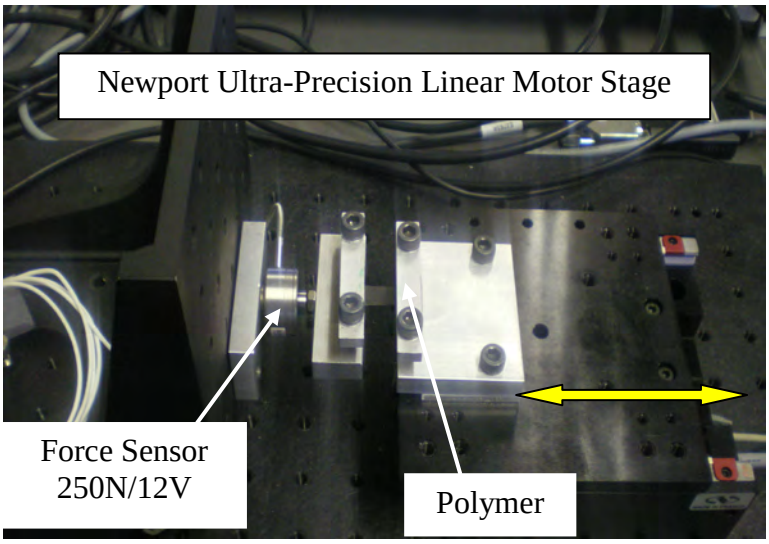

(a)

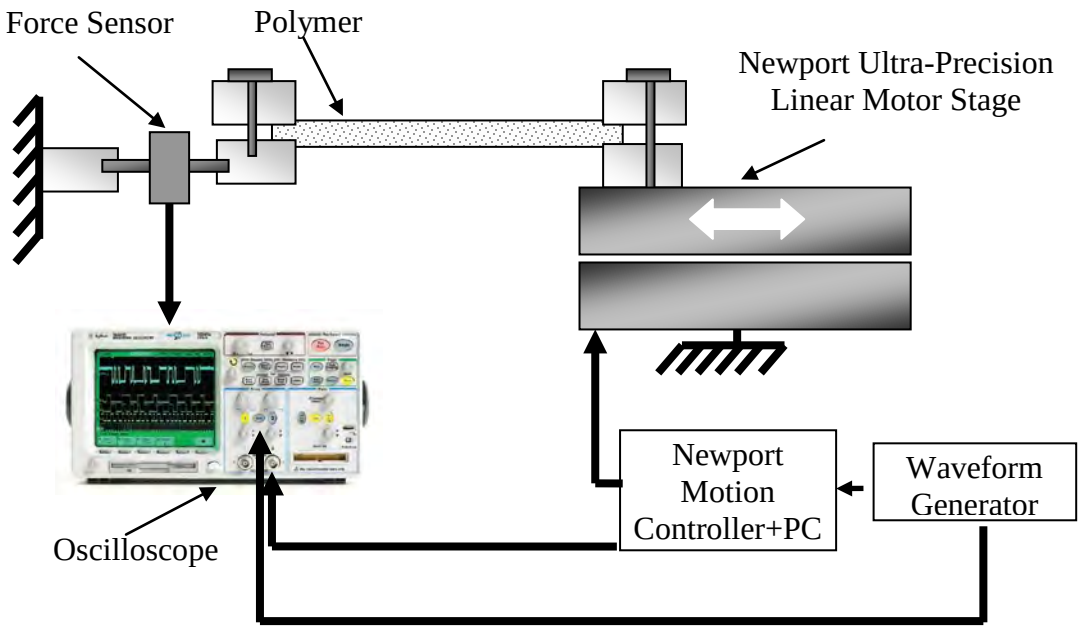

(b)

Fig. 3. 3 (a) Photograph Test bench of Young's modulus measurement; (b)Schematic of measuring system of Young's modulus

3.6 TSDC measurement

Thermal Stimulated Depolarization Current (TSDC) measurements were performed in order to investigate the exact quantity of charge stored on the surface and within the cellular PP. The stimulated current's spectrum versus the temperature can be used to obtain the important information of charges storing and de-trapping situation, which can also be a reference to understand the long-term storage mechanism in electrets. For these TSC experiments, a charged sample was placed in a test chamber with temperature control (Chamber VT7004, Vötsch Industrietechnik, Germany).

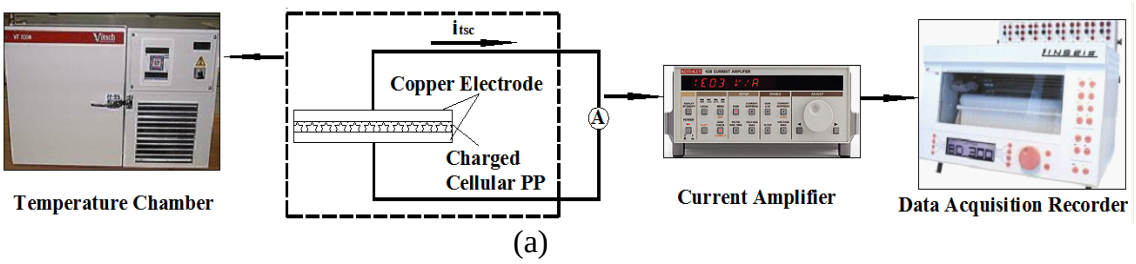

(a)

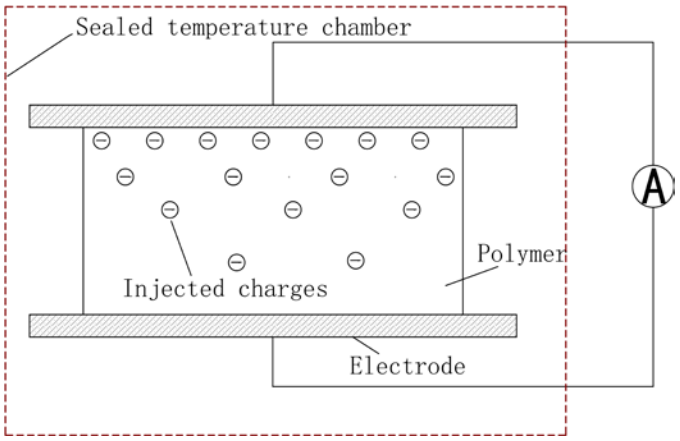

(b)

Fig. 3. 4 (a) The experimental process of the TSC technique; (b) Schematic of the TSDC technique

As shown in Fig. 3. 4, the two -surfaces-electroded sample was sandwiched between two copper plates, short-circuited and maintained at

23°C for one hour in order to release the surface charge, after which the temperature was linearly increased from 23°C to 140°C at a rate of 5°C/min. The TSDC current signal was measured with the help of a current amplifier. In the meantime, the over-all thermal-current spectrum of the tested sample was registered by a data acquisition recorder (BD300 Series Kipp & Zonen Vötsch Industrietechnik, Germany).

The total charge Q_{corona} within the cellular PP was calculated by integrating the TSC current, i_{tsc}, according to:

$$Q_{corona} = \int_0^t i_{tsc} dt \tag{3.1}$$

3.7 Differential scanning calorimetry measurement

3.7.1 Principle of data acquisition in the differential scanning calorimetry

Differential scanning calorimetry (DSC) is a useful tool for measuring heat capacity variations induced by phase transitions: i.e. melting, the glass transition or crystallization. It is a technique for measuring the energy necessary to establish a nearly zero temperature difference between a substance and an inert reference material, as the two specimens are subjected to identical temperature regimes in an environment heated or cooled at a controlled rate [141].

As shown in Fig. 3. 5, during the DSC experiment, the change of heat capacity is detected. Then, the equilibrium between sample and reference is disturbed. When the sample temperature is higher (exothermic event)

or lower (endothermic event) than the reference, this temperature difference is detected by a temperature controlling system and the differential heat flow between sample and reference can be calculated [142, 143]. In our studies we use the DSC to deduce the crystallinity of the film, for instance [144].

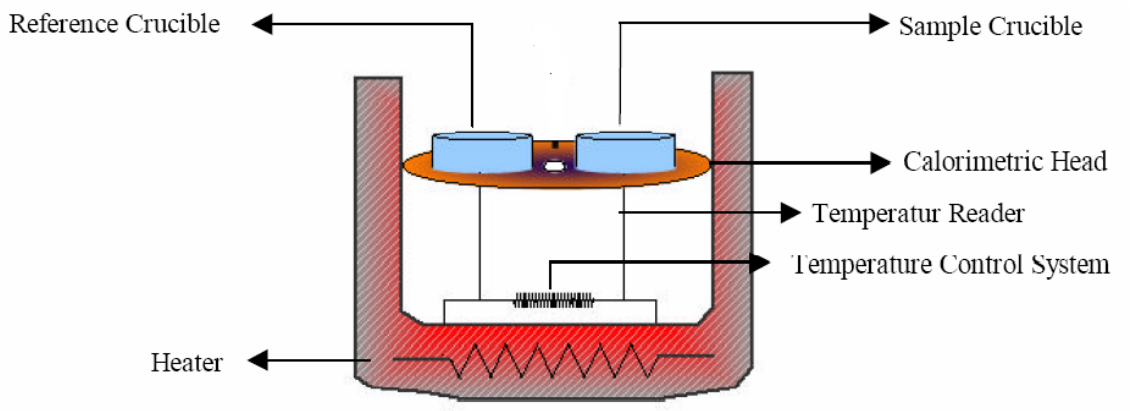

Fig. 3. 5 Scheme of DSC instrument [143]

3.7.2 Procedure of DSC test

The samples were placed in a closed aluminium crucible in the DSC equipment (DSC 131 evo Setaram France), where they were heated from 23°C to 200°C and cooled down to 23°C at a controlled rate of 10°C/min. The heat flow was recorded synchronously by a computer connected to the DSC equipment. In heat flux DSC, the sample and reference are connected by a low resistance heat flow path (a metal disc) symmetrically. The assembly is enclosed in a single furnace. Enthalpy or heat capacity changes in the sample cause a difference in its temperature relative to the reference [143].

3.7.3 Electrostrictive coefficient measurement

As shown in Fig. 3. 6, strain versus electric field was measured with the help of a non-contact capacitive measurement sensor (FOGALE MC 940) on disc-shaped samples with a precision on the order of 10 nm. Because PP were elastically much softer than ceramics and the samples were made into very thin films, great care must be taken in the strain measurements of PP to ensure the accuracy of the data when applied a electric field on it. For such soft film like materials flexure motion and mechanical clamping of a sample are two major causes of errors in the strain measurements.

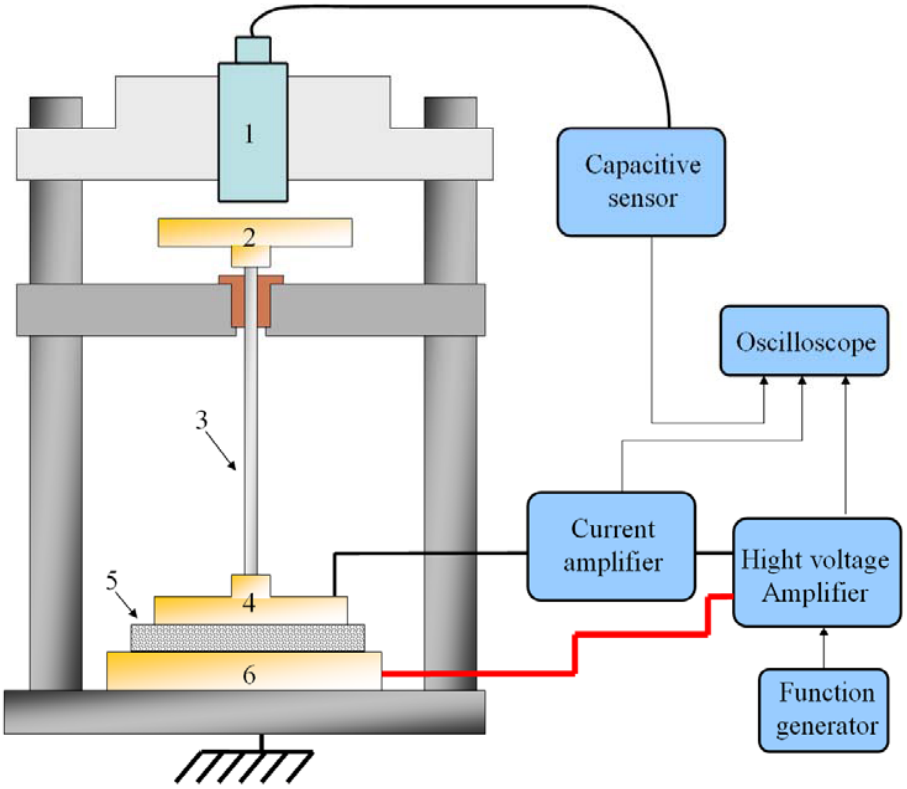

Pieces number	*Definition*
1	Capacitive sensor
2	Moving disc
3	Rod
4	Moving electrode
5	Polymer
6	Clamped electrode

Fig. 3. 6 The electrostrictive coefficient measurement setup

The film samples were placed on horizontal stainless steel discs (20 mm in diameter) in order to avoid measuring a parasitic flexure motion, and a second brass disc positioned on the top of the film rendered it possible to apply a bipolar electric field. The total weight of piece 2, 3 and 4 was 5g (equivalent to 156Pa) which was a suitable small stress, in order to avoid clamping of the sample. The sample was subjected to electric field with the help of a waveform generator for which the output was amplified through a high-voltage amplifier (TREK 609D-6). The frequency and the magnitude of the applied ac electric field were 0.1 Hz and 12.5 V/μm, respectively. During these strain versus electric field measurements, the electric polarization was calculated by integration of the measured current through the sample by means of a current amplifier.

3.8 Conclusion

Since the parameters in corona discharge set-up could influence the result of charge injection, the mesh size of inserted metal grid, applied high-voltage amplitude on the discharge electrode, sample dimension and distance between charged sample and electrode in corona discharge configurations, have been introduced. Then, after corona poling, in order to investigate the surface charge retaining ability, distribution situation and depolarization principle of retained charge, as well as thermal trace characterization after corona discharge treatment in cellular PP, the experiments such as Surface Potential Decay Test, Thermal Stimulated Depolarization Current (TSDC) experiment, and Differential Scanning Calorimetry (DSC) experiment have been designed. Then, with the aim to find the influence of stored charges on the electrostrictive performance of charged films, a set-up that can measure their deformation under an external applied electric field has been introduced.

It contained a non-contact capacitive sensor, current and voltage amplifier, oscilloscope, clamped electrode and supporting rod.

Chapter 4. Magnetoelectric results of laminate composites

4.1 Introduction

In recent years, it has been found that laminated composites made of magnetostrictive and piezoelectric materials possess superior ME performance owing to their giant product property effect between the magnetostrictive and piezoelectric effects. But very few studies have been devoted to the ME effect in laminate composites including magnetostrictive polymeric layer. For this reason, in this chapter, we have studied the ME effect based on magneto-elastic-electric effect in bi- and tri-layered composites consisting of thermoplastic polyurethane (PU) filled with magnetically hard magnetite Fe_3O_4 or Terfenol-D (TeD) magnetostrictive alloy. Moreover, a model, based on a driven damped oscillation system, has been developed to evaluate the influence of the first and second-order ME coefficients on the dc magnetic field-induced phase switching phenomenon between dynamic ME current and the applied ac magnetic field.

On the other hand, normal magnetic sensor based on Lorentz force effect can show an excellent linear response to magnetic field [64]. Based on the previous researches on the magnetoelectric effect from the direct coupling of the Lorentz force and piezoelectric effect, we have designed a series of ME experiment using PZT unimorph bender, PVDF film and PZT ceramic

disc and expected to obtain an excellent ME output by combining the Lorentz force effect with the piezoelectric effect without applying ac current directly on the samples as the previous ME experiments. Finally, the modelling of Lorentz forces induced ME effect in piezoelectric materials has been established.

4.2 Magnetoelectric effect of laminate polymer composites

4.2.1 ME coupling in PU composite/PVDF laminates

The polyurethane matrix filled with magnetically hard magnetite Fe_3O_4 or TeD is chosen in this experiment since it exhibits important magnetostrictive effect. While, the PVDF film is the soft polymer with piezoelectric effect. Thus, the ME coupling between different layers should be produced through the interaction between magnetostriction and piezoelectricity phenomena. The present study focuses to the experimental observation and the modelling of the ME effect at room temperature, in the bi- and tri-layered polymers. The experimental results and calculation details are presented in the following.

4.2.2 Experimental results and calculation details

The variation of the square of the output RMS value of the ME current generated by multilayered samples (PU+2 wt% Fe_3O_4 /PVDF, PU+50 wt% TeD /PVDF and PU+50 wt% TeD /PVDF/ PU+50 wt% TeD) dependence of the dc magnetic field is shown in Fig. 4. 1. The result shows that

these samples exhibit a quadratic-type variation of the squared current amplitude versus H_{dc}.

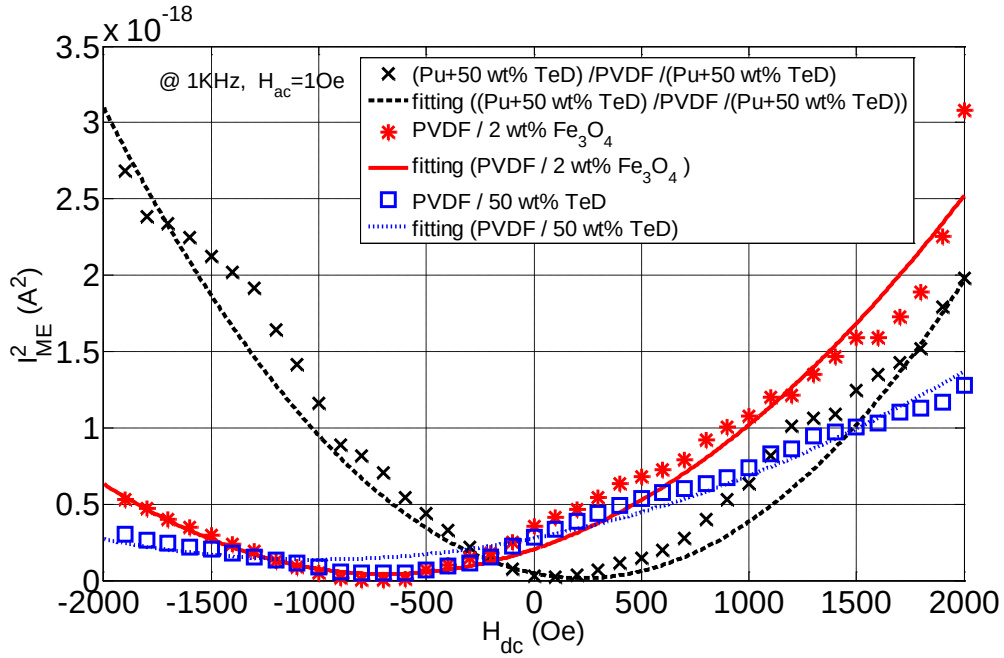

Fig. 4. 1 Experimental variation of the square of the ME current $I_{ME}^2(H_{dc})$ of the multilayer composites versus the (dc) magnetic field.
(Solid and dotted lines correspond to polynomial fits.)

As reported in [135], the observed output ME current in the multilayered samples can be attributed to three distinct contributions. Firstly, the stress induced by the eddy currents within the metal electrodes through the Lorentz force effect is transferred to the piezoelectric layer and generates electric charges [133, 135]. This effect will be presented in detail in the following. Secondly, the well known ME coupling based on a mechanical interaction between magnetostrictive and piezoelectric layers in laminate composites can be also defined as one of the contributions of the total ME current. Thirdly, the dielectric current generated by the parasitic voltage induced by the ac magnetic flux through the closed contour of the experimental loop, is an inductively coupled voltage between the electrodes of the samples which can be explained by the Lenz and Faraday's Laws [21, 133, 135]. In Refs.

[129, 131], the authors demonstrated that eddy current inducing magnetoelectric effect is predominant only at the electromechanical resonance frequency of the material. In this section, since the working frequency is 1 kHz, which is far away from the electromechanical resonance frequency of the studied ME composites, the influence of the eddy currents on the ME response can be neglected. Thus, the total output ME current includes the magnetostrictively induced current and the dielectric current which is directly proportional to the ac magnetic field and independent on the bias magnetic field.

Finally, the electric displacement of the samples may be written as

$$D = \frac{1}{2}\beta_p.H^2 + \alpha_{p.}H \tag{4.1}$$

where α_P is the linear polarization ME coefficient due to the "Lenz" voltage and β_p is the bilinear polarization ME coefficient due to the magnetostriction. Then, the corresponding output ME current is given by:

$$i_{ME} = A.\frac{\partial D}{\partial t} = j.A.\left[\beta_p.\left(H_{dc} + h_{ac}\right) + \alpha_p\right]\omega h_{ac} \tag{4.2}$$

where A is the total surface area of the electrodes. In Eq.(4.2), since only the experimental current at the frequency of the applied ac field is measured by the lock-in amplifier, the second-order term at the frequency *f* can be suppressed.

Consequently, the magnetoelectric current can be expressed as

$$i_{ME} = j.A.\alpha_{Ptotal}.\omega.h_{ac} \tag{4.3}$$

where $\alpha_{P\ \mathrm{total}}$ is the total ME coefficient:

$$\alpha_{Ptotal} = \alpha_p + \beta_p \left(H_{dc} + h_{ac} \right) \tag{4.4}$$

The total magnetoelectric coupling coefficient takes the form:

$$\alpha_{P\ \text{total}} = -j \frac{i_{ME}}{A.\omega h_{ac}} \tag{4.5}$$

So, the modulus of $\alpha_{P\ \text{total}}$ is:

$$\left| \alpha_{P\ \text{total}} \right| = \frac{I_{ME}}{A.\omega H_0} \tag{4.6}$$

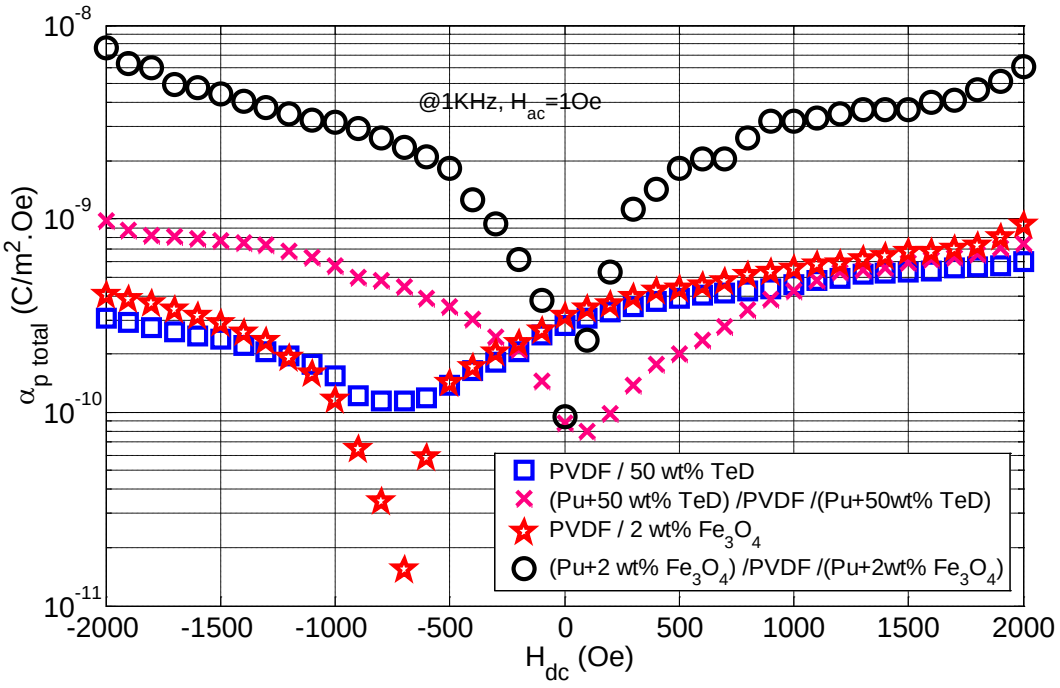

Fig. 4. 2 Variation of the total magnetoelectric coefficient of the multilayered composites versus the dc magnetic field.

The modulus values of the total ME coupling coefficients versus the bias magnetic field is shown in Fig. 4. 2. The highest ME coefficient

$|\alpha_{P\ \text{total}}| = 7.61\times10^{-9}$ C/m$^2\cdot$Oe is obtained at H_{dc}=-2000 Oe by the trilayered sample of (PU+2 wt% Fe_3O_4 /PVDF/ PU+2 wt% Fe_3O_4). The corresponding voltage coefficient is $\alpha_{E\ \text{total}}$= 75.33 V/m.Oe. This value is greater than that of the monolayer sample comprised of PU+ x% magnetic particles [132].

4.2.3 Modeling of the ME current of a multilayered sample

In order to interpret both the evolution of the total current and phase switching versus H_{dc}, and to distinguish the linear α_p and bilinear polarization ME coefficient β_p, the behavior of the ME effect in a multilayered sample is modeled. The schematic of the structure of the multi-layer composites has been shown in Fig. 4. 3, in which $\vec{F}$, $\vec{F}_1$ and $\vec{F}_2$ vectors indicate the mechanical coupling force between the composites layers.

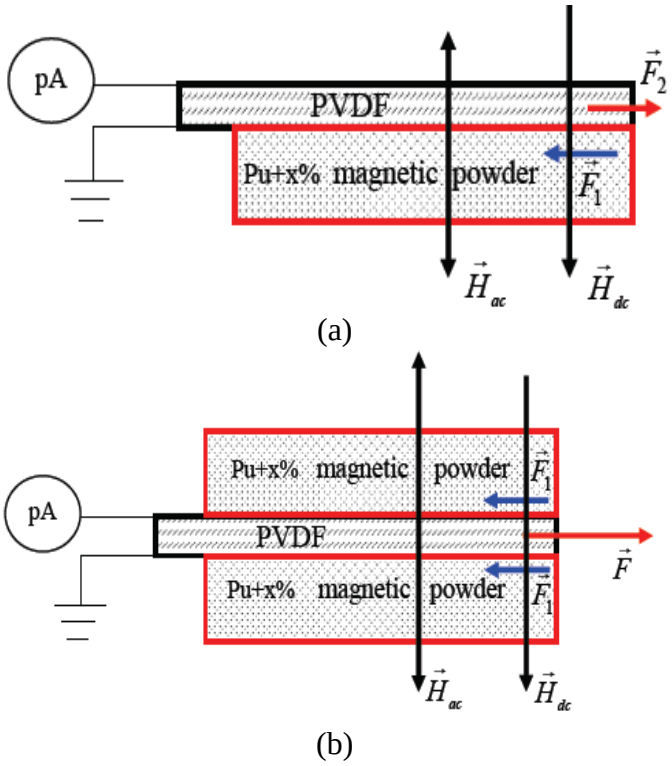

Fig. 4. 3 A schematic of the structure of the sandwiched composites, (a) bilayer sample. (b) trilayer sample;

The electric displacement vector of the piezoelectric PVDF layer may also be written as a function of the α_p coefficient and the transverse strain *S* triggered by the dynamic motion of the magnetostrictive layer (s):

$$D = e_{31}.S + \alpha_p.H \tag{4.7}$$

where e_{31} is the piezoelectric strain coefficient. Then, Eq.(4.8) is based on Eq.(4.7) and Eq.(4.1).

$$\beta_p H^2 = 2.\, e_{31} S \tag{4.8}$$

Furthermore, as shown in Fig. 4. 4, under the alternative magnetic field, the magnetic particles in the polymer matrix (PU+x wt% magnetic powder) vibrate and produce the force F_1 acting on this layer.

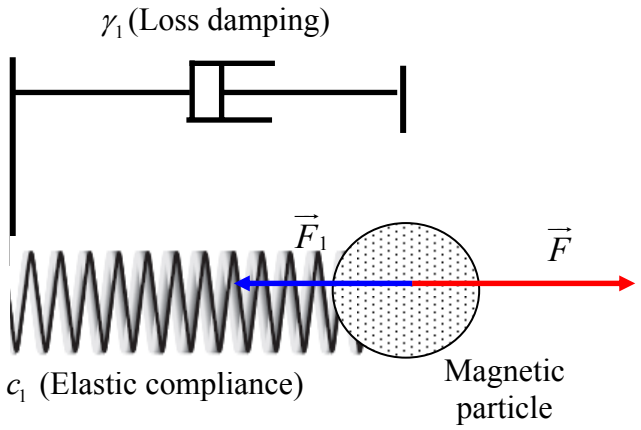

Fig. 4. 4 Schematic presentation of magnetic particulate in the magnetostrictive layer under magnetic field effect.

The induced force is a function of the square of the magnetic field, the velocity of the strain as well as the strain itself. It can thus be expressed as:

$$F_1 = A_1.T_1 = A_1.\left(c_1 S + \gamma_1 .\dot{S} + \delta_1 .H^2 \right) \tag{4.9}$$

Here, A_1 is the section surface. T_1, c_1 and γ_1 are the induced stress, the elastic compliance and the loss damping coefficient respectively. And δ_1 is the stress magnetostrictive coefficient relating the stress to the square of the magnetic field.

The piezoelectric layer generates a spring force F_2, where in this system the stress magnetostrictive coefficient δ_1, the loss coefficient and the elastic compliance are coupled between them.

$$F_2 = A_2.T_2 = A_2.\left(-c_2 S \right) \tag{4.10}$$

Here, A_2 is the section surface, T_2 the generated stress, and c_2 the elastic compliance coefficient of the piezoelectric layer.

The piezoelectric layer and the charged polymer were pasted together and if a perfect bonding interface is assumed, this implies that the two layers undergo the same strain *S*. In addition, because $F_1 = F_2$, we can deduce an equality:

$$A_1.\left(c_1 S + \gamma_1 .\dot{S} + \delta_1 .H^2 \right) = A_2.\left(-c_2 S \right) \tag{4.11}$$

Thus,

$$(A_1.c_1 + A_2.c_2)S + A_1.\gamma_1.\dot{S} = -A_1.\delta_1.H^2 \tag{4.12}$$

The applied sinusoidal magnetic field produces a sinusoidal deformation:

$$H_{ac} = H_0.e^{j\omega t} \tag{4.13}$$

$$S = S_0 e^{j\omega t} \tag{4.14}$$

Together with Eq.(4.12):

$$(A_1.c_1 + A_2.c_2)S + j.A_1.\gamma_1.\omega.S = -A_1.\delta_1.H^2 \tag{4.15}$$

We can get

$$\begin{aligned} S &= -\frac{A_1.\delta_1}{(A_1.c_1 + A_2.c_2) + j.A_1.\gamma_1.\omega}.H^2 \\ &= \left(\frac{-A_1.\delta_1.(A_1.c_1 + A_2.c_2)}{(A_1.c_1 + A_2.c_2)^2 + (A_1.\gamma_1.\omega)^2} - j\frac{-A_1^2.\delta_1.\gamma_1.\omega}{(A_1.c_1 + A_2.c_2)^2 + (A_1.\gamma_1.\omega)^2} \right) H^2 \end{aligned} \tag{4.16}$$

It can be simplified as:

$$S = \left(\lambda' - j\lambda''\right).H^2 \tag{4.17}$$

where λ' and λ'' are defined as:

$$\lambda' = \frac{-A_1.\delta_1.(A_1.c_1 + A_2.c_2)}{(A_1.c_1 + A_2.c_2)^2 + \left(A_1.\gamma_1.\omega\right)^2} \qquad \lambda'' = \frac{-A_1^2.\delta_1.\gamma_1.\omega}{(A_1.c_1 + A_2.c_2)^2 + \left(A_1.\gamma_1.\omega\right)^2} \tag{4.18}$$

For the tri-layered sample, there are two forces F_1 applied to both sides of the piezoelectric layer. Consequently,

$$F = 2.F_1 = 2.A_1.T_1 = 2.A_1.c_1.S + 2.A_1.\gamma_1.\dot{S} + 2.A_1.\delta_1.H^2 \tag{4.19}$$

and as a result,

$$\lambda' = \frac{-2.A_1.\delta_1.(2.A_1.c_1 + A_2.c_2)}{(2.A_1.c_1 + A_2.c_2)^2 + \left(2.A_1.\gamma_1.\omega\right)^2} \tag{4.20}$$

and

$$\lambda'' = \frac{-4.A_1^2.\delta_1.\gamma_1.\omega}{(2.A_1.c_1 + A_2.c_2)^2 + \left(2.A_1.\gamma_1.\omega\right)^2} \tag{4.21}$$

Thus, the electric displacement *D* can be written as:

$$D = e_{31}\left(\lambda' - j\lambda''\right).H^2 + \alpha_{p.}H = \frac{1}{2}\beta_p.H^2 + \alpha_{p.}H \tag{4.22}$$

Here, $\lambda = \lambda' - j\lambda''$ is the magnetostriction coefficient which is found to be a complex quantity since the modeling takes the damping effect (γ_1 coefficient) into account. The imaginary part λ'' represents the magnetostriction losses and consequently, both α_p and β_p coefficients must be treated as complex quantities [145]:

$$\alpha_p = \alpha_p' - j.\alpha_p'' \text{ and } \beta_p = \beta_p' - j.\beta_p'' \tag{4.23}$$

where the imaginary parts represent the ME losses.

The ME current can be thus expressed as:

$$i_{ME} = A\left[\begin{array}{l}\left(\beta_p''.\left(H_{dc} + h_{ac}\right) + \alpha_p''\right) \\ \qquad + j\left(\beta_p'.\left(H_{dc} + h_{ac}\right) + \alpha_p'\right)\end{array}\right]\omega h_{ac} \tag{4.24}$$

When $H_{dc} >> h_{ac}$, the h_{ac} term in the bracket concerning the magnetic field can be neglected. And the i_{ME} current can be written as:

$$i_{ME} = A\left[\begin{array}{c}\left(\beta_p^{''}.\left(H_{dc}\right)+\alpha_p^{''}\right)^2 \\ +\left(\beta_p^{'}.\left(H_{dc}\right)+\alpha_p^{'}\right)^2\end{array}\right]^{1/2} \omega h_{ac} \tag{4.25}$$

Finally, the magnitude of the ME current can be expressed as:

$$I_{ME} = \left|i_{ME}\right| = A\left[\begin{array}{c}\left(\beta_p^{''}.H_{dc}+\alpha_p^{''}\right)^2 \\ +\left(\beta_p^{'}.H_{dc}+\alpha_p^{'}\right)^2\end{array}\right]^{1/2} \omega H_0 \tag{4.26}$$

The H_{dc} dependence of the phase shift φ can be simulated as:

$$\varphi = arctg\left(\frac{\mathrm{Im}(i_{ME})}{\mathrm{Real}\,(i_{ME})}\right) = arctg\left(\frac{\beta_p^{'}.H_{dc}+\alpha_p^{'}}{\beta_p^{''}.H_{dc}+\alpha_p^{''}}\right) \tag{4.27}$$

The square of the magnitude of the ME current I_{ME} is

$$I_{ME}{}^2 = A^2.\left[\begin{array}{l}\left(\beta_p^{''2}+\beta_p^{'2}\right).\left(H_{dc}\right)^2 \\ +2.\left(\beta_p^{''}.\alpha_p^{''}+\beta_p^{'}.\alpha_p^{'}\right)H_{dc} \\ +\alpha_p^{''2}+\alpha_p^{'2}\end{array}\right].\left(\omega H_0\right)^2 \tag{4.28}$$

So

$$I_{ME}{}^2 = Z_1.H^2{}_{dc} + Z_2 H_{dc} + Z_3 \tag{4.29}$$

With:

$$\begin{cases} Z_1 = A^2.\left(H_0\omega\right)^2.\left(\beta_p^{"2} + \beta_p^{'2}\right) \\ Z_2 = 2.A^2.\left(H_0\omega\right)^2.\left(\beta_p^{"}.\alpha_p^{"} + \beta_p^{'}.\alpha_p^{'}\right) \\ Z_3 = A^2.\left(H_0\omega\right)^2\left(\alpha_p^{"2} + \alpha_p^{'2}\right) \end{cases} \quad (4.30)$$

We can deduce Z_1, Z_2 and Z_3 coefficients by a polynomial fit of the experimental curves of $I_{ME}{}^2$ versus H_{dc}, as shown in Fig. 4. 1. Finally, re-solving Eq.(4.27) and (4.30), gives the calculated results of coefficients $\alpha_p^{'}$, $\alpha_p^{"}$, $\beta_p^{'}$ and $\beta_p^{"}$ respectively, which are summarized in Tab. 4. 1.

Tab. 4. 1 Comparison between the calculated results of the different samples.

Sample	$\alpha_p^{'}$	$\alpha_p^{"}$	$\beta_p^{'}$	$\beta_p^{"}$	Phase switching	H_{dc0} of phase switching
	(pC/m^2Oe)		(pC/m^2Oe^2)		(deg.)	(Oe)
PU+ 2 wt% Fe_3O_4 /PVDF/ PU+ 2 wt% Fe_3O_4	96.50	-291.70	-2.59	0.95	-60 → 112	0
PU+ 50 wt% TeD /PVDF/ PU+ 50 wt% TeD	-43.61	-117.20	-0.09	0.41	-30 → 142	200
PU+ 2 wt% Fe_3O_4 /PVDF	44.37	-220.60	-0.04	0.29	-170 → 5	-800
PU+ 50 wt% TeD /PVDF	27.43	-247.50	0.16	0.16	-115 → 20	-1100

As shown in Fig. 4. 5 and Tab. 4. 1, the simulated curves calculated from Eq.(4.27), show that the phase shift versus the bias magnetic field from fit well the experimental results. It is clearly demonstrated the evolution of

the phase between the ME current and the applied ac magnetic field versus the applied bias magnetic field is related to linear and bilinear ME coefficients. In this case, the trilayered samples lead to a phase switching dc magnetic field (H_{dc0}) near zero for (PU+2 wt% Fe_3O_4 /PVDF/ PU+2 wt% Fe_3O_4), whereas a result of 2000 Oe was obtained for PU+50 wt% TeD /PVDF/ PU+50 wt% TeD). For the bi-layered samples, the switching point is always negative.

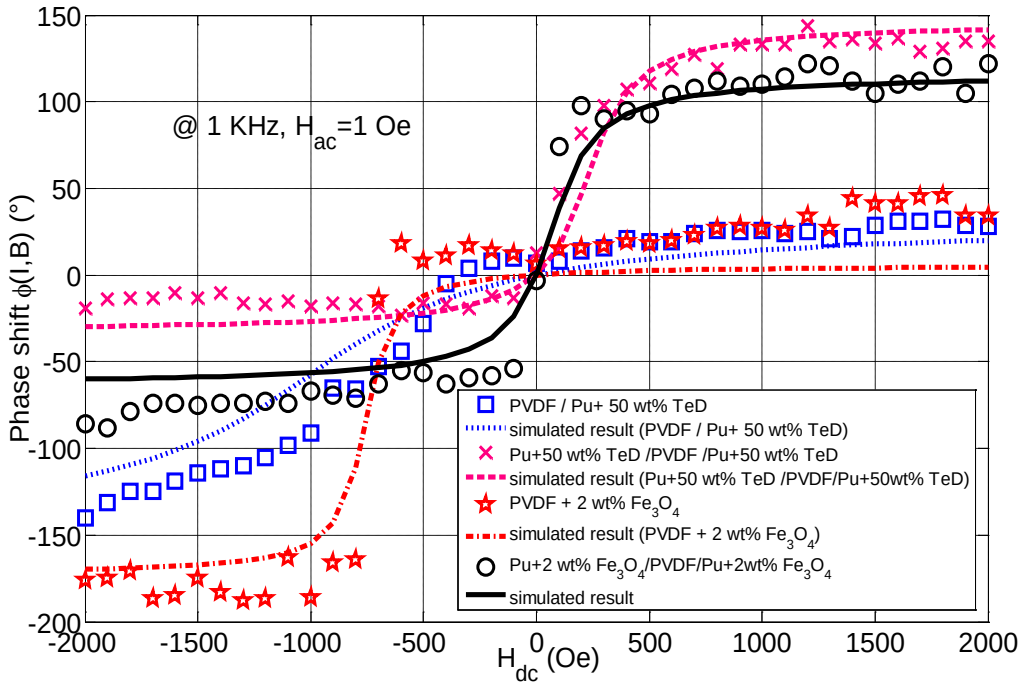

Fig. 4. 5 Variation of the phase shift between the ME current and the (ac) magnetic field versus the (dc) magnetic field.

4.2.4 Effect of the first and second ME coefficients on phase shift

The first and second ME coefficient are respectively given by $\alpha_p = \alpha_p^{'} - j\alpha_p^{''}$ and $\beta_p = \beta_p^{'} - j\beta_p^{''}$. The relationship between the two coefficients and the phase between the ME current and alternative applied magnetic field is given in Eq.(4.27). In order to study the influence of various coef-

ficients, the sample (PU+2 wt% Fe_3O_4)/PVDF/(PU+2 wt% Fe_3O_4) was selected and the value of one coefficient was varied as the other coefficient was kept constant.

4.2.5 Effect of the linear ME coefficient α_p

The value change of the real part of the ME coefficient α_p' causes a phase switching phenomenon in the dc magnetic field value H_{dc0}, which is shown in Fig. 4. 6. In addition, the value of $\varphi(i_{ME}, h_{ac})$ was almost constant for the highest values of the bias magnetic field.

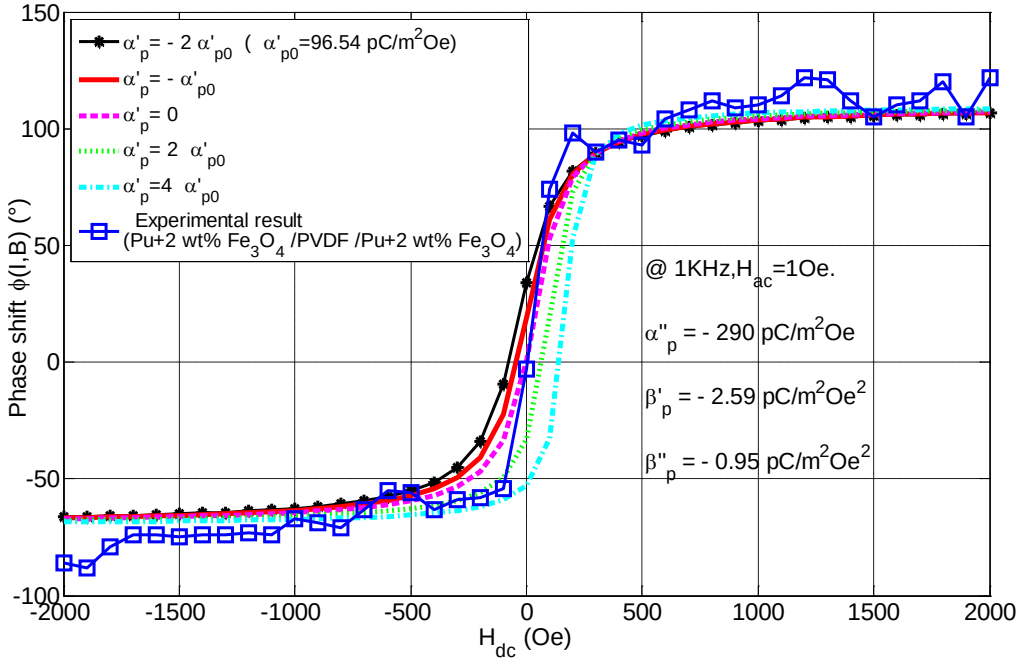

Fig. 4. 6 The influence of the real part of the linear ME coefficient α_p' (α_p'', β_p', β_p'' were taken as constant values).

As shown in Fig. 4. 7, the decrease of the imaginary part of the ME coefficient α_p'' leads to a decrease in the slope of the curve $\varphi(H_{dc})$ accompanied by a decrease of the absolute value of the phase shift. Moreover, $\varphi(H_{dc0})$ remains quasi null for a zero dc magnetic field.

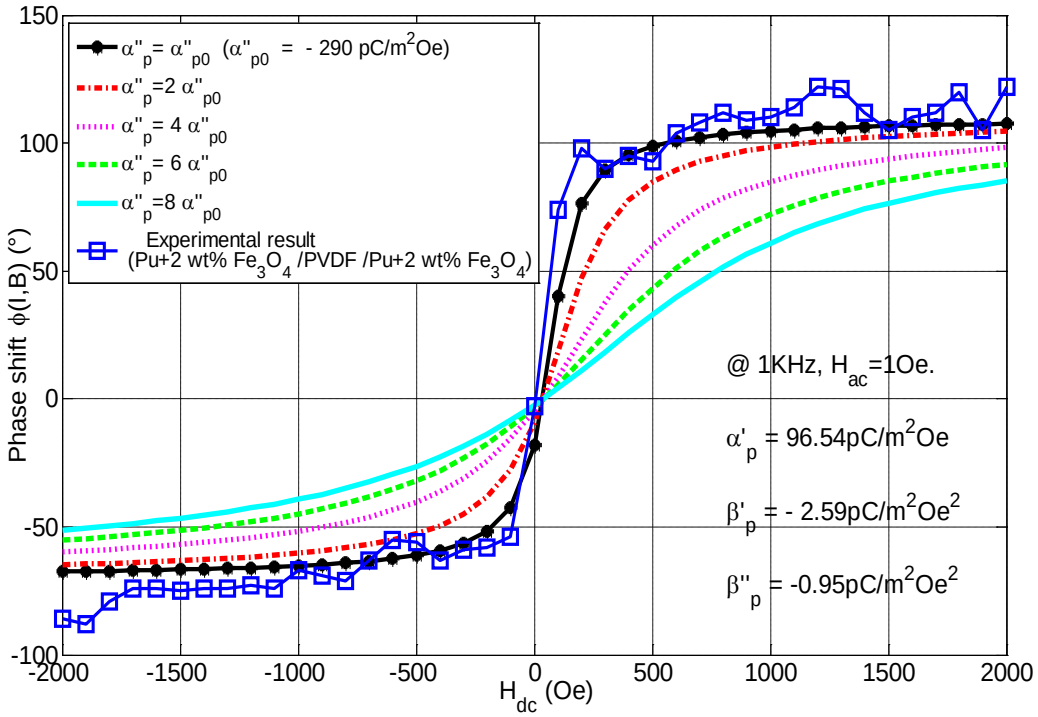

Fig. 4. 7 The effect of the imaginary part of the linear ME coefficient $\alpha_p^{"}$ ($\alpha_p^{'}$, $\beta_p^{'}$, $\beta_p^{"}$ were taken as constant values).

4.2.6 Effect of the bilinear ME coefficient β_p

The effect of the second ME coefficient $\beta_p = \beta_p^{'} - j\beta_p^{"}$ on the phenomenon of phase switching is shown in Fig. 4. 8 and Fig. 4. 9. Starting with the result of the sample ((PU+2 wt% Fe_3O_4)/PVDF/(PU+2 wt% Fe_3O_4)), decreasing the $\beta_p^{'}$ results in shift on the phase towards higher values and shift of the switching point towards higher H_{dc0} values increasing $\beta_p^{"}$ mainly shifts the phase towards higher phase values.

Consequently, from the fitting results, we can deduce that the model constructed in this part based on a driven damped oscillation system, can be used to evaluate the influence of the first and second-order ME coefficients on the dc magnetic field-induced phase switching phenomenon between dynamic ME current and the applied ac magnetic field.

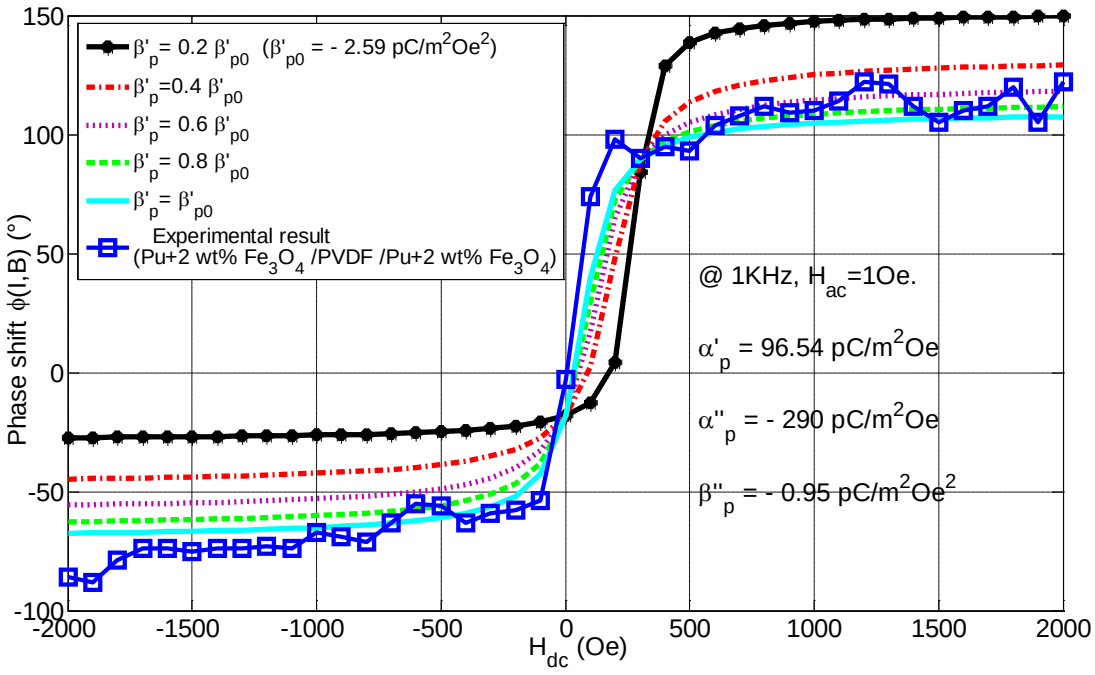

Fig. 4. 8 The effect of the real part of the bilinear ME coefficient $\beta_p^{'}$ (with $\alpha_p^{'}, \alpha_p^{"}, \beta_p^{"}$ taken as constant values.)

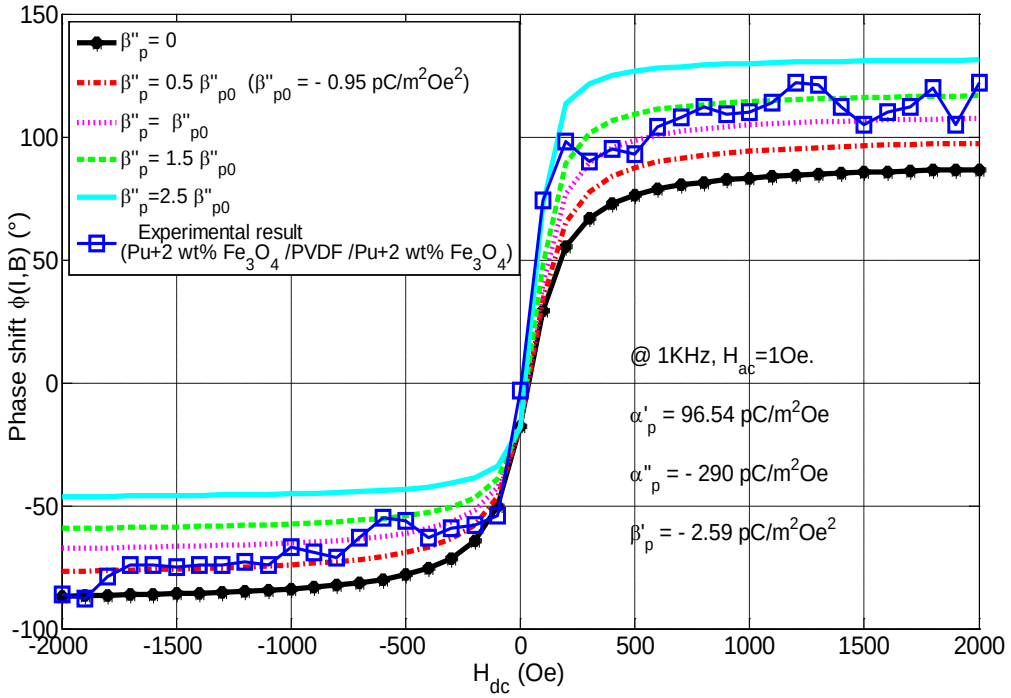

Fig. 4. 9 The influence of the imaginary part of the bilinear ME coefficient $\beta_p^{"}$ (with $\alpha_p^{'}, \alpha_p^{"}, \beta_p^{'}$ taken as constant values.)

4.3 Magnetoelectric effect induced by eddy current in piezoelectric unimorph bender

4.3.1 Early ME experiments on piezoelectric unimorph bender

4.3.1.1 Modelling of the piezoelectric unimorph bender

Eddy currents are currents induced in conductors, when it is exposed to a changing magnetic field due to variations of the field with time. The magnetic field will induce those small "rings" of current which will actually create internal magnetic fields opposing the change. The magnetic flux ϕ through the surface of the electrodes A can be written as:

$$\phi = \iint_A B \cdot dA \tag{4.31}$$

where magnetic induction vector B can be expressed as:

$$B = \mu_0 H_{dc} + \mu_0 h_{ac} \tag{4.32}$$

Then, induced electromotive forces (Emfs: e) loops in the metal electrode via the Lenz-Faraday equation:

$$e = -d\phi/dt \tag{4.33}$$

So, Emfs acting on the resistivity of the conductor can generate so called eddy currents which cause by such ac magnetic flux:

$$\phi_{ac} = \iint_A B_{ac} \cdot dA \tag{4.34}$$

In the field of physics, the Lorentz force is the force on a point charge or current loop due to electromagnetic fields. Here, when eddy currents exist in the silver electrodes, each current loop (*l*) locally induces an infinitesimal dynamic Lorentz force *F* on them which is expressed as the vector product:

$$dF = i_{eddy}(d\ell \times B) = \mu_0 i_{eddy}\left[d\ell \times (H_{dc} + h_{ac})\right] \tag{4.35}$$

where $d\ell$ is a vector element of the closed contour of the loop and i_{eddy} is the ac eddy current.

Since a homogeneous magnetic induction may be assumed in the piezoelectric ceramic, the global force $F = \int_L dF$ acting on the loop is null but each loop undergoes a moment *M* which is equal to:

$$M = m \times B = i_{eddy} s \times B = \mu_0 i_{eddy}\left[a \times (H_{dc} + h_{ac})\right] \tag{4.36}$$

where m is the magnetic moment of the eddy current loop and a is the area of the loop and *r* is the radius.

Finally, each electrode of the piezoelectric layer is subjected to the same moment:

$$M_{TOT} = \int_S \mu_0 k(r)\left[s \times (H_{dc} + h_{ac})\right] dr \tag{4.37}$$

where $k(r)$ is the eddy current surface density, which is unfortunately unknown [133], because the shape of the eddy current loops is unknown, owing to the rectangular shape of the sample.

Since the direction and magnitude of induced Lorentz force is given by the right-hand rule and its resulting moment on the sample depends on the different directions and magnitude of magnetic fields, we designed two possible configuration concerning to changing the magnetic field directions and four possible experimental configurations associated with different magnitudes of H_{ac} and H_{dc} , which are shown in Fig. 4. 10 and listed in Tab. 4. 2 respectively.

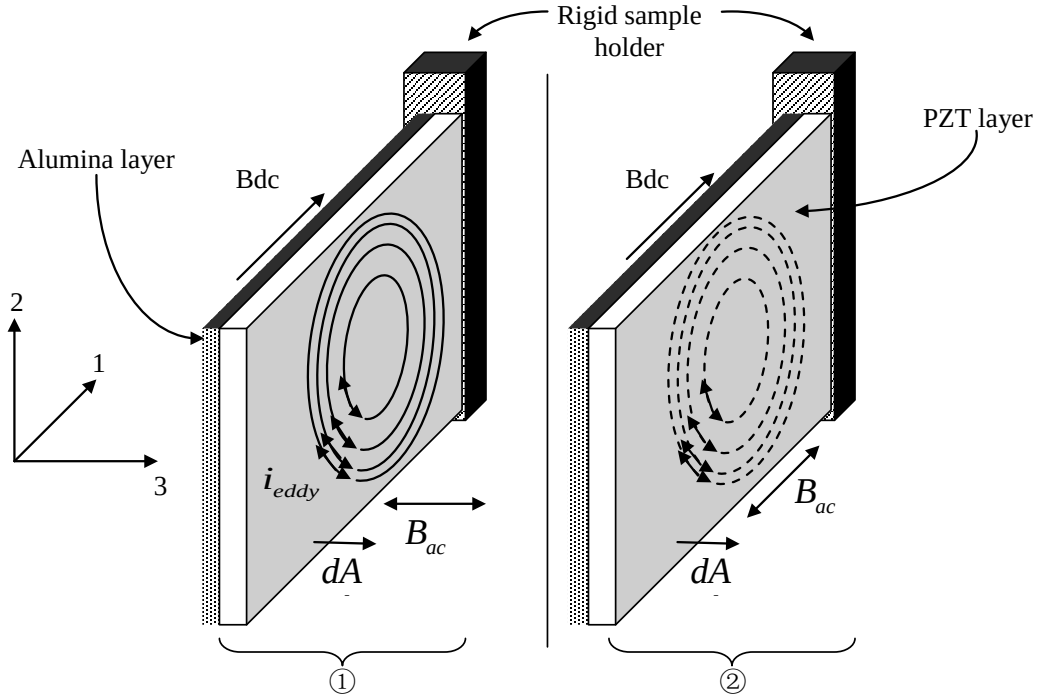

Fig. 4. 10 Schematic representation of the piezoelectric unimorph bender subjected to ac and dc magnetic fields. Two configurations (① and ②) provide the ac field direction. i_{ed} is the eddy current loop within the electrode

Tab. 4. 2 Different configurations of ME experiment on PZT unimorph bender

Configuration	Situation of H_{dc} and h_{ac}	Direction of Lorentz force	Direction of Moment
①	$H_{dc} >> h_{ac}$	"3"	"2"
①	H_{dc} =0	"1, 2"	"3"
②	$H_{dc} >> h_{ac}$	"3"	"2"
②	H_{dc} =0	"3"	"2"

In Fig. 4. 10, Cartesian coordinates were used to describe the two different configurations (① and ②). Our set up allowed applying the ac field perpendicular to the plane of the sample ("3" direction, configuration ①) or parallel ("1" direction, configuration ②). The dc magnetic bias was systematically applied along the "1" direction. The eddy current loops within the electrodes are also schematically shown in this drawing.

In these two cases, the induced moment is transferred to the PZT ceramic layer which is stress coupled with the silver electrodes, when the Lorentz forces exist. Consequently, piezoelectric charges are induced at the electrodes of the sample. Because of the different direction of applied magnetic flux and various ratios of the magnitudes of both h_{ac} and H_{dc} in the configuration ① or ②, the directions and magnitude of subjected moment on the cantilever bender change also.

4.3.1.2 Calculation of ME coefficient based on the experiment

Fig. 4. 11 shows the magnetoelectric current versus H_{dc} in both ① and ② configurations. With configuration ①, the measured magnetoelectric current i_{ME} presents a quite good linear response to the applied dc bias field change from -2000Oe to +2000Oe. This is a theoretically expected result when considering the proportionality between an applied external moment and the electrical charges (Q) generated at the electrodes of a piezoelectric unimorph bender [146].

$$Q = KM_{TOT} \tag{4.38}$$

where K is a constant coefficient which depends on the material characteristics of the PZT and alumina layers such as dimensions of each laminate, the piezoelectric coefficient of PZT layer and their elastic compliances. Thus, the magnetoelectric current in our study is given by

$$i_{ME} = \frac{dQ}{dt} = K\frac{dM_{TOT}}{dt} \tag{4.39}$$

In configuration ①, and when H_{dc}>>h_{ac}, the magnitude of moment M_{TOT} is proportional to H_{dc}, when the bender is subjected a given h_{ac} magnitude. So, according to Eq.(4.39), i_{ME} current is also proportional to H_{dc}, as experimentally found. Besides, its frequency is the same as that of $i_{eddy}(f)$. When there is no dc magnetic field, H_{dc} = 0, the ME current frequency is twice the frequency of i_{eddy} and h_{ac} according to Eq.(4.37), thus the current measured at the ac magnetic drive frequency f is null. In the case of configuration ②, the magnetoelectric current is very low (~1nA) and is H_{dc} independent. This result confirms that the ME coupling originates from eddy currents in silver electrodes that do not exist in the configuration ②. It is can be explained by the principle that B and dA vectors are perpendicular, thus the ac magnetic flux is null and consequently, no eddy currents and Lorentz forces are induced in this case. Noticeably, the ac flux magnitude is maximum in the configuration ① since B and dS vectors are parallel, yielding the highest eddy current magnitude. An apparent polarization ME coefficient $\alpha = \delta P/\delta H$ under H_{dc}= 500 Oe for instance, may be calculated using the following equation [21]:

$$\alpha = \frac{\left|i_{ME}(Hdc = 500Oe)\right|}{A\omega Hac} \tag{4.40}$$

We find α = 1.4×10^{-9} s/m, which is nearly of the same order of magnitude of ME coefficient of piezoelectric and magnetostrictive laminated composites measured at 1 kHz and under the same H_{dc} and h_{ac} field magnitudes, but applied along the length of the laminates [145]. Since the length

and thickness control the resonance frequency of cantilever beam, the piezo-electric beam can be made into different sizes and operates under different resonance frequencies [147].

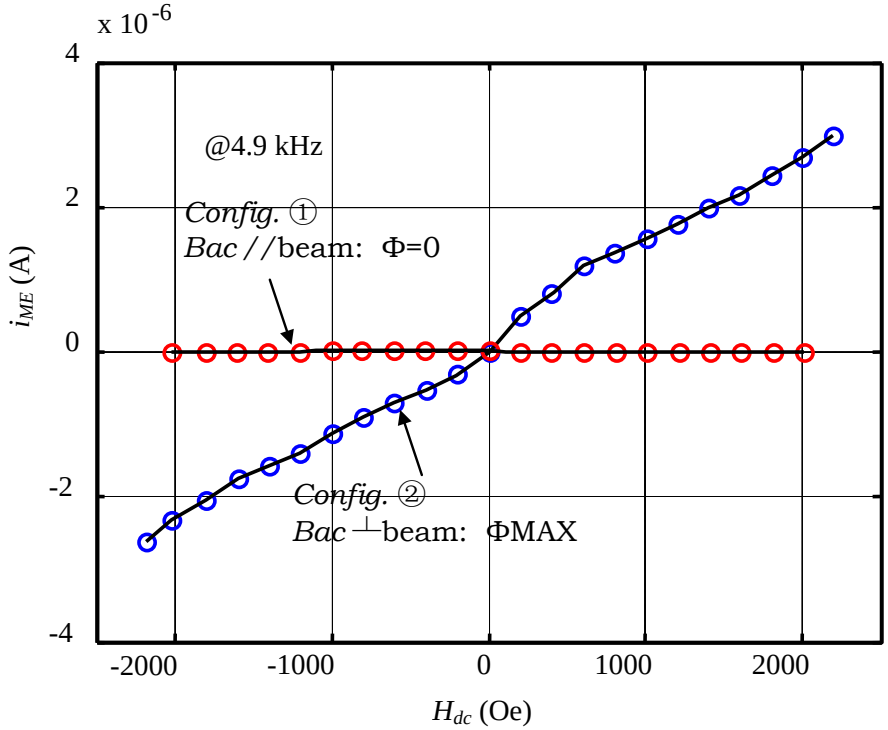

Fig. 4. 11 dc field dependence of the algebraic magnetoelectric current measured at the bending-mode resonance frequency (4.9 kHz) and H_{ac}=1 Oe, in the two configuration.

4.3.2 A developed ME sensor based on piezoelectric unimorph bender

Fig. 4. 12, (a) and (b) shows that the RMS voltage magnitude and vibrating velocity of unimorph bender are proportional to H_{dc} respectively, when applied ac magnetic field is 1Oe and frequency was kept at bending-mode resonance frequency of unimorph bender. As previously explained in § 2.3.2, the ac applied magnetic field was a rotating (vortex) one induced by a conducting wire carrying ac current located close to the clamped edge of the unimorph bender (Fig. 2. 3).

A linear ME response shown in Fig. 4. 12(a) was evidence that the voltage of unimorph bender is proportional to H_{dc}. This phenomenon can be explained as that with increase of dc magnetic field, the moment on the metal layer increased, which compliance with Eq.(4.36). Hence, vibration induced by moment will become intense gradually as dc magnetic field magnitude increased. As shown in [Fig. 4. 12(b)], the vibrating velocity magnitude versus algebraic H_{dc} exhibits the same behaviour. It is because of that with the increase of H_{dc} magnitude from 0Oe to +2400Oe, the moment increased together with bending vibration at direction "3". Then, transverse deformation enhanced the magnetoelectric response. Thus, dc magnetic field measurement can be realized by measuring magnetoelectric voltage of unimorph bender when it was subjected a certain ac magnetic field, such as 1Oe.

In order to investigate the magnetoelectric response and transverse deformation of the unimorph bender when the AC current amplitude in conducting wire changed, the measurement of bender's voltage and the velocity were made and their results were shown in [Fig. 4. 13 (a) and (b)]. Both figures show an approximate linear relation of magnetoelectric voltage and vibrating velocity versus ac current amplitude respectively, which can be explained by using Eq.(4.36) and (4.41).

$$B_{ac} = \frac{\mu_0 I_{AC}}{2\pi r} \tag{4.41}$$

where B_{ac}, I_{AC} and r are the ac magnetic flux density, ac current amplitude in conducting wire and its distance with unimorph bender respectively. The ac magnetic field through the surface of unimorph bender was proportional to ac current in wire. With increasing current amplitude, the ac magnetic field together with eddy currents in the metal electrode increased. Therefore, the transverse deformation induced magnetoelectric response was enhanced.

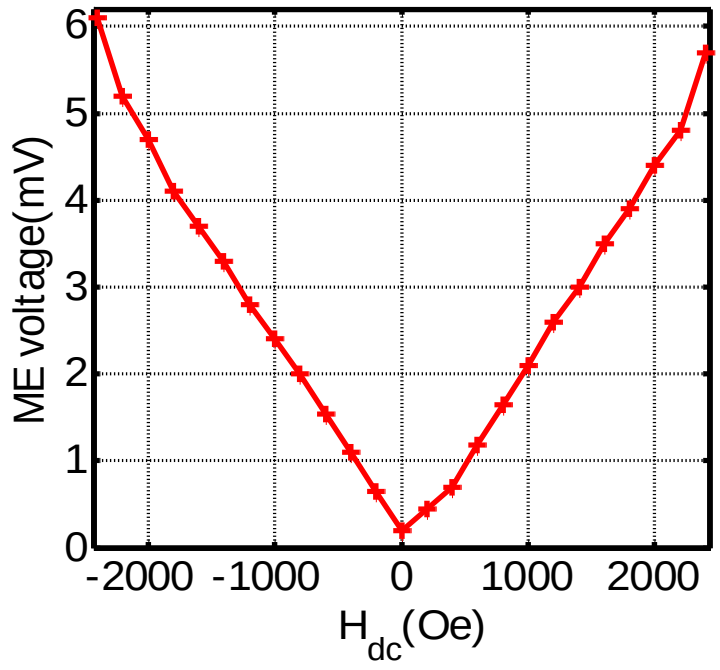

(a)

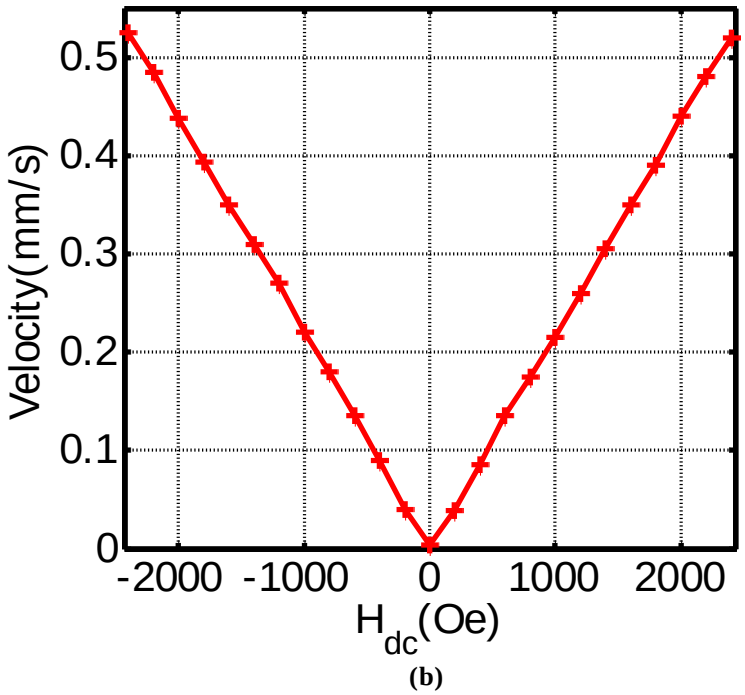

(b)

Fig. 4. 12 (a) RMS voltage of PZT unimorph bender versus dc magnetic field from -2400 Oe to +2400Oe (b) vibrating velocity of PZT unimorph bender versus the same dc magnetic field

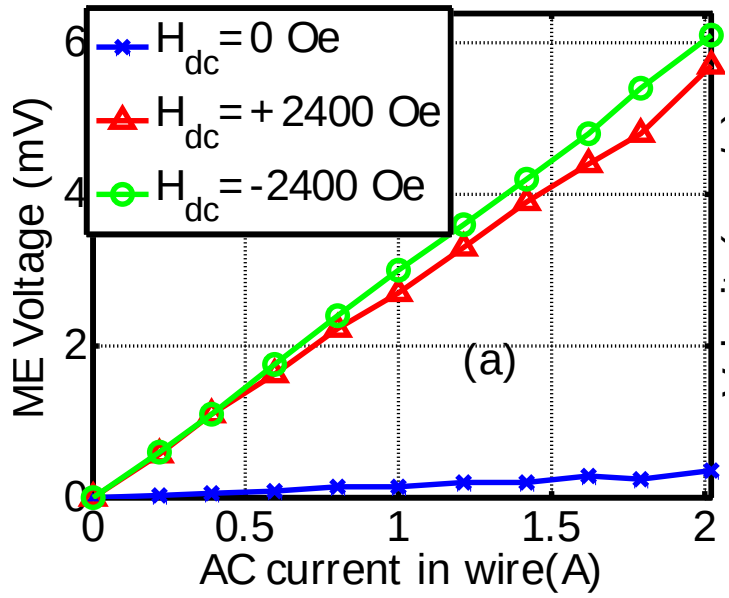

(a)

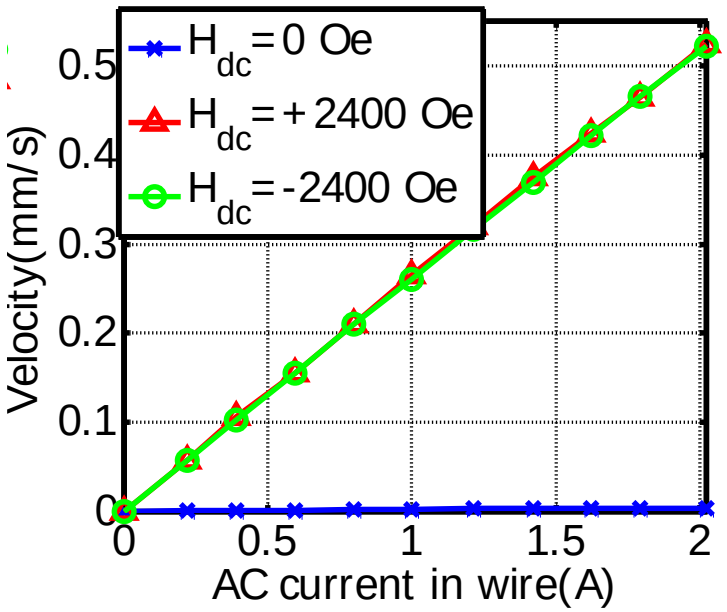

(b)

Fig. 4. 13 (a) RMS voltage of PZT unimorph bender versus ac current in conducting wire; (b) Vibrating velocity magnitude of PZT unimorph bender versus ac current in conducting wire

The vibrating mode of unimorph bender is shown by the schematic diagram of Fig. 4. 14. The vibration is following the thickness direction (direction 2). Finally, each electrode is subjected to the same moment as Eq.(4.36)

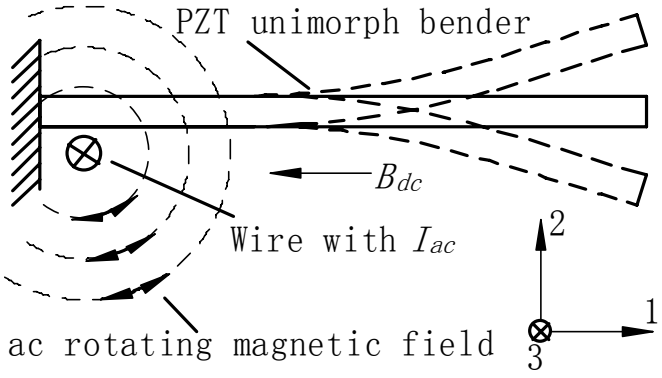

Fig. 4. 14 Schematic of vibrating mode of PZT unimorph sensor

Consequently, the ac magnetic field measurement can be realized by measuring the magnetoelectric voltage of piezoelectric cantilever beam when it was subjected under certain dc magnetic field such as 2400Oe.

The resulting ac electric field δE was estimated from the magnetoelectric voltage δV measured with a lock-in-amplifier. Then, the ME voltage coefficient α_E can be calculated using Eq.(4.42) [38, 134, 148], which can be considered the energy converting efficiency of our new type magnetoelectric sensor.

$$\alpha_E = \frac{1}{th}\left(\frac{\delta V}{\delta H}\right) \tag{4.42}$$

where, δV and δH are the induced voltage, intensity of applied ac magnetic field respectively. And th is the effective thickness of the piezoelectric phase. Because eddy currents in electrodes are sufficient to generate Lorentz forces, no extra magnetic phase is needed in this new magnetic field sensor.

The maximum magnetoelectric coefficient, 83.8mV/cm-Oe, is obtained for unimorph PZT sensor at 2400Oe d.c. magnetic field (bending-mode resonance frequency 560Hz) and 14.7 mV/cm-Oe at 500 Oe dc magnetic field at same resonance frequency.

4.3.3 ME effect caused by Lorentz force in a PVDF film

4.3.3.1 Mechanical model of bending PVDF film

Because of the contribution of Lorentz forces on the ME effect as discussed before, the piezoelectric PVDF film possesses a similar ME result as unimorph bender and the deflection of the sample will increase as the dc magnetic field increases, and thus enhanced value of output ME current can be obtained. Interestingly, since the PVDF sample is a heterogeneous polymer film, its bending behaviour may be fully modelled using bending pieozelectricity concept, which defines the relationship between the strain gradient in the thickness of the film and the induced electrical response. So for the soft piezoelectric film, a deflection is associated with its ME effect and the induced electric displacement D in the direction of the thickness can be expressed as [149]:

$$D = \varepsilon E + \eta \cdot 1/R \tag{4.43}$$

where D, ε, E are the electric displacement, electric field and the permittivity respectively. Since R is the radius of curvature, $1/R$ is equal to the gradient of the strain in the direction of thickness dS/dx_3. And η is defined as the bending piezoelectric stress constant of PVDF film which is equal to 80nC/m [149]. For the small deflections of the tested film:

$$1/R = 2y/l^2 \tag{4.44}$$

where y is film deflection and l is the length of the sample. Consequently, under short-circuit condition, the i_{ME} current can be obtained by:

$$i_{ME} = \frac{dD}{dt} A = \frac{2\eta}{l^2} \cdot \frac{dy}{dt} A \tag{4.45}$$

where A is sample surface. dy/dt is the bending velocity which can be measured using laser vibrometer system.

4.3.3.2 ME effect of bending PVDF film

Based on the model above, we can calculate the ME current caused by PVDF film deflection. The comparison between calculated and measured ME current is shown in Fig. 4. 15. From this result, we can conclude that the constructed model based on piezoelectric PVDF film deflections is in good agreement with the experimental magnetoelectric results. It is shown that with the magnitude increase of applied dc magnetic field, the induced Lorentz force and resulting deflection of the single piezoelectric PVDF film increases gradually. Thus, the ME current increases synchronously. The validity of the mechanical model is finally testified by this result.

Although, the rectangular shape PZT unimorph bender and PVDF film have been investigated and got significant ME coefficient, their shape quantitative modelling of eddy current induced ME effect difficult because Lorentz forces cannot be easily expressed. As shown in Fig. 4. 16, the trivial shape of eddy current loops which may be centered at different points of the electrodes make the calculation of Lorentz forces difficult. Consequently, in order to establish a model to calculate Lorentz force in the electrode, we have chosen to use piezoelectric ceramic disc which will be discussed in the following section of this chapter.

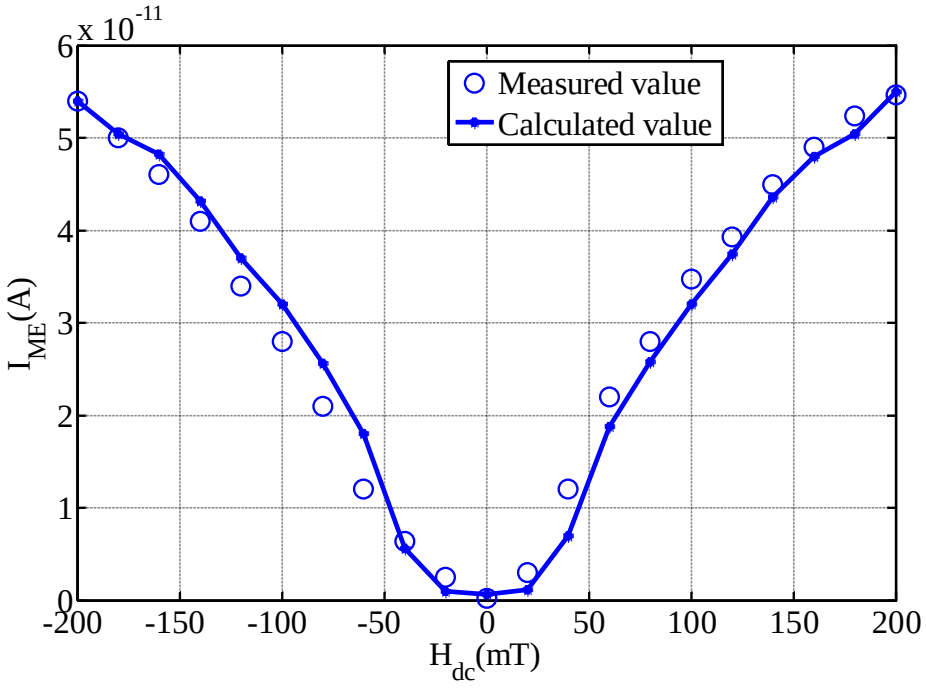

Fig. 4. 15 dc magnetic induction dependence of ME current

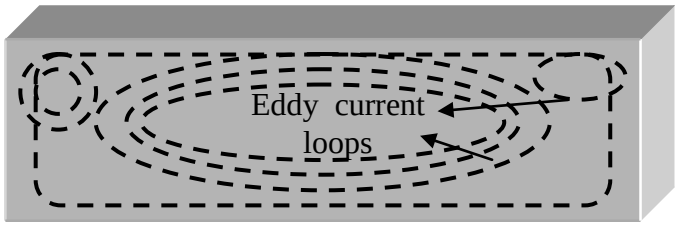

Fig. 4. 16 Schematic representation of possible eddy current loops in the rectangular shape sample

4.4 Magnetoelectric effect of single piezoelectric ceramic disc

4.4.1 Modelling of the magnetoelectric current induced by the Lorentz forces

For the piezoelectric disc, we can assume that circular and concentric eddy current loops exist in the disc shape electrodes, which can not be realized in the rectangular shape sample in the previous discussion. We have established both Cartesian and cylindrical (r, θ, z) three-dimensional coordinates which are used to express the Lorentz forces and associated stresses acting on the PZT ceramic disc when it is subjected to both ac and dc magnetic field (Fig. 4. 17).

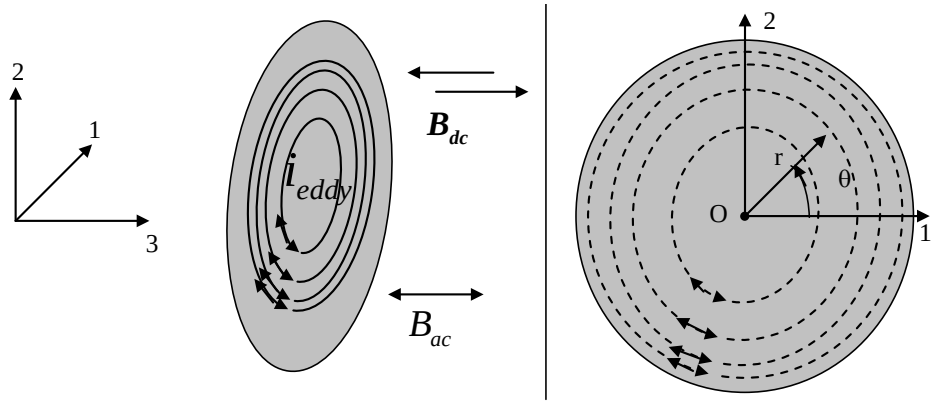

Fig. 4. 17 Schematic drawing of PZT ceramic disc in ac and dc magnetic field

The round shape of disc-form sample make the modelling of magnetoelectric coupling can be realized. The correspondence between the two systems of coordinates is: $r \rightarrow Axis\ 1$, $\theta \rightarrow Axis\ 2$, $z \rightarrow Axis\ 3$. In this case, the electrical polarization and magnetic fields directions are along the axis 3 and the sample's plane is parallel to the (1, 2) plane.

Since the thickness *th* of the disc sample is far less than its radius R, the radial mode piezoelectric response is largely predominant. In addition, because the ceramic sample is unclamped, the displacement (u_r), if it occurs, is only radial. The mechanical boundary conditions may be expressed as:

$$\begin{cases} T_1 \neq T_2 \neq 0 \\ T_3 = 0 \end{cases} \tag{4.46}$$

and

$$\begin{cases} S_1 \neq 0 \\ S_2 \neq 0 \\ S_3 = 0 \end{cases} \tag{4.47}$$

where T_i and S_i are the stress and the strain in the i-direction, respectively.

The electrical conditions (short-circuit) are:

$$\begin{cases} D_1 = D_2 = 0 \\ D_3 \neq 0 \end{cases} \tag{4.48}$$

and

$$E_1 = E_2 = E_3 = 0 \tag{4.49}$$

where D_i and E_i are the electric displacement and electric field in the i-direction. Thus, in these conditions, the constitutive piezoelectric equations are written in matrix notation as:

$$\begin{cases} S_1 = s_{11}^E T_1 + s_{12}^E T_2 \\ S_2 = s_{12}^E T_1 + s_{11}^E T_2 \\ D_3 = d_{31}(T_1 + T_2), \end{cases} \tag{4.50}$$

The expression of D_3 can be written as a function of the strain:

$$D_3 = e_{31}(S_1 + S_2) \tag{4.51}$$

Where the following relationship holds:

$$e_{31} = \frac{d_{31}}{s_{11}^E(1-\upsilon)} \tag{4.52}$$

where, s_{11}^E is the elastic compliance under the constant electric field, d_{31} is the transverse piezoelectric coefficient, e_{31} is the piezoelectric strain constant and υ is the planar Poisson's ratio. It may be assumed in a first approximation that $T_1=T_2=T$, then $S_1=S_2=S$. In other words, it means that the radial strain $S_r(=S_1)$ is constant whatever the radius value r ($S_r = \partial u_r/\partial r, S_\theta = S_2 = u_r/r$). Thus, the correlating between electrical and mechanical data can be used to simplify the Eqs.(4.50) and (4.51) as following:

$$\begin{cases} S_1 = (s_{11}^E + s_{12}^E)T_1 \\ D_3 = 2d_{31}T_1 \\ D_3 = 2e_{31}S_1 \end{cases} \tag{4.53}$$

According to the Lenz-Faraday equation, when the surface of the silver electrodes of the PZT ceramic disc is subjected on an ac magnetic flux, there are the electromotive forces $e_{eddy} = -d\phi/dt$ appearing around concentric loops in the metal electrode and consequently eddy currents i_{eddy} are present along these loops, owing to the conductive nature of silver. The specific shape of the ceramic and thus electrodes chosen for this study allows the development of concentric eddy current loops all having the same centre, the electrode one (O in Fig. 4. 17). It would be not the case for other particular shapes such as rectangular one. In this case, eddy current loops may appear

centred at different points of the metallic electrodes, thus making the calculation of Lorentz more difficult.

In order to give the theoretical expression of Lorentz forces and the corresponding stress in the electrodes thickness, it is necessary to determine the volume current density J associated to the eddy currents in the silver electrodes. Firstly, as shown in Fig. 4. 18, we can reasonably assume that current density does not depend on the coordinate in the "3" direction (thickness direction) because the depth penetration was estimated to be equal to 800 μm, which is much higher than the thickness of the silver electrodes (10 μm). Thus, J is constant in the cross-sectional area of the electrodes. Besides, owing to the symmetry of the studied sample, current density and consequently electromotive field E_{eddy} along the eddy current loop are independent upon the θ coordinate. Thus, according to the Ohm's Law:

$$J(r) = \gamma . E_{eddy}(r) \tag{4.54}$$

where r and γ is the radius of the current loop and the conductivity of silver respectively. Electric field and emf e_{eddy} are related to each other by:

$$e_{eddy} = \oint_l E_{eddy}(r) dl \tag{4.55}$$

where l is the circumference of the loop, $l = 2\pi r$. The generated emf is proportional to the rate of change of the magnetic flux. So,

$$E(r) = \frac{e_{eddy}}{2\pi . r} \tag{4.56}$$

Thus, current density at the distance r of the centre of the disc is:

$$J(r) = \frac{\gamma . e_{eddy}}{2\pi . r} = -\frac{\gamma}{2\pi . r}\frac{d\phi}{dt} \tag{4.57}$$

The magnetic flux ϕ defined by an integral over the surface:

$$\phi = b_{ac} . \pi . r^2 \tag{4.58}$$

since b_{ac} is applied perpendicularly to the electrodes plane and is assumed to be constant on the whole electrode surface. This assumption is valid because the diameter of the Helmoltz coils placed either side of the sample is twice larger than that of the ceramic, so magnetic induction b_{ac} is uniform in the airgap and equal to:

$$b_{ac} = B_{ac} . e^{j\omega t} \tag{4.59}$$

Finally, we get current density which is the electric current per unit area:

$$J(r) = -\frac{\gamma}{2\pi r}\frac{d\phi}{dt} = -j\frac{\gamma \omega r b_{ac}}{2} \tag{4.60}$$

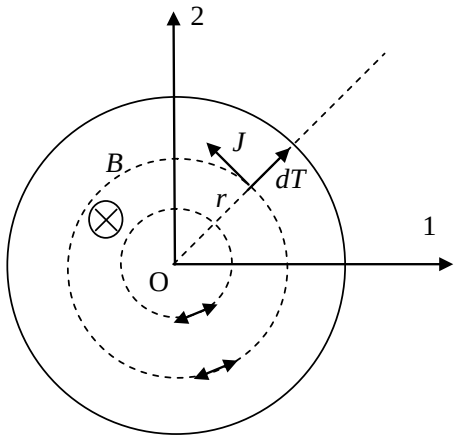

Fig. 4. 18 Infinitesimal Lorentz stress along radial direction induced by eddy current density *J* and applied magnetic induction *B*

The radial infinitesimal Lorentz force dF acting on an infinitesimal volume $d\tau$ of the electrode at the distance r of the centre O is given by the vector product:

$$dF = J \times B.d\tau = J \times B.th.r.d\theta.dr \tag{4.61}$$

And the corresponding infinitesimal stress acting on the area dA = $th.r.\mathrm{d}\theta$, (dA is the cross-sectional area of the electrodes and dA vector is parallel to the radial unit vector) is :

$$dT = \frac{dF}{dA} = J \times B.dr \tag{4.62}$$

where $B = b_{ac} + B_{dc}$. Finally, the macroscopic radial stress T_1 applied to the ceramic is given by :

$$T_1 = T = \int_0^R dT = \int_0^R -j\frac{\gamma\omega r b_{ac}(b_{ac} + B_{dc})dr}{2} \tag{4.63}$$

Thus,

$$T_1 = -1/4\, j\gamma\omega R^2 b_{ac}(b_{ac} + B_{dc}) \tag{4.64}$$

This so-called Lorentz stress is applied to the electrodes and it may be reasonably assumed that it is totally transferred to the piezoelectric ceramic and remains constant in the low sample's thickness (th=500 microns).

Finally, according to Eq.(4.53), the theoretical expression of the magnetoelectric current $i_{Lorentz}$ induced by Lorentz stress T is given by :

$$i_{Lorentz} = \frac{dD_3}{dt} A = 2d_{31} \frac{dT_1}{dt} A \tag{4.65}$$

where $A = \pi R^2$ is the total surface area of the electrodes, or

$$\begin{aligned} i_{Lorentz} &= -1/2\, j d_{31} \gamma \omega \pi R^4 [\, j\omega b_{ac} (b_{ac} + B_{dc}) + j\omega b_{ac}^2] \\ &= 1/2 d_{31} \gamma \omega^2 \pi R^4 [b_{ac} B_{dc} + 2b_{ac}^2] \end{aligned} \tag{4.66}$$

In the brackets of Eq.(4.66), only the first term $b_{ac}B_{dc}$ varies with the frequency f of the applied ac field ($b_{ac} = \mu_0 h_{ac} = \mu_0 H_{ac} e^{j\omega t}$), which is the measurement frequency of the experimental ME current. So, the second-order term ($2b_{ac}^2$) at the frequency *f*: is suppressed in the modelling. Then, the theoretical ME current which may be compared to the experimental one can be written as:

$$i_{Lorentz} = 1/2 d_{31} \gamma \omega^2 \pi R^4 b_{ac} B_{dc} \tag{4.67}$$

It should be noted that this equation is valid only for low frequencies far away from the resonance frequency f_r of the ceramic in the radial mode. However, the magnetoelectric current at $f_r = 2\pi/\omega_{res}$ may be modelled by multiplying the expression by the mechanical quality factor Q_m=38:

$$i_{Lorentz} = 1/2 Q_m d_{31} \gamma \omega_{res}^2 \pi R^4 b_{ac} B_{dc} \tag{4.68}$$

Fig. 4. 19 gives both the theoretical and experimental variations of algebraic ME current RMS values at resonance frequency f_r as a function of dc magnetic induction. As it is expected with calculation using Eq.(4.68), a linear relationship between experimental current and B_{dc} is observed with a slope value very similar to that of the theoretical result.

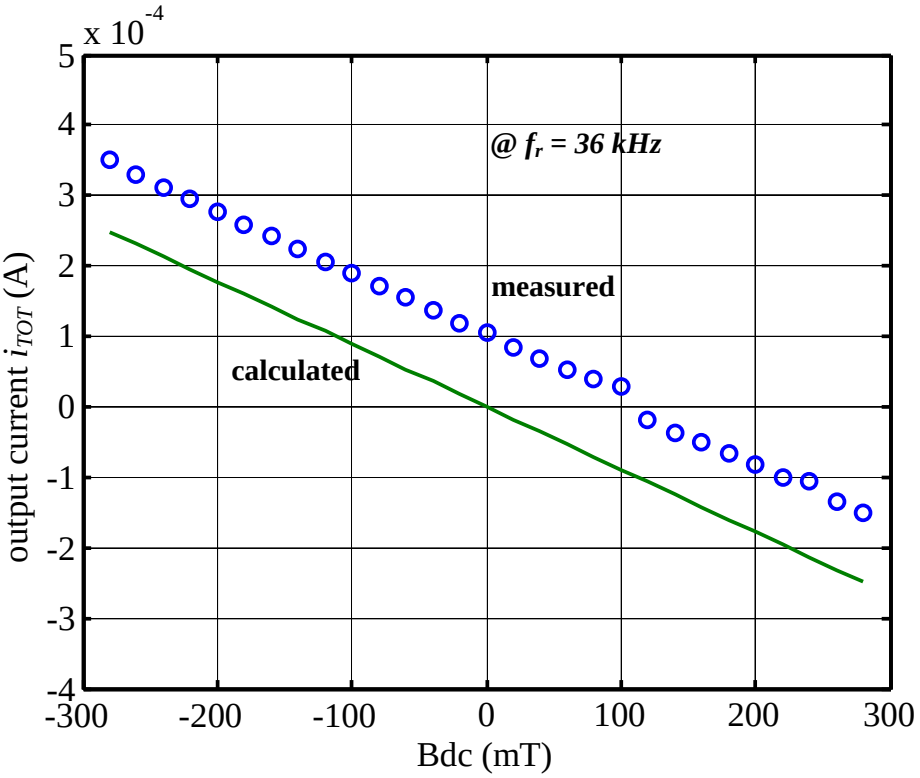

Fig. 4. 19 dc magnetic induction dependence of algebraic current magnitude.

However, there is still a clear difference between measured and calculated results, which remains constant whatever the dc magnetic induction value. This means that the modelling established in Eq.(4.68) needs to be improved by a supplementary current independent upon dc flux to be added to the Lorentz stress-induced current $i_{Lorentz}$. This current can be explained by the presence of a voltage induced by the ac magnetic flux ϕ_{loop} through the surface delimited by the experimental loop constituted of the ceramic connected by two wires to the current amplifier, as we reported in previous publications [21, 132] and was also mentioned by another group when studying magnetoelectric coupling in heteroepitaxial composite thin films [18].

In fact, the ceramic is supposed to be ideally short-circuited but it is not practically the case owing to the electrical impedance of the circuit can not be neglected. As a result, potential difference between the electrodes of

the sample should be taken into consideration through the Faraday and Lenz's Laws:

$$v_{loop} = -d\phi_{loop}/dt = -j\omega\phi_{loop} \tag{4.69}$$

where $\phi_{loop} = \Phi_{loop} e^{j\omega t}$, Φ_{loop} is the magnitude of ϕ_{loop}, which is a quantity in phase with hac. Consequently, dc field independent current, i_{loop} appears. It should be noticed that i_{loop} always exists since the magnetic flux ϕ_{loop} can never be totally suppressed. Then, the magnetic flux through the experimental loop and v_{loop} at a given frequency may be easily evaluated by measuring the output current at frequencies far from the resonance, for instance at 3 kHz, when B_{dc}=0. In these conditions, electromechanical coupling is weak as it is confirmed by the frequency dependence of macroscopic radial velocity measured at the edge of the ceramic which is shown in Fig. 4. 20 and it may be assumed that the current only originates from ϕ_{loop} and the theoretical expression is given by:

$$i_{loop} = jC\omega v_{loop} = C\omega^2\phi_{loop} \tag{4.70}$$

where C is the capacitance of the ceramic disc which was calculated by:

$$C = \frac{\varepsilon_{33}^{T}\pi R^2}{th} \tag{4.71}$$

where ε_{33}^{T} is the permittivity under constant stress. In Eq.(4.71), because of the high resistance R of the ceramic in (R/C) parallel configuration, the induced leakage current can be neglected.

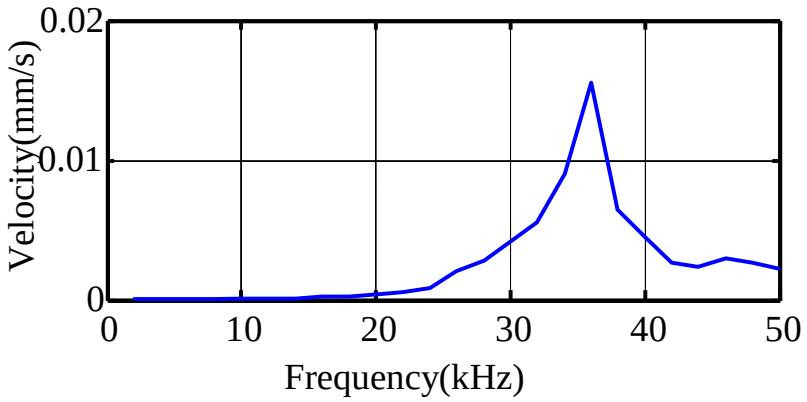

Fig. 4. 20 Frequency dependence of radial velocity showing electromechanical enhancement only in the vicinity of the resonance frequency (36 kHz)

Take the current measured at 3 kHz for example, i_{loop} (3 kHz)=2.5×10^{-7}A, magnitude of magnetic flux Φ_{loop}= 5.9×10^{-9} Wb and v_{loop} (3 kHz)= 1.1×10^{-4} V (rms values). Finally, it can be concluded that for the given setup, permanent magnetic flux magnitude Φ_{loop} is imposed to the loop, whatever the frequency and dc magnetic field. Consequently, the magnitude of the inductively coupled voltage between the electrodes v_{loop} increases linearly with the working frequency.

Then, when the experiment is undergone under the resonance frequency f_{res}, the electromechanical coupling of the sample in the radial mode is optimal, the $(v_{loop})_{res}$ voltage and the associated electric field E_3 are calculated by Eq.(4.72):

$$E_3 = \frac{(v_{loop})_{res}}{th} \tag{4.72}$$

Thus, the total output current i_{TOT} which is not only due to Lorentz forces and can be the sum of three different contributions.

$$i_{TOT} = i_{loop} + i_{Lorentz} + i_E \tag{4.73}$$

where $i_{Lorentz}$ is the contribution of the piezoelectric coupling related to Lorentz stress given by Eq. (4.68) and i_E is the contribution of the piezoelectric coupling related to the electric field.

4.4.2 Modelling of the output current when B_{dc}=0

Based on above theoretical total current, the piezoelectric current i_E may be calculated when $B_{dc} = 0$, i.e. the applied Lorentz stress T_1 is null, using the combination of the following piezoelectric equations with E and S as variables:

$$\begin{aligned} S_1 &= d_{31} E_3 \\ D_3 &= \varepsilon_{33}^S E_3 + 2 e_{31} S_1 \end{aligned} \tag{4.74}$$

where ε_{33}^S is the permittivity under constant strain and with the previous assumption: S_1=S_2

This yields

$$D_3 = \varepsilon_{33}^S E_3 + 2 Q_m e_{31} d_{31} E_3 \tag{4.75}$$

Then, the time derivative of Eq.(4.75) multiplied by the electrodes area A gives the i_E current at the resonance frequency f_r:

$$i_E = \frac{dD_3}{dt} A = (\varepsilon_{33}^S + 2 Q_m e_{31} d_{31}) \frac{dE_3}{dt} A \tag{4.76}$$

Since

$$E_3 = \frac{(v_{loop})_{res}}{th} = \frac{-j\omega_{res}\phi_{loop}}{th} \tag{4.77}$$

Thus, *when* $B_{dc}=0$, the theoretical total current i_{TOT} may be expressed as a function of ϕ_{loop} as:

$$i_{TOT} = i_{loop} + i_E = (\varepsilon_{33}^S + 2Q_m e_{31} d_{31}) \frac{\pi R^2 \omega_{res}^2}{th} \phi_{loop} \tag{4.78}$$

In Fig. 4. 19, when $B_{dc}=0$, experimental output current equals $(i_{TOT})_{meas} = 1.05 \times 10^{-4}$ A. While the calculated total current due to the dielectric and piezoelectric nature of the ceramic subjected to $(v_{loop})_{res}$ yields: $(i_{TOT})_{calc} = 1.11 \times 10^{-4}$ A($i_{loop} = 2.27 \times 10^{-5}$A and $i_E = 8.83 \times 10^{-5}$A). So it yields $(v_{loop})_{res} = 1.33$ mV at the resonance frequency.

A good agreement between experimental and calculated currents confirms the three types of contributions to the total current at the resonance frequency as predicted before, which include: 1) piezoelectric current due to the applied Lorentz stress, 2) piezoelectric current due to the inductively coupled electric field and 3) the dielectric loop current. Besides, the validity of the established modelling also confirms the validity of the assumption concerning the radial strain in Eqs.(4.53) and (4.74) : $S_1=S_2$ and $T_1=T_2$.

4.4.3 Modelling of the output current when $B_{dc} \neq 0$

In order to model the dc magnetic induction dependence of the i_{TOT} at f_r, the piezoelectric Eq. (4.74) can be used, which gives the electric displacement with the electric field and resulting strain. The corresponding current versus time derivative of E_3 and S_1 is:

$$i_{TOT} = \frac{dD_3}{dt} A = \varepsilon_{33}^S \frac{dE_3}{dt} A + 2e_{31} \frac{dS_1}{dt} A \tag{4.79}$$

Thus

$$i_{TOT} = \varepsilon_{33}^S \frac{\pi R^2}{th} \omega_{res}^2 \phi_{loop} + 2e_{31} \frac{v_S \pi R^2}{R} \tag{4.80}$$

where v_S is the radial strain velocity: $v_S = R \cdot dS_1/dt$. In our ME experimental setup, the vibrating velocity v_S can be simultaneously determined at the edge of the ceramic by the laser vibrometer. Besides, at f_r, both the strain S_1 and velocity are the result of the two excitation sources: the mechanical one (Lorentz stress) and electrical one (magnetically induced electric field). Hence, the induced strain is expected to be modelled by the following piezo-electric equation with stress and electric field as independent variables:

$$S_1 = (s_{11}^E + s_{12}^E)T_1 + d_{31}E_3 \tag{4.81}$$

Thus, radial velocity at the resonance frequency can be expressed as:

$$\begin{aligned} v_S = R\frac{dS_1}{dt} &= Q_m \left[(s_{11}^E + s_{12}^E)\frac{dT_1}{dt} + d_{31}\frac{dE_3}{dt} \right] \\ &= Q_m \left[\frac{1}{4}(s_{11}^E + s_{12}^E)\gamma\omega_{res}^2 R^2 b_{ac} B_{dc} + d_{31}\omega_{res}^2 \frac{\phi_{loop}}{th} \right] \end{aligned} \tag{4.82}$$

Consequently, we got:

$$v_S = R\frac{dS_1}{dt} = Q_m \left[\frac{1}{4}(s_{11}^E + s_{12}^E)\gamma\omega_{res}^2 R^2 b_{ac} B_{dc} + d_{31}\omega_{res}^2 \frac{\phi_{loop}}{th} \right] \tag{4.83}$$

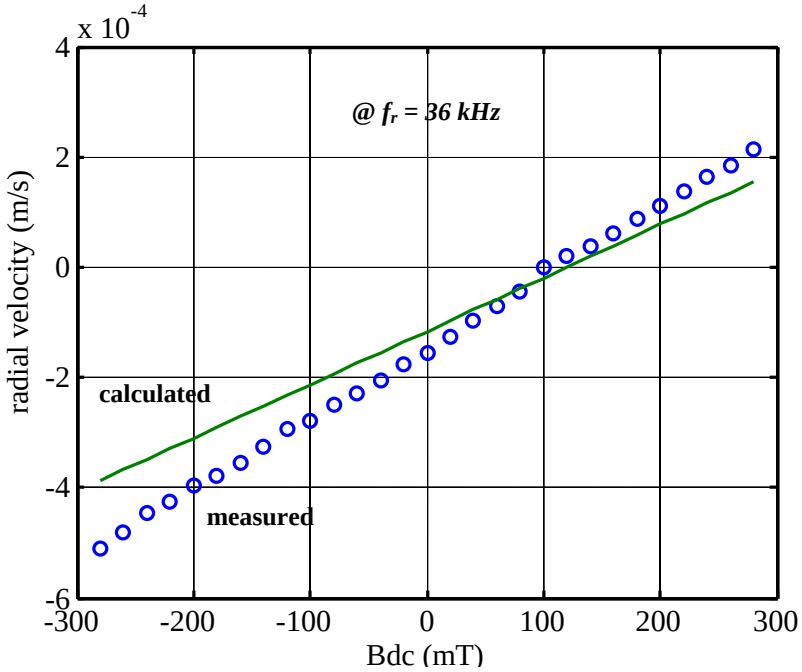

Fig. 4. 21 Radial strain velocity V.S. Bdc

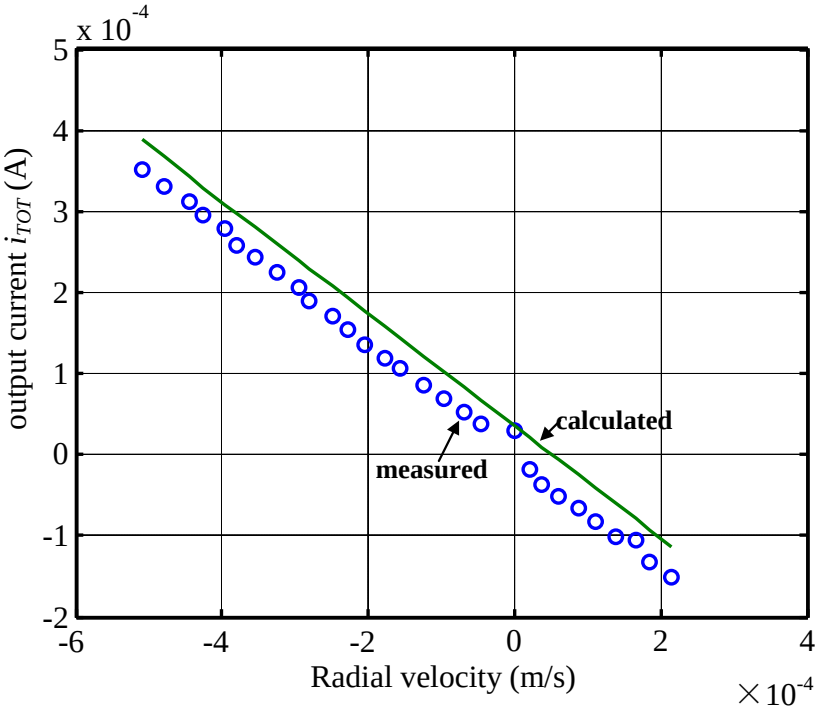

Fig. 4. 22 Output current V.S. radial strain velocity

Comparison between measured radial velocity by Eq.(4.83) and its calculated value against dc magnetic field at f_r has been shown in Fig. 4. 21. It presents the good agreement between measured and calculated results. Experimental v_S shows a good linear variation. Finally, in Fig. 4. 22, i_{TOT} is linearly dependent of the velocity v_S, and is consistent with theoretical i_{TOT} calculated by Eq. (4.80).

4.5 Conclusion

In summary, we have observed that the best ME voltage coefficient is given by the trilayered sample of (PU+2wt%Fe_3O_4/PVDF/ PU+2wt%Fe_3O_4), presenting a voltage coefficient is 75.33V/m-Oe, which is greater than that obtained with the other sample as well as that obtained for the monolayer consisited of PU+x% magnetic particles. A model based on a driven damped oscillation system, to evaluate and study the influence of the first and second-order ME coefficients on the dc magnetic field-induced phase switching phenomenon, has been developed.

On the other hand, it is experimentally shown that ac magnetic field induce eddy currents and the presence of applied dc magnetic field generate Lorentz forces in the metal electrodes acting on piezoelectric compounds such as PZT unimorph bender, single sheet PVDF film and PZT ceramic disc. A magnetically induced piezoelectric current is obtained at the sample electrodes and is the result of the product property between magnetic forces and piezoelectricity. In this case, the ME coupling does absolutely not require magnetic component, compared with ME effect originating from the product property between magnetostriction and piezoelectricity (laminate composites).The major difference with previously published ME coupling implying Lorentz forces and piezoelectric effect is that there is no need of current supply directly with connecting wires. The eddy currents in silver electrodes are

sufficient to generate Lorentz forces. The ME response is linear with H_{dc}, contrary to magnetostrictive composites, which is very interesting for dc magnetic field detection applications. Besides, the similar ME result is observed in single piezoelectric PVDF film. Its mechanical model has bee testified by the measured ME result. Thus, the eddy current induced magnetoelectric effect is expected to be observable in piezoelectric ceramics and polymers, provided their electrodes are subjected to ac magnetic flux.

Chapter 5. Electrostrictive performance of the charged cellular PP

5.1 Introduction

After corona poling, there are a number of the charges injected in the cellular PP. The charge storage ability of electrets plays an important part of the application of electromechanical-transducer. Thus, some experiments need to be undergone to examine the charge storage mechanism. Based on the results of the surface potential decay test, TSDC and DSC experiments described in this chapter, the charge retain ability and deposit situation of cellular PP after corona poling has been examined. Then, it is used to explain the enhanced electrostrictive effect of the charged sample. A mathematic model which can explain the increase in electrostrictive coefficient and relative permittivity has been established.

5.2 Charge storage mechanism analysis on the charged cellular PP

5.2.1 Surface potential decay tendency

The industrial manufactured cellular PP film has two distinct surfaces: one is very smooth and another is rougher. Fig. 5. 1 is plotted with the surface potential normalized by initial surface potential V(0) against the total measurement time (500s), where the smooth and rough surfaces are exposed to corona treatment respectively.

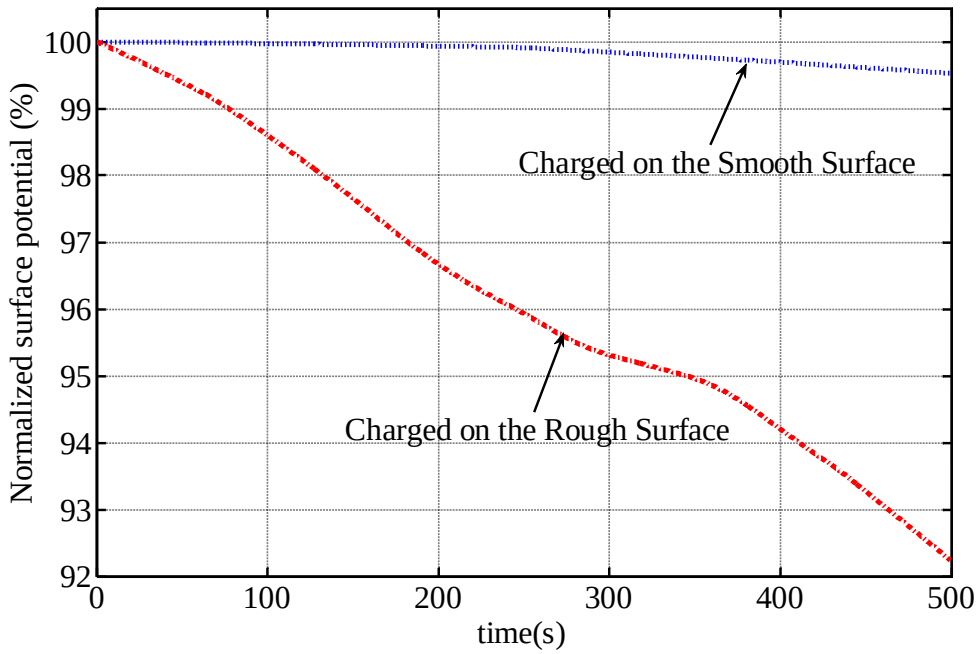

Fig. 5. 1 A comparison of the normalized surface potential (V(t)/V(0)) between two charged surfaces of different roughness.

It was found that the initial surface potential V(0) for both surfaces was approximately the same at the beginning of the measurement: -4 kV, for

the sample charged on the rough surface and the same value for the sample charged on the smooth side. On the contrary, the normalized surface potential decay rate for the smooth surface (0.7 % from 0s to 500s) was much lower than for the rough surface (8%).

The decay of the surface potential was more pronounced for the rough surface due to its contact area with air being larger than that of the smooth surface. Consequently, more surface charges could be released versus time. The effect of the samples' roughness has been already mentioned in another study [5]. This experiment reveals that the roughness of the cellular PP does not affect the charge injection as the same surface potential is observed, but affects its surface potential decay quantitatively. Consequently, cellular PP with corona poling on the smooth surface was applied in the following experiments.

5.2.2 Charge storage analysis through TSDC measurements

Fig. 5. 2 shows the TSDC current versus the temperature. For the non-charged sample, no TSDC current was measured from 23°C to 140°C. For the corona charged samples, on the other hand, three peaks can be clearly seen on the curve: the first one - designated the peak a - at 60°C with a maximum current value of 5pA; the second peak - designated the peak b - at 86°C with a maximum current value of 10pA, and the third one - designated the peak c - at 128°C with a maximum current of 4pA. The two former peaks have been mentioned in a previous investigation [5]. As expected for the non-charged samples, no TSDC peak was observed due to the fact that PP is a dielectric for which no free charge exists without corona poling treatment. In contrast, for the charged samples, the existence of peaks was evidence of charges having been injected within the sample during the corona treatment and of these charges having been maintained at different depth within the sample after the treatment [106, 131, 150, 151]. Specifically, the second and

the third peaks which are more diffuse clearly concern a thermal activated phenomenon of free charges displacement and should concern electron that are more deeply injected within the samples. Then, by using Eq.(3.1), the absolute value of the total quantity of injected charges was found to be equal to 23.9 nC.

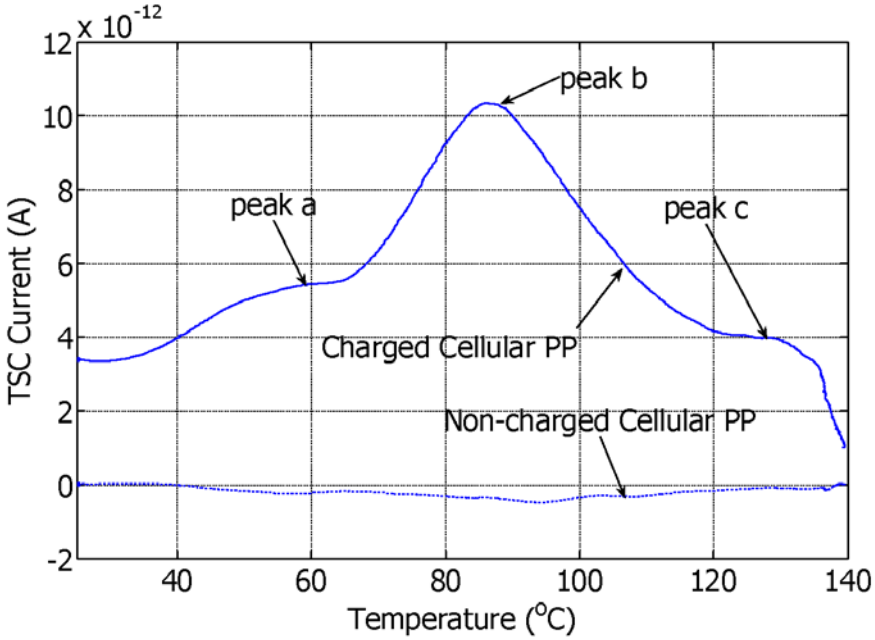

Fig. 5. 2 TSDC current measurements versus temperature for non-charged and charged cellular PP

5.2.3 Charge quantity comparison among different applied corona voltage

In order to investigate the influence of different corona voltage of the discharge needle on the quantity of injected charge. We apply high-voltage from -15kV to -30kV, and calculate the quantity based on the TSDC experiment results in each case. Fig. 5. 3 depicts the variation of released charges versus temperature after the corona treatment for various corona

voltages applied on the needles. This quantity of charges was calculated through integration of the measured TSDC current.

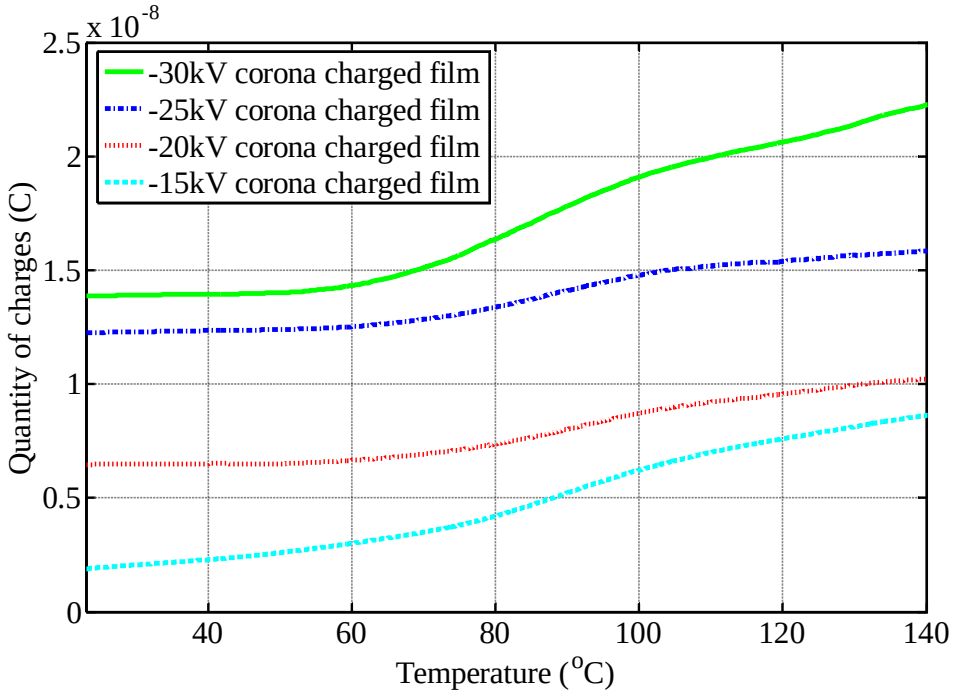

Fig. 5. 3 The total quantity of charges in cellular PP under the corona voltage from -30kV to -15kV.

In these curves, we can observe that a smooth increase in released charges with a step of almost from 60°C to 100°C. This step correspondes to the two diffuse peaks denoted a and b, which can be also observed in the curve of TSDC result. This smooth increase phase indicate that the charge stored in the shallow energy traps of cellular PP released slowly with the increase in temperature. Then, the total quantity of released charges versus temperature, which is equal to the charges injected by the corona process, was found to increase with the corona voltage applied on the needles from 9.1 nC at -15 kV to 23.9 nC at -30 kV. As previously explained, the charges that were more deeply injected were progressively released, leading to the smooth increase in the charge.

As expected, the quantity of released charges, which was equal to the quantity of injected charges, increased as the potential applied to the needles was raised. This phenomenon was imposed by the fact that a higher corona voltage helps to enhance Paschen's breakdown [106] of the air between the needles and the sample, as well as that of the voids inside the cellular PP. Therefore, the quantity of charges corresponded to the various applied voltages in corona discharge.

5.3 Analysis on crystallinity

5.3.1 Measured DSC traces of cellular PP

Fig. 5. 4 shows the thermal behavior, as measured by DSC experiments, of non-charged and -30kV-charged cellular PP. For the two samples and for the first thermal cycle on the charged cellular PP, a first peak can be observed at 127°C. After integration of the heat flow, the corresponding enthalpy, ΔH, was equal to 0.82 J/g for the non-charged sample and 2.38 J/g for that charged at -30 kV. For both materials, a second peak was observed at 169°C. The corresponding enthalpy was equal to 62.57 J/g and 75.49 J/g respectively for the non-charged and charged materials. During the cooling, a third peak was observed for the two samples at a same temperature of 114°C. The enthalpy value was 72.69 J/g for the non-charged sample and 73.2 J/g for the -30 kV charged sample.

For the second thermal cycle applied on the charged sample, a DSC trace close to that of the non-charged sample can be observed, showing that this sample has recovered the properties exhibited before the corona treatment. As a consequence, the large increase in the enthalpy for the first peak

and the slight one for the two other peaks can be unambiguously attributed to the corona injection.

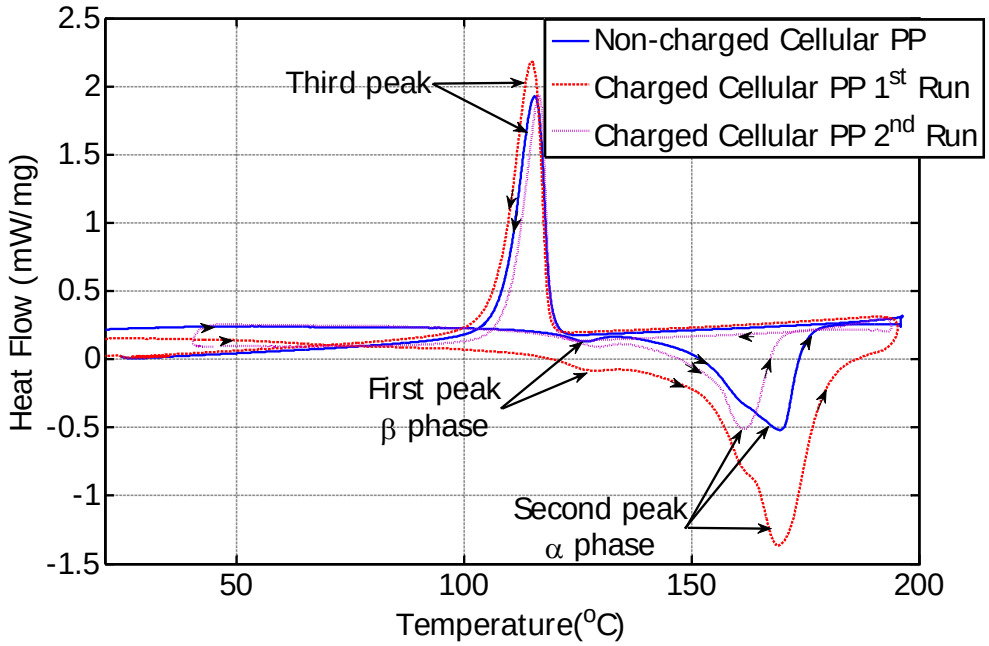

Fig. 5. 4 DSC traces of charged and non-charged cellular PP

As previously reported, commercial PP is mainly composed of two crystalline phases named as α phase and β phase [152]. The melting temperatures of the major α phase and of the β phase are generally given around 160°C and around 130°C respectively [152, 153]. Consequently, in good agreement with these results, the first peak observed in DSC at 127°C is believed to be due to the β phase melting and the second one observed at 169°C is due to the α phase melting. The third peak observed during the cooling procedure at 114°C is due to the crystallization of the melting.

By using the following Eqs.(5.1) and (5.2), the percentage of crystallinity of β phase (H_β) and α phase (H_α) within the sample can be calculated by assuming that the melting enthalpy of 100% α- and β-crystalline phase is 178 J/g and 168J/g respectively [142, 152, 153]. The obtained results are summarized in Tab. 5. 1. Even though the mechanism is not well understood,

the corona injection has clearly increased the content of the β phase and slightly increased the content of the α phase.

$$H_{\alpha}(\%) = \left(\Delta H_m^{\alpha} / \Delta H\right) \times 100 \tag{5.1}$$

$$H_{\beta}(\%) = \left(\Delta H_m^{\beta} / \Delta H\right) \times 100 \tag{5.2}$$

The peak a and b observed on the TSC curve did not correspond to any event on the DSC diagram. As a consequence, it is reasonable to assume that they have no link with the melting temperature of the α and β phases. These peaks are probably due to the space charges which are not deeply injected in the polymer. The peak c observed on the TSC curve occurs at a temperature closed to the melting temperature of the β phase and is probably due to the release of the trapped charges at the β phase interface.

Tab. 5. 1 Calculated percentage crystallinity of β phase and α phase

Material	β-crystalline phase	α-crystalline phase
Non-charged cellular PP	0.49%	35.2%
-30kV-charged PP	1.42%	42.4%

In addition, a corona discharge treatment gives rise to the incorporation of various chemical groups containing oxygen into the films, mainly C=O [101], which was in agreement with of XPS (X-ray Photoelectron Spectroscopy) measurement result in Ref. [121]. The main polymer chains were broken and rearranged by macromolecular motions, and the dipole moment was formed within the film [154]. Consequently, the melting enthalpy for the -30kV-corona-charged sample was higher than the corresponding value for the non-charged material.

5.3.2 Wide angle X-ray Differaction spectra of cellular PP

In addition, the Wide Angle X-ray Diffraction (WAXD) spectra are shown in following Fig. 5. 5 and the area of each peak of 2θ were listed in Tab. 5. 2. WAXD measurements have been performed at MATEIS Laboratory, INSA Lyon. The slight but evident increase in the integral intensity of WAXD peaks of corona-charged cellular PP was an evidence of increased crystallinity at the surface of charged sample [152].

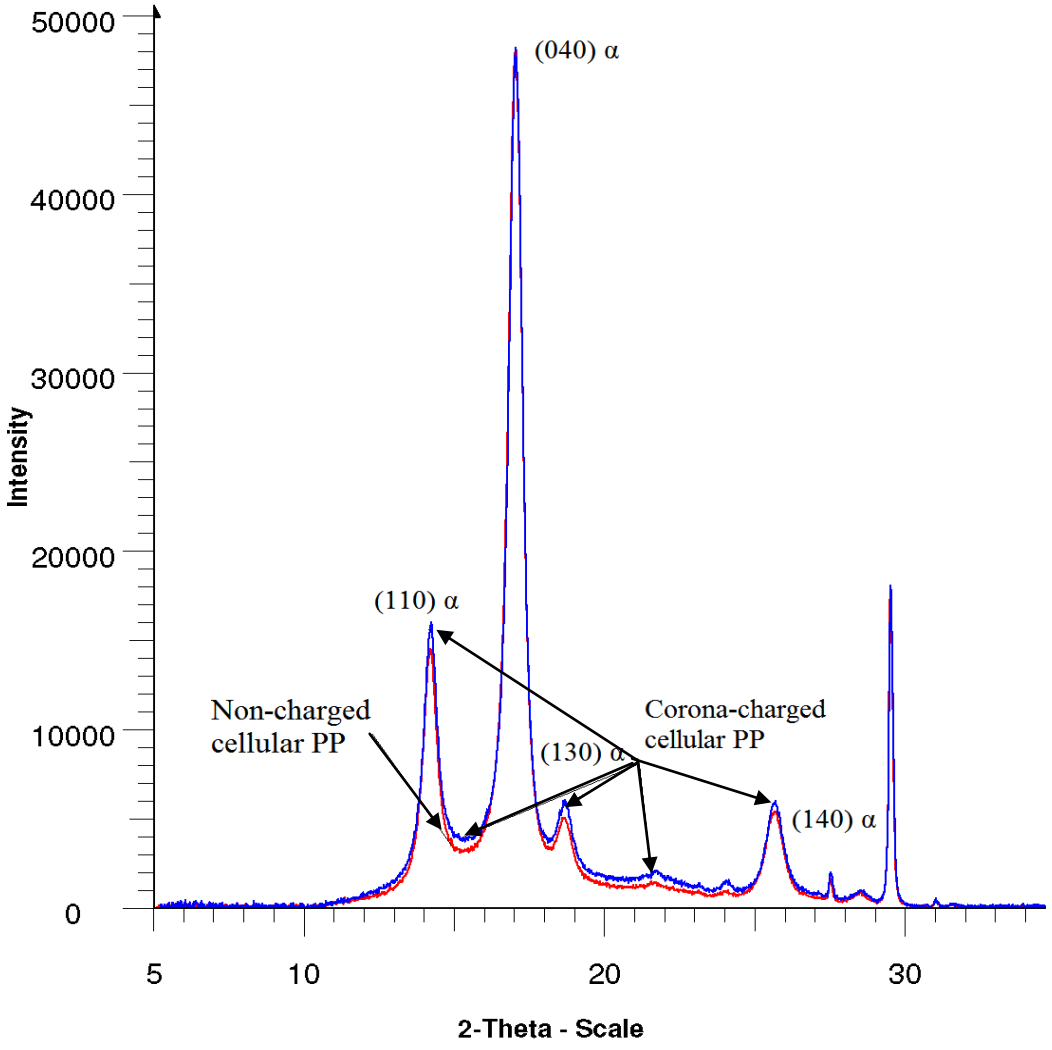

Fig. 5. 5 WAXD spectra of non-charged and corona-charged cellular PP

As shown in Fig. 5. 5 and Tab. 5. 2., concerning the α peak, we observe a small increase of the peaks of intensity and a small decrease of the FWHH (Full Width at the Half-Height) which were in good agreement with the enthalpy increase of the α phase contents observed on DSC.

Tab. 5. 2 Integral of intensity of cellular PP at each WAXD peaks V.S. 2θ

2θ (deg)	Peak name	Integral of intensity Non-charged cellular PP	Integral of intensity Corona-charged cellular PP
14.2	(110) α	73.17	89.81
17	(040) α	210.6	209.3
18.6	(130) α	23.44	32.56
25.6	(140) α	27.92	32.94

5.4 Electrostrictive performance of charged cellular PP

5.4.1 Electrostriction measurements results

Tab. 5. 3 gives the low electric field (0.5 V/mm) permittivity at 0.1 Hz, i.e., the same frequency of the applied electric field for strain measurements. It can be seen that the corona treatment also almost doubled the value of the permittivity, probably by inducing a space charge polarization that contributed to the permittivity value [91, 106]. This is also called interfacial polarization and is present in polymers having large structural in homogeneities. If the density of electric charges in the material is increased by corona

poling, the low frequency interfacial polarization is enhanced and permittivity may be significantly higher, as observed. Besides, the increase in the crystallinity of PP films induced by charge injection may also contribute to the better dielectric response, since this latter primarily originates from the crystalline phase of the polymer [3].

Tab. 5. 3 Relative permittivity of tested cellular PP at 0.1 Hz

Material	ε_r (0.1Hz)
Non-charged cellular PP	1.20
-30kV-charged PP	2.31

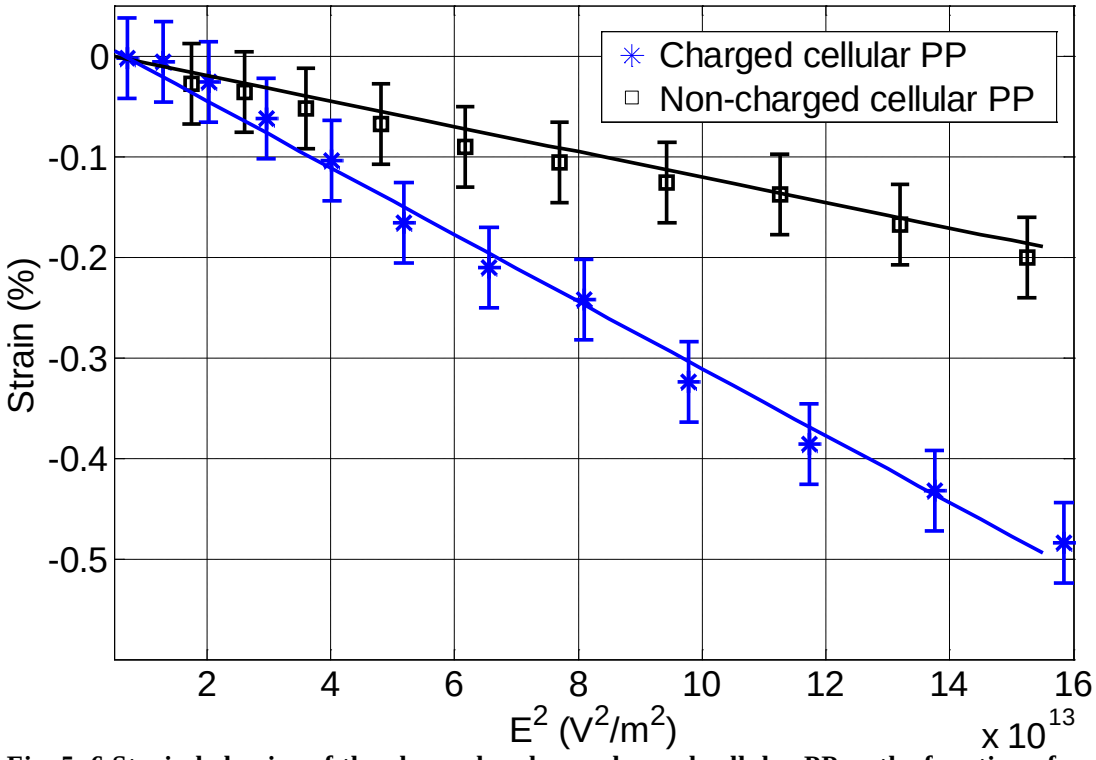

Fig. 5. 6 Strain behavior of the charged and non-charged cellular PP as the function of the square of the driving electric field.

Fig. 5. 6 presents curves of strain versus the square of the electrical field for the non-charged and the -30kV-charged samples, at 0.1 Hz. For both

materials, a linear dependence is observed confirming that the applied electric field dependence of the strain is quadratic. This result clearly indicates that the origin of the strain was mainly electrostrictive and/or induced by Maxwell stress effect. As a consequence, S_3 can be expressed according to:

$$S_3 = M_{33}^{*} \cdot E_3^{\,2} \tag{5.3}$$

By using the permittivity data from Tab. 5. 3 together with Young modulus of cellular PP measured in our laboratory (1GPa), the percentage contribution of the Maxwell effect ($-(\varepsilon_r.\varepsilon_0 / Y)\ E_3^{\,2}$) to the strain was found equal to 0.081% for the non-charged PP and 0.07% for the -30 kV-charged material. Consequently, the Maxwell effect can be neglected and the overall contribution to the strain is clearly due to the pure electrostrictive effect.

The apparent electrostriction coefficient may, be evaluated in both cases with the formula: $M_{33}^{*}=S_3/E_3^{\,2}$, giving a value of 1.3×10^{-17} m²/V² for the non-charged sample and 3.1×10^{-17} m²/V² for its -30kV-charged counterpart.. The charge-related electrostrictive coefficient, Q_{33}, can be calculated using $M_{33}=Q_{33}\varepsilon_0^{\,2}(\varepsilon_r\text{-}1)^2$ and gives the value 4.2×10^{6} m^4C^{-2} for the non-charged PP and 0.23×10^{6} m^4C^{-2} for the charged material. These values have been confirmed by a direct polarization measurement when performing the strain versus electric field experiment and the Q_{33} calculation from $S_3=Q_{33}P_3^{\,2}$. Interestingly, charge injection with corona poling decreases the Q_{33} coefficient of PP films, like conductive fillers such as carbon black (CB) incorporated in electrostrictive polymer matrices like polyurethane (PU) films [155]. But in this CB/PU composite system, global electrostrictive response (M_{33} coefficient) is also enhanced.

It is worthwhile to note that the observed increase in the strain is mainly due to an increase in the permittivity and that corona treatment was able to greatly enhance the ability of the cellular PP to become electrically strained [9, 91, 106]. The enhanced strain in thin film is a consequence of

nonuniform space-charge distribution across the thickness direction [156]. Due to the corona poling, the charges injected from the non-electroded surface were trapped in the film and then, formed a space charge layer, which augmented the electrostatic capacitance of charged sample [157]. Then, since the effect of the poling field was to orient the molecules of charged PP, the dipole moments pointed in the same direction, which would lead to electrostatic interactions between neighboring additives. The presence of an appropriate space-charge between two additives would force that dipole (additive)-charge- dipole (additive) system behaves as a unit. The combined mass and volume of such a unit would be much greater than a single dipole, thus hindering reorientation increasing the amount of stress [158]. Also the new dipole-charge-dipole system can be responsible for the enhanced electrostrictive effect in the poled system. Therefore, the charge in the bulk of the polymer would correlate the motion of the supplementary dipoles [130]. In addition, the charge storage capability of polymer electret material is also determined by the chemical nature of the polymer [18].

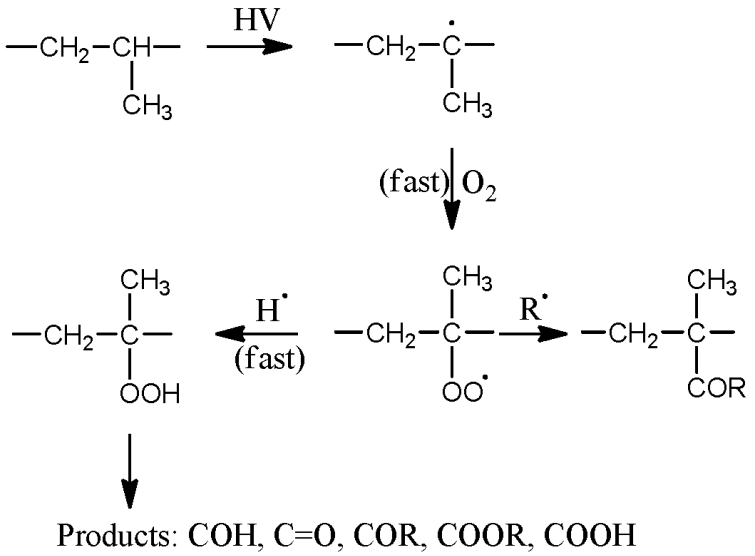

Fig. 5. 7 The oxidized polar groups generated in corona poling [101, 156]

As shown in Fig. 5. 7, N.Sellin et al. analyzed oxidized polar groups on the film surface by infrared spectroscopy (FTIR/ATR) technique and con-

firmed the presence of oxidized polar groups in corona poled PP films, mainly, C=O, C-O and COH [101, 159].

5.4.2 Electrical modelling based on charged cellular PP

Furthermore, based on the experimental data and interpretations given in Refs.[6, 14], in which space charge distribution of PP films has been investigated, a simplified model of charged cellular PP is proposed, in order to explain the beneficial effect of injected charges on the dielectric properties.

In Fig. 5. 8, ρ is the charge density (ρ<0), whose value is assumed to be equal in every layer. Divergence of electric field E can be obtained from Maxwell's equations:

$$\nabla \vec{E} = \frac{\rho}{\varepsilon} \tag{5.4}$$

where ε is the permittivity. Then,

$$\frac{dE}{dx} = \frac{\rho}{\varepsilon} \tag{5.5}$$

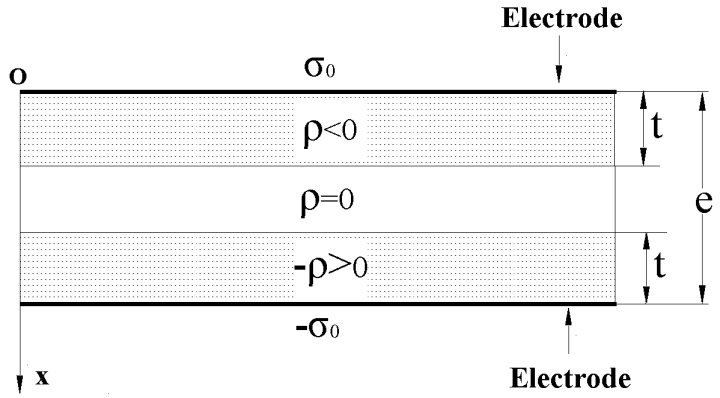

Fig. 5. 8 Simplified model of corona-charged cellular PP

Electric field can be expressed as:

$$\begin{aligned} E(x) &= \frac{\rho}{\varepsilon}x + E(0) \qquad (x < t) \\ E(x) &= E(0) + \frac{\rho}{\varepsilon}t \qquad (t < x < e - t) \\ E(x) &= E(0) + \frac{\rho}{\varepsilon}(e - x) \qquad (e - t < x < e) \end{aligned} \tag{5.6}$$

And then by integrating of the electrical field along the thickness of the sample, we got:

$$\int_0^e \vec{E}d\vec{l} = -\int_{V(0)}^{V(e)} dV \tag{5.7}$$

We got the potential V on the sample which can be expressed by

$$V(0) - V(e) = \frac{\rho}{\varepsilon}t(e - t) + E(0)e \tag{5.8}$$

Together with $V(0)$-$V(e)$=Q/C and Q=$\sigma_0 S$, capacitance of sample is calculated by

$$C_{cellularPP} = \frac{S}{\frac{e}{\varepsilon} + \frac{\rho}{\sigma_0 \varepsilon}t(e - t)} \tag{5.9}$$

For the non-charged film, ρ is around to be null and $C_{cellular\text{PP}}$= ε.S/e. For charged sample, as ρ <0 and σ_0>0:

$$\frac{e}{\varepsilon} + \frac{\rho}{\sigma_0 \varepsilon}t(e - t) < \frac{e}{\varepsilon} \tag{5.10}$$

and

$$C_{cellular\mathrm{PP}}^{\text{charged}} > C_{cellular\mathrm{PP}}^{\text{mon-charged}} \tag{5.11}$$

Consequently, capacitance and relative permittivity of charged cellular PP are greater than non-charged film, which lead to increase in strain in charged film as well.

5.5 Conclusion

In this part, we have demonstrated that after corona poling, electrostrictive response of cellular PP was enhanced, which is due to the non-uniform distribution of free injected charge and its displacement. Increase in the electrical-field-induced strain and permittivity were explained experimentally by using TSC, DSC and permittivity measurements, as well as a simple dielectric model. Larger strain responses and higher permittivity were observed for the charged sample as opposed to for the neat one. It appears that the injected charges contributed to induce a space charge polarization within the samples which highly contributed to the permittivity and the induced strain.

Chapter 6. Conclusions and future work

The motivation for the work was twofold. Firstly, we have studied on magnetoelectric performance of the laminated polymer composites and establishing mathematic models of each case. Secondly, the charge storage mechanism and the resulting enhanced electrostrictive effect on the cellular polypropylene after its corona poling has been analysed.

6.1 Main conclusions on magnetoelectric effect

In our works, we report on the direct magnetoelectric effect observed in bi- and trilayered polymers consisting of polyvinylidene fluoride (PVDF) and polyurethane (PU) filled with magnetically hard magnetite Fe_3O_4 or Terfenol-D(TeD) magnetostrictive material. A model, based on a driven damped oscillation system, has been developed to evaluate and study the influence of the first and second-order ME coefficients on the dc magnetic field-induced phase switching phenomenon between dynamic ME current and the applied ac magnetic field.

Aside from ME effects in multi-layer laminated composite materials, another novel and better performance of ME behaviour or developments indicating future fields of ME effect research have been discussed in this paper. The presented ME effect is an alternative to the product property between magnetostriction and piezoelectricity and is rather based on the product prop-

erty between Lorentz forces and piezoelectricity. The originality of this ME coupling is that Lorentz forces are located in the metal electrodes of the piezoelectric material and originate from eddy currents induced by ac magnetic flux within them. By this way, a ME coupling is finally achieved with only one piezoelectric material, in which no magnetic phase is required, and no direct ac current supply on the sample is necessary, eddy currents in electrodes are sufficient to generate Lorentz forces. Of course, optimal ac field orientation is required, i.e., ac magnetic field must be applied perpendicular to the electrodes to reach maximum flux. Consequently largest eddy currents magnitude and stress and strain magnitude may be achieved, yielding large direct piezoelectric response.

Then, the similar ME effect can be obtained using a PVDF film and a simple piezoelectric ceramic disc. Besides, owing to the circular shape of the disc, calculation of the Lorentz forces, and associated stresses can be realized, which was not the case for the rectangular unimorph bender in the former ME experiments. So, the measured output magnetoelectric current of a single piezoelectric disc was successfully modelled using piezoelectric equations providing the inductively coupled voltage between the electrodes of the ceramic is taken into account. The total output current can be attributed to three important sources: 1) The stress induced by the eddy currents within the metal electrodes through the Lorentz force effect is transferred to the piezoelectric layer and generates electric charges. This stress is increased by the dc bias field appliance. 2) The well known ME coupling based on a mechanical interaction between magnetostrictive and piezoelectric layers in laminate composites. 3) The dielectric current generated by the parasitic voltage induced by the ac magnetic flux through the closed contour of the experimental loop, is an inductively coupled voltage between the electrodes of the samples which can be explained by the Lenz and Faraday's Laws.

It is found that a good correlation between theoretical and experimental results can be got from the model. The ME response is linear with the

magnitude of dc magnetic field. In addition, combined radial velocity measurements validated the contribution of both radial stress and magnetically induced electric field. Finally, it was found that anisotropic dc field sensing can also be sensitively achieved at room temperature with only a single piezoelectric ceramic.

6.2 Main conclusions on electrostrictive effect

In view of the importance that the cellular PP electret in the field of EAP. We reported on our ongoing investigations of dipolar-charged cellular PP electrets. The results of surface potential decay tendency showed that the surface roughness influenced corona poling effect. The sample charged on smooth surface could keep surface charge for a longer time than the sample charged on its rough surface. Then, the results of electrostrictive effect demonstrated that after corona poling, electrostrictive response of cellular PP was enhanced. Increase in the electrical-field-induced strain and permittivity were explained experimentally by using TSC, DSC and permittivity measurements, as well as a simple dielectric model. It was shown with TSC measurements that the corona treatment at room temperature could inject charges at various depths, which were the main factor that enhanced electromechanical response of the -30 kV-charged sample. From permittivity measurements and electrical-field-induced strain experiments, higher permittivity and larger strain responses were observed for the charged sample as opposed to for the neat one. It appeared that the injected charges contributed to induce a space charge polarization within the samples which highly contributed to the permittivity and consequently the induced strain. In addition, by means of DSC measurements, from the chemical viewpoint, it was demonstrated that the corona treatment increased the crystallinity of cellular PP, which is consistent with the in-

crease in the dielectric response. Finally, a simplified model based on space charges with distinct polarity trapped in the vicinity of sample surfaces was also proposed in order to explain the increase in the effective permittivity and strain after corona poling.

6.3 Future work

Based on the previous researching experiences on the magenetoelectric effect of the composite materials, it would be promising for application that ac magnetic flux inducing eddy current within the electrodes of the other soft piezoelectric polymer. Comparing with stiff piezoelectric ceramic, the polymer has many merits, such as simpler structure, easier to fabricate and it is not as fragile as PZT unimorph bender. However, the design idea and magnetoelectric response of the unimorph bender in this work are precious and will promise to be applied widely. Furthermore, In order to develop it for practical applications, the set-up of the ME sensor must be improved to become more compact and portable, probably by using small permanent magnets to replace the giant electromagnets in ME experiment.

Because the Lorentz force induced magnetoelectric effect in unimorph bender and PVDF film is caused by eddy current within their electrodes, the current density will influence their magnetoelectric responses and vibrating velocity. Using different metal as electrodes with various conductivities should change the eddy current density and cause the different bending modes of benders. Thus, the ME effect and actuation mode of samples probably can be influenced by this way.

Since the complete mechanism of the electrostriction enhancement is not yet fully understood, other experiments and advanced technologies such as Laser Induced Pressure Pulse (LIPP) method, Photo Stimulated Current (PSC) method should be used to test the space-charge distribution in cellular

polymer, in order to enhance the understanding of space-charge storage mechanism in the sample. In addition, using corona discharge set up and forming the dipole within the composite embedded with magnetic particles seems to be another novel source of magnetoelectric effect, which is also the important link between two research topics in this thesis.

Furthermore, the experiment on the high-voltage corona charged polymer promise to be put into application such as micro electret generator that can retain the charges over an extensive period of time.

List of figures

List of tables

List of publications

1 GUIFFARD B., GUYOMAR D., BELOUADAH R. and **ZHANG J. W.,** "Piezomagnetic losses in bilayered magnetostrictive/piezoelectric composites: Effect of Terfenol-D content on the magnetoelectric susceptibility," ***Materials Letters***, **63**, 2584-2586, 2009.

2 GUIFFARD B., GUYOMAR D., GARBUIO L., BELOUADAH R., **ZHANG J. W.** and COTTINET P. J., "Eddy current induced magnetoelectricity in a piezoelectric unimorph bender," ***Applied Physics Letters***, **96**, 044105, 2010.

3 GUIFFARD B., **ZHANG J. W.**, GUYOMAR D., GARBUIO L., COTTINET P. -J. and BELOUADAH R., "Magnetic field sensing with a single piezoelectric ceramic disk: Experiments and modeling," ***Journal of Applied Physics***,**108**, 094901, 2010.

4 BELOUADAH R., GUYOMAR D., GUIFFARD B. and **ZHANG J.W.**, "Phase switching phenomenon in magnetoelectric laminate polymer composites: Experiments and modeling" ***Physica B: Condensed Matter***. **406**, 2821-2826, 2011

5 **ZHANG J. W.**, LEBRUN L., GUIFFARD B., BELOUADAH R., GUYOMAR D., GARBUIO L., COTTINET P.-J. and QIN L., "Enhanced Electromechanical Performance of Cellular Polypropylene Electrets Charged at High Temperature" ***Journal of Physics D: Applied Physics***. **44**, 415403, 2011

6 **ZHANG J. W.**, LEBRUN L., GUIFFARD B., COTTINET P.-J., GUYOMAR D., GARBUIO L. and BELOUADAH R., "Influence of corona poling on the electrostrictive behavior of cellular polypropylene films" ***Sensors & Actuators: A. Physical***, 2011 (In press)

International conference

7 GUIFFARD B, GUYOMAR D, **ZHANG J.W. ,** BELOUADAH R., GARBUIO L., and COTTINET P.-J. "Magnetoelectric effect in electroactive compounds without

magnetic ordering", **Materials Science & Technology (MS&T'10),** Houston, Texas, Oct.17-21, 2010

8 **ZHANG J. W.**, GUIFFARD B., LEBRUN L., and GUYOMAR D. "A Multi-functional Magnetoelectric Sensor Based on Eddy Current in Cantilevered Piezoelectric Unimorph Bender", **the 8th IEEE International Conference on Mechatronics and Automation (ICMA)**, Beijing, August 7-10, 2011.

References

[1] FIEBIG M., "Revival of the magnetoelectric effect," *Journal of Physics D-Applied Physics,* vol. 38, pp. R123-R152, 2005.

[2] ZHANG Q. M., SU J., KIM C. H., TING R. and CAPPS R., "An experimental investigation of electromechanical responses in a polyurethane elastomer," *Journal of Applied Physics,* vol. 81, pp. 2770-2776, 1997.

[3] GUIFFARD B., GUYOMAR D., SEVEYRAT L., CHOWANEK Y., BECHELANY M., CORNU D. and MIELE P., "Enhanced electroactive properties of polyurethane films loaded with carbon-coated SiC nanowires," *Journal of Physics D-Applied Physics,* vol. 42, 2009.

[4] GHOSH T. K., SHANKAR R. and SPONTAK R. J., "Mechanical and actuation behavior of electroactive nanostructured polymers," *Sensors and Actuators a-Physical,* vol. 151, pp. 46-52, 2009.

[5] ONO R., NAKAZAWA M. and ODA T., "Charge storage in corona-charged polypropylene films analyzed by LIPP and TSC methods," *IEEE Transactions on Industry Applications,* vol. 40, pp. 1482-1488, 2004.

[6] ZHANG B., ZHOU Y. X., WANG N. H., LIANG X. D., GUAN Z. C. and TAKADA T., "Polarity reversal charging of polypropylene films under DC corona discharge," *Journal of Electrostatics,* vol. 63, pp. 657-663, 2005.

[7] SAKANE Y., SUZUKI Y. and KASAGI N., "The development of a high-performance perfluorinated polymer electret and its application to micro power generation," *Journal of Micromechanics and Microengineering,* vol. 18, p. 104011, 2008.

[8] LINDNER M., HOISLBAUER H., SCHWODIAUER R., SIMONA B. G. D. and BAUER S., "Charged cellular polymers with "ferroelectretic" behavior," *IEEE Transactions on Dielectrics and Electrical Insulation,* vol. 11, pp. 255-263, 2004.

[9] QIU X. L., MELLINGER A., WEGENER M., WIRGES W. and GERHARD R., "Barrier discharges in cellular polypropylene ferroelectrets: How do they

influence the electromechanical properties?," *Journal of Applied Physics,* vol. 101, pp. 1-7, 2007.

[10] QIU X. L., MELLINGER A., WIRGES W. and GERHARD R., "Dielectric barrier discharges during the generation of ferroelectrets: Optical spectroscopy for process monitoring," *2007 Annual Report Conference on Electrical Insulation and Dielectric Phenomena,* pp. 828-831, 2007.

[11] MONTANARI G. C., FABIANI D., CIANI F., MOTORI A., PAAJANEN M., GERHARD-MULTHAUPT R. and WEGENER M., "Charging properties and time-temperature stability of innovative polymeric cellular ferroelectrets," *IEEE Transactions on Dielectrics and Electrical Insulation,* vol. 14, pp. 238-248, 2007.

[12] WEGENER M. and BAUER S., "Microstorms in cellular polymers: A route to soft piezoelectric transducer materials with engineered macroscopic dipoles," *Chemphyschem,* vol. 6, pp. 1014-1025, 2005.

[13] BAUER S., BAUER-GOGONEA S., DANSACHMULLER M., GRAZ I., LEONHARTSBERGER H., SALHOFER H. and SCHWODIAUER R., "Modern electrets," *2003 IEEE Ultrasonics Symposium Proceedings,* vol. 1-2, pp. 370-376, 2003.

[14] TANG M. M., AN Z. L., XIA Z. F. and ZHANG X. Q., "Electret properties and chemical modification of cellular polypropylene films," *Journal of Electrostatics,* vol. 65, pp. 203-208, 2007.

[15] GASANLY N. M., AYDINLI A. and SALIHOGLU O., "Thermally stimulated current observation of trapping centers in undoped GaSe layered single crystals," *Crystal Research and Technology,* vol. 36, pp. 295-301, 2001.

[16] GIACOMETTI J. A. and CAMPOS J. S. C., "Constant Current Corona Triode with Grid Voltage Control - Application to Polymer Foil Charging," *Review of Scientific Instruments,* vol. 61, pp. 1143-1150, 1990.

[17] FERREIRA G. F. L. and FIGUEIREDO M. T., "Corona Charging of Electrets - Models and Results," *IEEE Transactions on Electrical Insulation,* vol. 27, pp. 719-738, 1992.

[18] NAN C. W., BICHURIN M. I., DONG S. X., VIEHLAND D. and SRINIVASAN G., "Multiferroic magnetoelectric composites: Historical perspective, status, and future directions," *Journal of Applied Physics,* vol. 103, pp. 1-35, 2008.

[19] PRIYA S., ISLAM R., DONG S. X. and VIEHLAND D., "Recent advancements in magnetoelectric particulate and laminate composites," *Journal of Electroceramics,* vol. 19, pp. 147-164, 2007.

[20] MA J., HU J. M., LI Z. and NAN C. W., "Recent Progress in Multiferroic Magnetoelectric Composites: from Bulk to Thin Films," *Advanced Materials,* vol. 23, pp. 1062-1087, 2011.

[21] GUYOMAR D., GUIFFARD B., BELOUADAH R. and PETIT L., "Two-phase magnetoelectric nanopowder/polyurethane composites," *Journal of Applied Physics,* vol. 104, p. 074902, 2008.

[22] CURIE P., "Sur la symétrie dans les phénomènes physiques symétrie d'un champ électrique et d'un champ magnétique," *J. Physique,* vol. 3eme series, 1894.

[23] BRACKE L. P. M. and VANVLIET R. G., "A Broad-Band Magnetoelectric Transducer Using a Composite-Material," *International Journal of Electronics,* vol. 51, pp. 255-262, 1981.

[24] DZYALOSHINSKII I. E., "On the magneto-electrical effect in antiferromagnetics," *Soviet Physics-JETP,* vol. 37, pp. 628-629, 1959.

[25] ASTROV D. N., "The magnetoelectric effects," *Soviet Physics-JETP,* vol. 11, pp. 708-709, 1960.

[26] FOLEN V. J., RADO G. T. and STALDER E. W., "Anisotropy of the Magnetoelectric Effect in Cr_2O_3," *Physics Review Letter,* vol. 6, pp. 607-608, 1961.

[27] RADO G. T. and FOLEN V. J., "Observation of the magnetically induced magnetoelectric effect and evidence for antiferromagnetic domains," *Physical Review Letter,* vol. 7, pp. 310-311, 1961.

[28] RYU J., PRIYA S., UCHINO K. and KIM H. E., "Magnetoelectric effect in composites of magnetostrictive and piezoelectric materials," *Journal of Electroceramics,* vol. 8, pp. 107-119, 2002.

[29] CHANG C. M. and CARMAN G. P., "Experimental evidence of end effects in magneto-electric laminate composites," *Journal of Applied Physics,* vol. 102, p. 124901, 2007.

[30] BOOMGAARD J. V. D., TERRELL D. R., BORN R. A. J. and GILLER H. F. J. I., "An in-situ grown eutectic magnetoelectric composite material: Part I composition and unidirectional solidification," *Journal of Materials Science,* vol. 9, pp. 1705-1709, 1974.

[31] SRINIVASAN G., RASMUSSEN E. T., GALLEGOS J., SRINIVASAN R., BOKHAN Y. I. and LALETIN V. M., "Magnetoelectric bilayer and multilayer structures of magnetostrictive and piezoelectric oxides," *Physical Review B,* vol. 64, p. 214408, 2001.

[32] DONG S. X., LI J. F. and VIEHLAND D., "Ultrahigh magnetic field sensitivity in laminates of TERFENOL-D and $Pb(Mg_{1/3}Nb_{2/3})O_3$-$PbTiO_3$ crystals," *Applied Physics Letters,* vol. 83, pp. 2265-2267, 2003.

[33] RYU J. H., PRIYA S., CARAZO A. V., UCHINO K. and KIM H. E., "Effect of the magnetostrictive layer on magnetoelectric properties in lead zirconate titanate/terfenol-D laminate composites," *Journal of the American Ceramic Society,* vol. 84, pp. 2905-2908, 2001.

[34] NAN C. W., LIU L., CAI N., ZHAI J., YE Y., LIN Y. H., DONG L. J. and XIONG C. X., "A three-phase magnetoelectric composite of piezoelectric ceramics, rare-earth iron alloys, and polymer," *Applied Physics Letters,* vol. 81, pp. 3831-3833, 2002.

[35] CAI N., ZHAI J., NAN C. W., LIN Y. and SHI Z., "Dielectric, ferroelectric, magnetic, and magnetoelectric properties of multiferroic laminated composites," *Physical Review B,* vol. 68, p. 224103, 2003.

[36] ZHENG H., WANG J., LOFLAND S. E., MA Z., MOHADDES-ARDABILI L., ZHAO T., SALAMANCA-RIBA L., SHINDE S. R., OGALE S. B., BAI F., VIEHLAND D., JIA Y., SCHLOM D. G., WUTTIG M., ROYTBURD A. and RAMESH R., "Multiferroic $BaTiO_3$-$CoFe_2O_4$ nanostructures," *Science,* vol. 303, pp. 661-663, 2004.

[37] ZHOU J. P., HE H. C., SHI Z. and NAN C. W., "Magnetoelectric $CoFe_2O_4$/$Pb(Zr_{0.52}Ti_{0.48})O_3$ double-layer thin film prepared by pulsed-laser deposition," *Applied Physics Letters,* vol. 88, p. 013111, 2006.

[38] RYU J., CARAZO A. V., UCHINO K. and KIM H. E., "Magnetoelectric properties in piezoelectric and magnetostrictive laminate composites," *Japanese Journal of Applied Physics Part 1-Regular Papers Short Notes & Review Papers,* vol. 40, pp. 4948-4951, 2001.

[39] GAO J. Q., DAS J., XING Z. P., LI J. F. and VIEHLAND D., "Comparison of noise floor and sensitivity for different magnetoelectric laminates," *Journal of Applied Physics,* vol. 108, p. 084509, 2010.

[40] HILL N. A., "Why are there so few magnetic ferroelectrics?," *Journal of Physical Chemistry B,* vol. 104, pp. 6694-6709, 2000.

[41] ZHAO T., SCHOLL A., ZAVALICHE F., LEE K., BARRY M., DORAN A., CRUZ M. P., CHU Y. H., EDERER C., SPALDIN N. A., DAS R. R., KIM D. M., BAEK S. H., EOM C. B. and RAMESH R., "Electrical control of antiferromagnetic domains in multiferroic $BiFeO_3$ films at room temperature," *Nature Materials,* vol. 5, pp. 823-829, 2006.

[42] KIMURA T., GOTO T., SHINTANI H., ISHIZAKA K., ARIMA T. and TOKURA Y., "Magnetic control of ferroelectric polarization," *Nature,* vol. 426, pp. 55-58, 2003.

[43] KAMBE T., KOMATSU T., MICHIUCHI T., HAYAKAWA H., OHISHI D., HANASAKI N., YOSHII K. and IKEDA N., "Magneto-electric effect in charge-ordered $LuFe_2O_4$," presented at the International Conference on Magnetism (ICM 2009), 2010.

[44] PARK J. Y., PARK J. H., JEONG Y. K. and JANG H. M., "Dynamic magnetoelectric coupling in "electronic ferroelectric" $LuFe_2O_4$," *Applied Physics Letters,* vol. 91, p. 152903, 2007.

[45] CHUNG TIEN-KAN "Magnetoelectric coupling in layered thin film and nanostructure," Doctor of Philosophy, Mechanical Engineering, University of California, Los Angeles, 2009.

[46] SUCHTELEN V., "Product properties: a new application of composite materials," *Philips Research Report,* vol. 27, pp. 28-37, 1972.

[47] BOOMGAARD J. V. D., RUN A. M. J. G. V. and SUCHTELEN J. V., "Piezoelectric-piezomagnetic composites with magnetoelectric effect," *Ferroelectrics,* vol. 14, pp. 727-728, 1976.

[48] SRINIVASAN G., "Review on Giant Magnetoelectric effect in Oxide ferromagnetic/ferroelectric Layered Structures," *Condensed Matter,* vol. 0401607, pp. 1-9, 2004.

[49] VAN RUN A. M. J. G., TERRELL D. R. and SCHOLING J. H., "An in situ growneutectic magnetoelectric composite material.Part 2:Physical properties," *Journal of Materials Science,* vol. 9, pp. 1710-1714, 1974.

[50] ISLAM R. A., BEDEKAR V., POUDYAL N., LIU J. P. and PRIYA S., "Magnetoelectric properties of core-shell particulate nanocomposites," *Journal of Applied Physics,* vol. 104, p. 104111, 2008.

[51] ISLAM R. A., RONG C. B., LIU J. P. and PRIYA S., "Effect of gradient composite structure in cofired bilayer composites of $Pb(Zr_{0.56}Ti_{0.44})O_3$-$Ni_{0.6}Zn_{0.2}Cu_{0.2}Fe_2O_4$ system on magnetoelectric coefficient," *Journal of Materials Science,* vol. 43, pp. 6337-6343, 2008.

[52] MORI K. and WUTTIG M., "Magnetoelectric coupling in terfenol-D/polyvinylidenedifluoride composites," *Applied Physics Letters,* vol. 81, pp. 100-101, 2002.

[53] DONG S. X., ZHAI J. Y., PRIYA S., LI J. F. and VIEHLAND D., "Tunable Features of Magnetoelectric Transformers," *IEEE Transactions on Ultrasonics Ferroelectrics and Frequency Control,* vol. 56, pp. 1124-1127, 2009.

[54] DONG S. X., ZHAI J. Y., LI J. F. and VIEHLAND D., "Near-ideal magnetoelectricity in high-permeability magnetostrictive/piezofiber laminates with a (2-1) connectivity," *Applied Physics Letters,* vol. 89, p. 252904, 2006.

[55] CAI N., NAN C. W., ZHAI J. Y. and LIN Y. H., "Large high-frequency magnetoelectric response in laminated composites of piezoelectric ceramics, rare-earth iron alloys and polymer," *Applied Physics Letters,* vol. 84, pp. 3516-3518, 2004.

[56] GREVE H., WOLTERMANN E., QUENZER H. J., WAGNER B. and QUANDT E., "Giant magnetoelectric coefficients in $(Fe_{90}Co_{10})_{78}Si_{12}B_{10}$-AlN thin film composites," *Applied Physics Letters,* vol. 96, p. 182501, 2010.

[57] ZHANG J. X., DAI J. Y., SO L. C., SUN C. L., LO C. Y., OR S. W. and CHAN H. L. W., "The effect of magnetic nanoparticles on the morphology, ferroelectric, and magnetoelectric behaviors of CFO/P(VDF-TrFE) 0-3 nanocomposites," *Journal of Applied Physics,* vol. 105, p. 054102, 2009.

[58] MA J., SHI Z. and NAN C. W., "Magnetoelectric properties of composites of single $Pb(Zr,Ti)O_3$ rods and Terfenol-D/epoxy with a single-period of 1-3-type structure," *Advanced Materials,* vol. 19, pp. 2571-2573, 2007.

[59] DONG S. X., LI J. F. and VIEHLAND D., "Longitudinal and transverse magnetoelectric voltage coefficients of magnetostrictive/piezoelectric laminate composite: Theory," *IEEE Transactions on Ultrasonics Ferroelectrics and Frequency Control,* vol. 50, pp. 1253-1261, 2003.

[60] DONG S. X., LI J. F. and VIEHLAND D., "Longitudinal and transverse magnetoelectric voltage coefficients of magnetostrictive/piezoelectric laminate composite: Experiments," *IEEE Transactions on Ultrasonics Ferroelectrics and Frequency Control,* vol. 51, pp. 794-799, 2004.

[61] NAN C. W., "Magnetoelectric Effect in Composites of Piezoelectric and Piezomagnetic Phases," *Physical Review B,* vol. 50, pp. 6082-6088, 1994.

[62] O'DELL T. H., *The electrodynamics of magneto-electric media*. Amsterdam: North-Holland: American Elsevier Pub. Co., 1970.

[63] WANG Y., HU J., LIN Y. and NAN C. W., "Multiferroic magnetoelectric composite nanostructures," *NPG Asia Materials,* vol. 32, pp. 61-68, 2010.

[64] JIA Y. M., TANG Y. X., ZHAO X. Y., LUO H. S., OR S. W. and CHAN H. L. W., "Additional dc magnetic field response of magnetostrictive/piezoelectric magnetoelectric Laminates by Lorentz force effect," *Journal of Applied Physics,* vol. 100, p. 126102, 2006.

[65] JIA Y. M., ZHOU D., LUO L. H., ZHAO X. Y., LUO H. S., OR S. W. and CHAN H. L. W., "Magnetoelectric effect from the direct coupling of the Lorentz force from a brass ring with transverse piezoelectricity in a lead zirconate titanate (PZT) disk," *Applied Physics a-Materials Science & Processing,* vol. 89, pp. 1025-1027, 2007.

[66] LEUNG C. M., OR S. W. and HO S. L., "dc magnetoelectric sensor based on direct coupling of Lorentz force effect in aluminum strip with transverse piezoelectric effect in $0.7Pb(Mg_{1/3}Nb_{2/3})O_3$-$0.3PbTiO_3$ single-crystal plate," *Journal of Applied Physics,* vol. 107, pp. -, 2010.

[67] NAN C. W., LI M., FENG X. Q. and YU S. W., "Possible giant magnetoelectric effect of ferromagnetic rare-earth-iron-alloys-filled ferroelectric polymers," *Applied Physics Letters,* vol. 78, pp. 2527-2529, 2001.

[68] VOPSAROIU M., BLACKBURN J. and CAIN M. G., "A new magnetic recording read head technology based on the magneto-electric effect," *Journal of Physics D-Applied Physics,* vol. 40, pp. 5027-5033, 2007.

[69] EERENSTEIN W., MATHUR N. D. and SCOTT J. F., "Multiferroic and magnetoelectric materials," *Nature,* vol. 442, pp. 759-765, 2006.

[70] CHENG Z. Y., BHARTI V., XU T. B., XU H. S., MAI T. and ZHANG Q. M., "Electrostrictive poly(vinylidene fluoride-trifluoroethylene) copolymers," *Sensors and Actuators a-Physical,* vol. 90, pp. 138-147, 2001.

[71] BAR-COHEN Y., SHERRIT S. and LIH S. S., "Characterization of the electromechanical properties of EAP materials," *Smart Structures and Materials 2001: Electroactive Polymer Actuators and Devices,* vol. 4329, pp. 319-327, 2001.

[72] XU H. S., CHENG Z. Y., BHARTI V., WANG S. X. and ZHANG Q. M., "All-polymer electromechanical systems consisting of electrostrictive poly(vinylidene fluoride-trifluoroethylene) and conductive polyaniline," *Journal of Applied Polymer Science,* vol. 75, pp. 945-951, 2000.

[73] DEARING S. S., MORRISON J. F. and IANNUCCI L., "Electro-active polymer (EAP) "dimple" actuators for flow control: Design and characterisation," *Sensors and Actuators a-Physical,* vol. 157, pp. 210-218, 2010.

[74] KIM J., YUN S. and SONG C., "Performance of Electro-active paper actuators with thickness variation," *Sensors and Actuators a-Physical,* vol. 133, pp. 225-230, 2007.

[75] BAR-COHEN Y. and BREAZEAL C., *Biologically-inspired intelligent Robots* vol. PM122: SPIE Press, 2003.

[76] BAR-COHEN Y., "Electroactive polymers as artificial muscles - capabilities, potentials and challenges," in *Handbook on Biomimetics,* Y. Osada, Ed., ed: NTS Inc., 2000, pp. 936-950.

[77] COTTINET P.-J., GUYOMAR D., GUIFFARD B., LEBRUN L. and C. PUTSON, "Electrostrictive Polymers as High-Performance Electroactive

Polymers for Energy Harvesting," in *Piezoelectric Ceramics*, E. Suaste-Gomez, Ed., ed: InTech, 2010, pp. 185-208.

[78] BAR-COHEN YOSEPH, *Electroactive polymer (EAP) actuators as artificial muscles : reality, potential, and challenges*, 2nd ed. Bellingham, Wash.: SPIE Press, 2004.

[79] PUNNING A., ANTON M., KRUUSMAA M. and AABLOO A., "A biologically inspired ray-like underwater robot with electroactive polymer petoral fins," presented at the IEEE Mechatronics and Robotics (MechRob'04), Aachen, Germany, 2004.

[80] ZHAO X. H. and SUO Z. G., "Electromechanical instability in semicrystalline polymers," *Applied Physics Letters*, vol. 95, p. 031904, 2009.

[81] MYERS D. L. and ARNOLD B. D., "Electret Media For HVAC Filtration Applications," *International. Nonwovens Journal*, vol. 12, pp. 43-54, 2003.

[82] GUTMANN F. , "The Electret," *Reviews of Modern Physics*, vol. 20, pp. 457-472, 1948.

[83] Available: http://ether.sciences.free.fr/electrets.htm

[84] GIACOMETTI J. A., FEDOSOV S. and COSTA M. M., "Corona charging of polymers: Recent advances on constant current charging," *Brazilian Journal of Physics*, vol. 29, pp. 269-279, 1999.

[85] SESSLER G. M. and WEST J. E., "Self-biased condenser microphone with high capacitance," *J. Acoust. Soc. Am*, vol. 34, pp. 1787-1788, 1962.

[86] GERHARD-MULTHAUPT R. and IEEE DIELECTRICS AND ELECTRICAL INSULATION SOCIETY., *7th International Symposium on Electrets : (ISE 7) : Berlin, 25-27 September 1991 : proceedings*. New York, NY: IEEE, 1991.

[87] JASPER W. J., MOHAN A., HINESTROZA J. and BARKER R., "Degradation Processes in Corona-Charged Electret Filter-Media with Exposure to Ethyl Benzene," *Journal of Engineered Fibers and Fabrics*, vol. 2, pp. 19-24, 2007.

[88] LU T. J. and SESSLER G. M., "An Experimental-Study of Charge-Distributions in Electron-Beam Irradiated Polypropylene Films," *IEEE Transactions on Electrical Insulation*, vol. 26, pp. 228-235, 1991.

[89] LO H. W. and TAI Y. C., "Parylene-based electret power generators," *Journal of Micromechanics and Microengineering*, vol. 18, p. 104006, 2008.

[90] SESSLER G. M., *Elecctrets*, 3rd Edition ed.: Laplacian Press, 1998.

[91] SESSLER G. M. and HILLENBRAND J., "Electromechanical response of cellular electret films," *Applied Physics Letters,* vol. 75, pp. 3405-3407, 1999.

[92] ZHANG Q. M., BHARTI V. and ZHAO X., "Giant electrostriction and relaxor ferroelectric behavior in electron-irradiated poly(vinylidene fluoride-trifluoroethylene) copolymer," *Science,* vol. 280, pp. 2101-2104, 1998.

[93] LIU Y. M., REN K. L., HOFMANN H. F. and ZHANG Q. M., "Investigation of electrostrictive polymers for energy harvesting," *IEEE Transactions on Ultrasonics Ferroelectrics and Frequency Control,* vol. 52, pp. 2411-2417, 2005.

[94] DIACONU I. and DOROHOI D., "Properties of polyurethane thin films," *Journal of Optoelectronics and Advanced Materials,* vol. 7, pp. 921-924, 2005.

[95] LEBRUN L., GUYOMAR D., GUIFFARD B., COTTINET P. J. and PUTSON C., "The Characterisation of the harvesting capabilities of an electrostrictive polymer composite," *Sensors and Actuators a-Physical,* vol. 153, pp. 251-257, 2009.

[96] GUILLOT F. M., JARZYNSKI J. and BALIZER E., "Measurement of electrostrictive coefficients of polymer films " *Journal of the Acoustical Society of America* vol. 110, pp. 2980-2990, 2001.

[97] BOKOV A. A. and YE Z. G., "Giant electrostriction and stretched exponential electromechanical relaxation in $0.65Pb(Mg_{1/3}Nb_{2/3})O_3$-$0.35PbTiO_3$ crystals," *Journal of Applied Physics,* vol. 91, pp. 6656-6661, 2002.

[98] FENG Z. Y., HE T. H., XU H. Q., LUO H. S. and YIN Z. W., "High electric-field-induced strain of $Pb(Mg_{1/3}Nb_{2/3})O_3$-$PbTiO_3$ crystals in multilayer actuators," *Solid State Communications,* vol. 130, pp. 557-562, 2004.

[99] GUILLOT F. M. and BALIZER E., "Electrostrictive effect in polyurethanes," *Journal of Applied Polymer Science,* vol. 89, pp. 399-404, 2003.

[100] QIU X., XIA Z. and WANG F., "Piezoelectricity of single- and multi-layer cellular polypropylene film electrets," *Frontiers of Materials Science in China,* vol. 1, pp. 72-75, 2007.

[101] SELLIN N. and CAMPOS J. S., "Surface composition analysis of PP Films treated by corona discharge " *Materials Research,* vol. 6, pp. 163-166, 2003.

[102] HILLENBRAND J., ZHANG X., ZHANG Y. and SESSLER G. M., "Pressure-treated cellular polypropylene with large piezoelectric coefficients," *2003 Annual Report Conference on Electrical Insulation and Dielectric Phenomena,* pp. 40-43, 2003.

[103] WEGENER M., WIRGES W., FOHLMEISTER J., TIERSCH B. and GERHARD-MULTHAUPT R., "Two-step inflation of cellular polypropylene films: void-thickness increase and enhanced electromechanical properties," *Journal of Physics D-Applied Physics,* vol. 37, pp. 623-627, 2004.

[104] MELLINGER A., WEGENER M., WIRGES W., MALLEPALLY R. R. and GERHARD-MULTHAUPT R., "Thermal and temporal stability of ferroelectret films made from cellular polypropylene/air composites," *Ferroelectrics,* vol. 331, pp. 189-199, 2006.

[105] NEUGSCHWANDTNER G. S., SCHWODIAUER R., BAUER-GOGONEA S., BAUER S., PAAJANEN M. and LEKKALA J., "Piezo- and pyroelectricity of a polymer-foam space-charge electret," *Journal of Applied Physics,* vol. 89, pp. 4503-4511, 2001.

[106] PAAJANEN M., WEGENER M. and GERHARD-MULTHAUPT R., "Understanding the role of the gas in the voids during corona charging of cellular electret films - a way to enhance their piezoelectricity," *Journal of Physics D-Applied Physics,* vol. 34, pp. 2482-2488, 2001.

[107] ZHANG X., HILLENBRAND J. and SESSLER G. M., "Piezoelectric d_{33} coefficient of cellular polypropylene subjected to expansion by pressure treatment," *Applied Physics Letters,* vol. 85, pp. 1226-1228, 2004.

[108] GRIGSBY LEONARD L., *Electric power generation, transmission, and distribution*. Boca Raton: CRC Press, 2007.

[109] HAMZA A. S. H. A., MOHMOUD S. A. and GHANIA S. M., "Environmental pollution by magnetic field associated with power transmission lines," *Energy Conversion and Management,* vol. 43, pp. 2443-2452, 2002.

[110] MOORE A. D., *Electrostatics and its applications*. New York,: Wiley, 1973.

[111] WONG P. S. and SASTRE A., "Simultaneous Ac and Dc Magnetic-Field Measurements in Residential Areas - Implications for Resonance Theories of Biological Effects," *IEEE Transactions on Power Delivery,* vol. 10, pp. 1906-1912, 1995.

[112] SESSLER G. M., "Physical Principles of Electrets," *Topics in Applied Physics,* vol. 33, pp. 13-80, 1987.

[113] KOGOMA M. and OKAZAKI S., "Raising of Ozone Formation Efficiency in a Homogeneous Glow-Discharge Plasma at Atmospheric-Pressure," *Journal of Physics D-Applied Physics,* vol. 27, pp. 1985-1987, 1994.

[114] CARLEY J. F. and KITZE P. T. , "Corona-discharge treatment of polyethylene films. I. Experimental work and physical effects," *Polymer Engineering & Science,* vol. 18, pp. 326-334, 1978.

[115] NG S. H., WU Y. X., WANG Z. F. and WANG Z. P., "Corona discharge assisted thermal bonding of polymer microfluidic devices," *Microsystem Technologies-Micro-and Nanosystems-Information Storage and Processing Systems,* vol. 16, pp. 1181-1186, 2010.

[116] GROZA A., SURMEIAN A., GANCIU M. and POPESCU I. I., "Infrared spectral investigation of organosilicon compounds under corona charge injection in air at atmospheric pressure," *Journal of Optoelectronics and Advanced Materials,* vol. 7, pp. 2545-2548, 2005.

[117] TRINH N. G., "Partial Discharge .19. Discharge in Air .1. Physical-Mechanisms," *IEEE Electrical Insulation Magazine,* vol. 11, pp. 23-29, 1995.

[118] CHEN J. H. and DAVIDSON J. H., "Model of the negative DC corona plasma: Comparison to the positive DC corona plasma," *Plasma Chemistry and Plasma Processing,* vol. 23, pp. 83-102, 2003.

[119] CHEN J. H. and DAVIDSON J. H., "Ozone production in the negative DC corona: The dependence of discharge polarity," *Plasma Chemistry and Plasma Processing,* vol. 23, pp. 501-518, 2003.

[120] LOWKE J. J. and D'ALESSANDRO F., "Onset corona fields and electrical breakdown criteria," *Journal of Physics D-Applied Physics,* vol. 36, pp. 2673-2682, 2003.

[121] YOVCHEVA T. A., AVRAMOVA I. A., MEKISHEV G. A. and MARINOVA T. S., "Corona-charged polypropylene electrets analyzed by XPS," *Journal of Electrostatics,* vol. 65, pp. 667-671, 2007.

[122] ERHARD D. P., LOVERA D., GIESA R., ALTSTADT V. and SCHMIDT H. W., "Influence of Physical Aging on the Performance of Corona-Charged Amorphous Polymer Electrets," *Journal of Polymer Science Part B-Polymer Physics,* vol. 48, pp. 990-997, 2010.

[123] ARITA Y., SHIRATORI S. S. and IKEZAKI K., "A method for detection and visualization of charge trapping sites in amorphous parts in crystalline polymers," *Journal of Electrostatics,* vol. 57, pp. 263-271, 2003.

[124] YAGISHITA A., YAMANOUCHI H. and IKEZAKI K., "Charge trapping sites in spherulitic polypropylene," *Japanese Journal of Applied Physics Part 1-Regular Papers Short Notes & Review Papers,* vol. 38, pp. 2053-2058, 1999.

[125] SHI W., DING Y. J., FANG C., PAN Q. and GU Q., "Investigation of charge effects on poling and stability for corona-poled polymer films," *Applied Physics a-Materials Science & Processing,* vol. 77, pp. 567-570, 2003.

[126] BAMJI S. S., KAO K. J. and PERLMAN M. M., "Polymer Electrets Corona Charged at High-Temperature," *Journal of Electrostatics,* vol. 6, pp. 373-379, 1979.

[127] SCHWODIAUER R., GOGONEA S. B., BAUER S., HEITZ J., ARENHOLZ E. and BAUERLE D., "Charge stability of pulsed-laser deposited polytetrafluoroethylene film electrets," *Applied Physics Letters,* vol. 73, pp. 2941-2943, 1998.

[128] XIA Z. F., GERHARD-MULTHAUPT R., KUNSTLER W., WEDEL A. and DANZ R., "High surface-charge stability of porous polytetrafluoroethylene electret films at room and elevated temperatures," *Journal of Physics D-Applied Physics,* vol. 32, pp. 83-85, 1999.

[129] DAMAMME G., LEGRESSUS C. and DEREGGI A. S., "Space charge characterization for the 21st century," *IEEE Transactions on Dielectrics and Electrical Insulation,* vol. 4, pp. 558-584, 1997.

[130] PAULEY M. A., GUAN H. W. and WANG C. H., "Poling dynamics and investigation into the behavior of trapped charge in poled polymer films for nonlinear optical applications," *Journal of Chemical Physics,* vol. 104, pp. 6834-6842, 1996.

[131] BABA A. and IKEZAKI K., "Thermally Stimulated Currents from Corona-Charged Polypropylene Films - a Thermal Effect of Vacuum Deposition of Metallic Electrodes," *Journal of Applied Physics,* vol. 57, pp. 359-365, 1985.

[132] GUYOMAR D., MATEI D. F., GUIFFARD B., LE Q. and BELOUADAH R., "Magnetoelectricity in polyurethane films loaded with different magnetic particles," *Materials Letters,* vol. 63, pp. 611-613, 2009.

[133] GUIFFARD B., GUYOMAR D., GARBUIO L., BELOUADAH R., ZHANG J. and COTTINET P. J., "Eddy current induced magnetoelectricity in a piezoelectric unimorph bender," *Applied Physics Letters,* vol. 96, p. 044105, 2010.

[134] GUIFFARD B., GUYOMAR D., BELOUADAH R. and ZHANG J., "Piezomagnetic losses in bilayered magnetostrictive/piezoelectric composites: Effect of Terfenol-D content on the magnetoelectric susceptibility," *Materials Letters,* vol. 63, pp. 2584-2586, 2009.

[135] GUIFFARD B., ZHANG J. W., GUYOMAR D., GARBUIO L., COTTINET P. J. and BELOUADAH R., "Magnetic field sensing with a single piezoelectric ceramic disk: Experiments and modeling," *Journal of Applied Physics,* vol. 108, p. 094901, 2010.

[136] LLOVERA P. and MOLINIE P., "New methodology for surface potential decay measurements: Application to study charge injection dynamics on polypropylene films," *IEEE Transactions on Dielectrics and Electrical Insulation,* vol. 11, pp. 1049-1056, 2004.

[137] MADY F., RENOUD R., GANACHAUD J. P. and BIGARRE J., "Potential decay experiments for the characterization of electron transport. Modelling

and discussion," *Physica Status Solidi B-Basic Solid State Physics*, vol. 242, pp. 2089-2106, 2005.

[138] MOLINIE P., "Charge injection in corona-charged polymeric films: potential decay and current measurements," *Journal of Electrostatics*, vol. 45, pp. 265-273, 1999.

[139] MOLINIE P., GOLDMAN M. and GATELLET J., "Surface-Potential Decay on Corona-Charged Epoxy Samples Due to Polarization Processes," *Journal of Physics D-Applied Physics*, vol. 28, pp. 1601-1610, 1995.

[140] MANDOC M. M., ADAMS M. L. C., DINGEMANS G., TERLINDEN N. M., VAN DE SANDEN M. C. M. and KESSELS W. M. M., "Corona Charging and Optical Second-Harmonic Generation Studies of the Field-Effect Passivation of C-Si by Al_2O_3 Films," *35th IEEE Photovoltaic Specialists Conference*, 2010.

[141] UNIVERSITY OF CAMBRIDGE WEBSITE OF DEPARTMENT OF MATERIALS SCIENCE. Available: http://www.msm.cam.ac.uk/phasetrans/2002/Thermal2.pdf

[142] KONG Y. and HAY J. N., "The enthalpy of fusion and degree of crystallinity of polymers as measured by DSC," *European Polymer Journal*, vol. 39, pp. 1721-1727, 2003.

[143] TECHNISCHE UNIVERSITÄT BERLIN DEPARTMENT OF CHEMISTRY Available: http://www.chemie.tu-berlin.de/uploads/media/DSC.pdf

[144] UJHELYIOVA A., MARCINCIN A. and LEGEN J., "DSC analysis of polypropylene-low density polyethylene blend fibres," *Fibres & Textiles in Eastern Europe*, vol. 13, pp. 129-132, 2005.

[145] ZHAI J. Y., LI J. F., VIEHLAND D. and BICHURIN M. I., "Large magnetoelectric susceptibility: The fundamental property of piezoelectric and magnetostrictive laminated composites," *Journal of Applied Physics*, vol. 101, p. 014102, 2007.

[146] WANG Q. M., DU X. H., XU B. M. and CROSS L. E., "Theoretical analysis of the sensor effect of cantilever piezoelectric benders," *Journal of Applied Physics*, vol. 85, pp. 1702-1712, 1999.

[147] MUKHERJEE N., SHUKLA A., ROSEMAN R. D. and THOMPSON D. F., "Experimental determination of bending resonances of millimeter size PVF2 cantilevers," *Sensors*, vol. 3, pp. 263-275, 2003.

[148] BABU S. N., BHIMASANKARAM T. and SURYANARAYANA S. V., "Magnetoelectric effect in metal-PZT laminates," *Bulletin of Materials Science*, vol. 28, pp. 419-422, 2005.

[149] FUKADA E., SESSLER G. M., WEST J. E., BERRAISSOUL A. and GUNTHER P., "Bending Piezoelectricity in Monomorph Polymer-Films," *Journal of Applied Physics,* vol. 62, pp. 3643-3646, 1987.

[150] CAO W. Q., GU H. S., ZHOU T. S. and KUANG A. X., "Improved thermally stimulated current techniques and quenching polarization of polypropylene," *Materials & Design,* vol. 22, pp. 3-6, 2001.

[151] KRESSMANN R., "Linear and nonlinear piezoelectric response of charged cellular polypropylene," *Journal of Applied Physics,* vol. 90, pp. 3489-3496, 2001.

[152] NATH D. C. D., BANDYOPADHYAY S., YU A. B., ZENG Q. H., DAS T., BLACKBURN D. and WHITE C., "Structure-property interface correlation of fly ash-isotactic polypropylene composites," *Journal of Materials Science,* vol. 44, pp. 6078-6089, 2009.

[153] XIE X. L., LI R. K. Y., TJONG S. C. and MAI Y. W., "Structural properties and mechanical behavior of injection molded composites of polypropylene and sisal fiber," *Polymer Composites,* vol. 23, pp. 319-328, 2002.

[154] SUZER S., ARGUN A., VATANSEVER O. and ARAL O., "XPS and water contact angle measurements on aged and corona-treated PP," *Journal of Applied Polymer Science,* vol. 74, pp. 1846-1850, 1999.

[155] WONGTIMNOI K., GUIFFARD B., BOGNER-VAN DE MOORTELE A., SEVEYRAT L., GAUTHIER C. and CAVAILLE J. Y., "Improvement of electrostrictive properties of a polyether-based polyurethane elastomer filled with conductive carbon black" *Composites Science and Technology,* vol. 71, pp. 885-892, 2011.

[156] SU J., ZHANG Q. M., and TING R. Y., "Space-charge-enhanced electro-mechanical response in thin-film polyurethane elastomers" *Applied Physics Letters*, vol. 96, p. 386, 1997.

[157] FUJII M., TOHYAMA K., TOKORO M., KOSAKI Y., MURAMOTO Y., HOZUMI N. and NAGAO M., "Space charge behavior in polymer film based on increment of capacitance under AC high field" *Electrical Engineering in Japan*, vol. 141, pp. 8-6, 2002

[158] ZHANG J. W., LEBRUN L., GUIFFARD B., BELOUADAH R., GUYOMAR D., GARBUIO L., COTTINET P.-J. and LIU Q., "Enhanced electromechanical performance of cellular polypropylene electrets charged at a high temperature" *Journal of Physics D-Applied Physics*, vol. 44 p. 415403, 2011

[159] MATSUDA Y., SAITO Y. and TASAKA S., "Dipole Polarization Formed on Surface of Polypropylene Electrets," *IEEE Transactions on Dielectrics and Electrical Insulation,* vol. 17, pp. 1015-1020, 2010.

French part

Chapitre 1

La première partie de ce chapitre est consacré à la définition de l'effet magnéto-électrique (ME) sous ses deux aspects : direct et inverse. Le premier se traduit par l'apparition d'une polarisation électrique induite sous l'action d'un champ magnétique alors que le second correspond à l'apparition d'une aimantation sous l'action d'un champ électrique.

On distingue deux grandes familles de matériaux ME. La première famille est celle des monocristaux intrinsèquement magnétoélectriques comme Cr_2O_3, $BiFeO_3$, $TbMnO_3$ et $LuFe_2O_4$ qui présentent un couplage faible. La seconde famille est celle des matériaux composites dont l'effet ME repose sur le concept de propriété produite entre l'effet magnétostrictif et l'effet piézoélectrique. Ainsi, des composites 1-3 à fibres ou des composites 0-3 à particules et des matériaux composites à base d'oxydes laminés de type 2-2 ont été particulièrement étudiés. Par contre, peu de travaux sur les composites laminés utilisant des couches polymères magnétostrictifs ont été réalisés.

La suite de cette partie est consacrée à une présentation des applications les plus courantes: stockage de données, capteurs de champs magnétiques et actionneurs.

L'effet magnéto-électrique peut être également induit sans phase magnétique par un couplage entre l'effet piézoélectrique et les forces de Lo-

rentz induites par le champ magnétique dans les électrodes d'un élément piézoélectrique. Ce concept de propriété produite sans l'effet magnétostrictif est développé sur deux exemples.

La seconde partie de ce chapitre s'intéresse à l'effet électrostrictif qui constitue la deuxième thématique de cette thèse. Les polymères électroactifs présentent de nombreux avantages par rapport aux matériaux massifs classiques. Ils sont peu coûteux à produire, faciles à mettre en œuvre sous des formes très variés ou sur des grandes surfaces. Après une rapide revue des différentes familles de polymères électroactifs et de leurs applications, les équations fondamentales de l'électrostriction sont présentées. Une attention toute particulière est apportée aux électrets. Ces matériaux sont capables de stocker de façon permanente des charges électriques par exemple en utilisant la technique de charge basée sur l'effet Corona. Ils permettront donc d'étudier l'influence de charges électriques injectées sur les performances en électrostriction d'un matériau diélectrique.

Chapitre 2

Ce chapitre traite des différentes techniques expérimentales mises en jeu au laboratoire pour étudier l'effet magnéto-électrique. Il présente en particulier la technique de synthèse utilisée pour réaliser des composites à base de matrices polymères. Celle-ci est basée sur la dispersion de particules magnétiques dans une matrice de polyurethane (PU). Pour cela, des granules commerciales de PU sont mises en solution dans le solvant DMF avant d'y incorporer les particules magnétiques dans la quantité souhaitée. Celles-ci sont ensuite dispersées à l'aide d'une sonde à ultrasons qui garantit une distribution homogène des particules dans le film. Une attention toute particulière est apportée au séchage afin de garantir une bonne élimination du solvant. Ce film ainsi préparé est associé à un film piézoélectrique de PVDF. La déformation mécanique induite par magnétostriction dans le composite à base de PU sera convertie en signal électrique par effet piézoélectrique direct grâce au film de PVDF.

Il discute également du développement de systèmes originaux présentant un effet magnétoélectrique sans la présence de phase magnétique (magnétostrictive). En effet, par application d'un champ magnétique alternatif, des courants de Foucault peuvent être induits dans les électrodes métalliques recouvrant un matériau piézoélectrique. Ces courants en présence d'un champ magnétique continu produisent une force de Lorentz dans l'électrode qui se transmet au matériau piézoélectrique. Celui-ci va délivrer un signal électrique par effet piézoélectrique inverse. Trois types de matériaux piézoélectriques ont été étudiés : un film commercial de PVDF, un disque céramique piézoélectrique et une structure unimorphe type poutre constituée d'une céramique piézoélectrique sur un substrat métallique.

Ce chapitre décrit enfin les bancs de mesures utilisés pour quantifier dans ces différents types de système l'effet magnéto-électrique mais également leur déformation mécanique.

Chapitre 3

Ce chapitre est consacré à la présentation des différents équipements utilisés pour charger un échantillon de polypropylène et pour contrôler les propriétés électriques après sa charge.

Le premier équipement consiste en un montage de type triode Corona réalisé au laboratoire à partir de deux générateurs haute tension[5, 125]. Il utilise quatre aiguilles et d'une grille en métal positionnée au voisinage de l'échantillon. Chacun de ces éléments est porté à un potentiel négatif choisi par l'utilisateur. Ce montage permet de fixer le potentiel de surface de l'échantillon et la quantité de charges injectées.

Le second est un voltmètre électrostatique (Model 541 Trek) qui permet de suivre la variation dans le temps du potentiel de surface de l'échantillon de polypropylène.

Le troisième est un système commercial qui mesure la réponse en fréquence d'un échantillon diélectrique et donne ainsi accès à la valeur de sa permittivité (1255A Frequency response Analyser and 1296 Dielectric Interface Solartron) .

Le quatrième est un dispositif réalisé au laboratoire qui permet la mesure du Module d'Young. Il utilise un moteur linéaire qui permet de soumettre un échantillon à un cycle contrôlé de déplacement et d'un capteur de force qui permet de connaître la force appliquée.

Le cinquième permet la mesure des courants thermo-stimulés à l'aide d'une étuve (Chamber VT7004, Vötsch Indutrieteknik, Germany) qui permet d'appliquer un profil thermique défini sur l'échantillon et d'un amplificateur de courant associés à un enregistreur de données [142-144]. Cette mesure permet de calculer la quantité de charges injectées mais également de

déterminer à quel type de mécanisme est du le courant mesuré (relaxation dipolaire, déplacement de charges…)

Le sixième est un équipement de Calorimétrie Différentielle DSC (DSC 131 evo Setaram) qui permet de suivre toute transformation ou transition de phase dans un matériau. Cette mesure complète la mesure de courant thermo-stimulé en précisant si le courant observé est également lié à une transformation structural du matériau.

Chapitre 4

Ce chapitre regroupe les résultats de mesures magnétoélectriques effectuées sur différents types d'échantillons. Le premier type concerne des composites laminés associant des polymères composites magnétostrictifs et des matériaux piézoélectriques. Pour ces composites, une modélisation du courant induit par l'effet magnétoélectrique a été réalisée en prenant en compte les pertes. Ce modèle permet de décrire correctement l'ensemble des résultats expérimentaux observés. Les valeurs des coefficients sont données pour différentes familles de composites.

Le second type concerne l'utilisation de la force de Lorentz sur les électrodes d'un matériau piézoélectrique pour délivrer un signal électrique commandé par le champ magnétique. Dans ce cas, comme il a été dit précédemment, il n'y a pas besoin de phase magnétique pour induire l 'effet. La réponse magnétoélectrique de tels dispositifs est linéaire avec le champ magnétique continu alors qu'elle est usuellement quadratique. Ceci ouvre donc des perspectives intéressantes pour réaliser des capteurs de champ magnétique.

Un modèle du courant électrique disponible a été réalisé, en bon accord avec les mesures expérimentales.

Chapitre 5

Ce chapitre est consacré à la caractérisation du polypropylène avant et après une décharge Corona. Un premier résultat montre l'intérêt d'utiliser des polymères avec un état de surface peu rugueux. En effet, la rugosité favorise l'échange des charges de surface avec l'environnement et par conséquent diminue la diffusion de ces charges dans le polymère. Ceci se voit essentiellement sur la diminution plus rapide du potentiel de surface dans le cas d'une surface plutôt rugueuse. L'analyse des courants thermo-stimulés a montré que la charge injectée augmentait avec le potentiel appliqué sur les aiguilles et que l'injection de charges s'est faite à des niveaux plus ou moins profonds. Un des pics de courant apparaît au voisinage de la température de fusion de la phase β du polypropylène. Par conséquent, on peut donc envisager que suite à l'injection Corona des charges électriques ont été piégées à l'interface existant entre la phase β et la phase α et qu'elles sont dé-piégées à la fusion de la phase β. Les deux autres pics de courant ne sont associés à aucun autre évènement décelable en analyse thermique. Un des effets de la décharge Corona a été d'augmenter légèrement la cristallinité du polypropylène. L'effet de l'injection de charge sur l'électrostriction du polypropylène est fort car il se traduit par un doublement de la permittivité et de la déformation sous champ électrique. Cette augmentation de la permittivité peut s'expliquer par un modèle simple qui distribue en volume les charges injectées. Cette distribution volumique est également compatible avec le développement d'un processus dipolaire au sein du matériau.

FOLIO ADMINISTRATIF

THESE SOUTENUE DEVANT L'INSTITUT NATIONAL DES SCIENCES APPLIQUEES DE LYON

NOM : **ZHANG** DATE de SOUTENANCE : **13 Décembre 2011**
(avec précision du nom de jeune fille, le cas échéant)

Prénoms : **Jiawei**

TITRE : ***NANOCOMPOSITES MULTIFONCTIONNELS POUR L'ACTIONNEMENT MECANIQUE ET LA CONVERSION MAGNETO-ELCTRIQUE***

NATURE : **Doctorat** Numéro d'ordre : 2011-ISAL-0132

Ecole doctorale : **EEA**

Spécialité : **Electronique-Electrotechnique-Automatique**

RESUME :
L'effet magnétoélectrique (ME) se traduit par la possibilité d'induire une magnétisation à l'aide d'un champ électrique (effet direct) ou celle d'induire une polarisation électrique à l'aide d'un champ magnétique (effet inverse). Les composites laminés qui possèdent de grands coefficients ME ont généré beaucoup d'intérêt dans le domaine des capteurs, des modulateurs, des interrupteurs et des inverseurs de phase. Dans cette thèse, nous présentons les performances de composites dits laminés à deux ou trois couches. Il a été montré que l'on pouvait obtenir des performances en conversion magnéto-électrique directe en associant des phases magnétostrictives et piézoélectriques. Une modélisation de leur comportement basée sur un oscillateur mécanique a été proposée. Elle a été en particulier utilisée pour simuler le couplage mécanique entre deux couches.
Une autre approche pour développer des dispositifs originaux a consisté à utiliser un champ magnétique alternatif pour induire des courants de Foucault dans des électrodes métalliques et une Force de Lorentz en présence d'un deuxième champ magnétique continu. Si ces électrodes recouvrent un matériau piézoélectrique, la force de Lorentz sera alors convertie en signal électrique suivant l'effet direct. Cette approche permet donc de développer des dispositifs de conversion électromagnétique sans phase magnétique. Différents prototypes utilisant un bimorphe piézoélectrique, un film de PVDF et une céramique piézoélectrique ont été réalisés et caractérisés. Un signal électrique proportionnel à la composante continue du champ magnétique a été mis en évidence, ce qui ouvre des applications pour la détection magnétique. Cette thèse s'est également intéressée à l'augmentation du coefficient d'électrostriction par injection de charges électriques en utilisant la technique de décharge Corona. Cette étude a été réalisée sur du polypropylène, connu pour sa capacité à stocker des charges électriques. Le mécanisme de stockage de charge et l'effet sur l'électrostriction ont été étudiées par la mesure du potentiel de surface, la mesure des courants thermo-stimulés, la calorimétrie différentielle et l'interférométrie Laser. L'injection de charges a contribué à une augmentation de la permittivité et par la même à celle du coefficient d'électrostriction, en accord avec un modèle simple de distribution de charges dans l'échantillon.

MOTS-CLES : **L'effet Magnétoélectrique, Composite, Triode Corona, Electrostriction, Polymère,**

Laboratoire (s) de recherche : **Laboratoire de Génie Electrique et Ferroélectricité, LGEF , INSA de Lyon**

Directeur de thèse: **Prof. Laurent LEBRUN**
Co-directeur de thèse: **Prof. Benoit GUIFFARD**

Président de jury : **Prof. Daniel GUYOMAR**

Composition du jury :

Dr. François BAUER
Dr. Yves BERNARD (HDR)
Prof. Benoit GUIFFARD
Prof. Daniel GUYOMAR
Prof. Colette LACABANNE
Prof. Laurent LEBRUN